Development of milk exosome-based probes for biomedical imaging

by

María Isabel González Gutiérrez

A dissertation submitted by in partial fulfillment of the requirements for the degree of Doctor in

Biomedical Science and Technology

Universidad Carlos III de Madrid

Advisor(s):

Dr. Beatriz Salinas Rodríguez
Dr. Manuel Desco Menéndez

Tutor:

Dr. Manuel Desco Menéndez

[Defense Month]

"If you can dream it, you can do it. Always remember that this whole thing was started with a dream and a mouse"

Walter Elias Disney.

ACKNOWLEDGEMENTS

Ahora sí, ha llegado el momento. Intentaré ser breve, sin olvidarme nada entre estas letras. GRACIAS. Gracias a esta tesis por darme tantos momentos y personas.

Empezaré por lo que más cerca me pilla, por Sondas. Gracias a Bea por dejarme unirme a este grupo, a esta experiencia. Gracias por todísimas (es que son muchas) las oportunidades que me has ofrecido, por creer en mí y por las charletas en los *Bistro* francesitos de Lyon. Que me llamen pelota, pero gracias por ser más que una mera directora de tesis. Gracias también a todo el que ha pasado y pasa cada día por este grupo tan variopinto que es Sondas y ha dejado en él un poquito de sí, pero permitidme quedarme con Gorka y Mario. Con el primero porque, pese a no cumplir su promesa de resistir conmigo hasta el final de esta tesis, ha sido mi hermano mayor, el hombro de Hulk en el que apoyarme y también el Drama King por excelencia. Y con el segundo por ser el Berto Romero de esta Andreu Buenafuente, mi manual de informática básica y mi compañero de tés, dulces o amargos, pero siempre reconfortantes.

En esta misma planta, voy a agradecerle a Elena Calidad sus abrazos mañaneros y esos suspiros que han puesto banda sonora a mi trabajo. También agradecerle a Manolo su punto de vista crítico, ese que te empuja a superarte. Y a todos los demás, presentes y pasados, Rebeca, Jorge, Elena Irish, Vicente, Diego, Nico, Lorena, Trajana y un largo etcétera, por contribuir a que haya sido un placer llegar a trabajar al LIM cada día.

Qué pena que no siga en la pecera y que me tenga que ir lejos a buscarle, pero no se me olvida incluir a mi Dani Rolín en esta líneas. Decirte que has sido y, por suerte, continúas siendo como un Obi-Wan para esta joven *padawan*. A buen entendedor…

Me levanto de la silla y bajo a un despacho pequeñito, el de Sandra, Yolanda y María. Y un poquito de Dani Calle también. Gracias a los cuatro porque aquí pasamos infinitas horas al día y es un regalo tener a quien te ayuda a levantar la vista del cuaderno y respirar, a base de cariño y cachondeo de los buenos.

Como además he tenido varios hospedadores a lo largo de este camino, voy a pararme a agradecerles todo lo que he aprendido con ellos y que me hayan hecho sentir una más de sus grupos. Aquí se incluyen los desayunos tempraneros con Iria, la cerveza fresquita de los viernes en el CNIO y la más fresquita aún entre muniqueses.

No se me puede olvidar uno de los gracias más grandes para mis padres y mi Ezequiel, que no han estado físicamente a mi lado en el laboratorio, pero han sido y son un apoyo incondicional donde soporto mi futuro científico. Y mi futuro en general.

Y acabo dándome las gracias a mí misma, por aprovechar y disfrutar tanto toda esta "suerte". Por haber aprendido a ser *sakura* en la nieve.

ABSTRACT

Exosomes are extracellular vesicles naturally secreted by living cells, intended for the exchange of information between them. Their physicochemical characteristics, featured by nanometric size and lipid bilayer structure, make them similar to the synthetic liposomes designed to be applied in the field of biomedicine. In addition, exosomes have associated an intrinsic biological role, which confers them natural tropism to certain tissues and pathological processes. Taken together, these characteristics suggest the potential use of exosomes as natural platforms to design new nanoprobes for molecular imaging, overcoming the limitations presented by nanoparticles traditionally used in this research field, generally associated with their toxicity and in vivo stability. As source of exosomes, milk stands out due to its high content of these nanovesicles, with proven functionality as carriers of molecules and drugs.

The main goal of this thesis was to develop milk exosome-based probes for the detection of several pathologies by molecular imaging. To reach this aim, the project was divided in four specific objectives, as follows: i) establishing an optimal protocol for the isolation of exosomes from, in this case, commercial goat milk, according to the milk characteristics and the resources available in the research laboratory, ii) exploring alternative strategies for the radioactive and fluorescent labeling of exosomes, overcoming the limitations of current approaches, iii) determining the in vivo pharmacokinetics and biodistribution of the exosome-based probes, to elucidate their natural behavior in healthy mice and iv) evaluating the capacity of the exosome-based probes to target inflammatory processes, as potential nanoplatforms for diagnosis.

Thus, **first contribution** of this thesis is to describe for first time an isolation protocol based on the combination of physical and biological approaches to obtain pure and homogeneous milk exosome samples. By means of physicochemical, proteomic and biological characterization, the efficacy of the biophysical protocol was demonstrated, as well as the exosomal nature of the isolated vesicles and their non-toxicity in healthy mice.

The second contribution of this thesis is based on the development of new chemical strategies for the labeling of exosomes with both radioisotopes and fluorophores. In the case of the radiochemical labeling, exosomes were labeled with Technetium-99, by the passive incorporation of this isotope into the nanovesicle structure. The main advantages of this straightforward approach is that it does not require a chelator for the coordination of the radiometal and employs mild conditions that avoid the chemical modification or degradation of the exosomes. The second chemical approach presented in this thesis is the fluorescent labeling of exosomes. Current methodologies for the fluorescent labeling of exosomes involve advanced knowledge of genetic engineering or result in unstable fluorescent probes that can lead to false positives. This thesis proposes a labeling strategy based on the covalent binding of commercial fluorophores to the functional groups available on the exosome surface. This strong chemical bond ensures the stability of the nanoprobe, preventing the release of the fluorophore. In both cases,

physicochemical characterization of the resulting molecular probes showed that the original properties of the exosomes are not altered after the corresponding labeling.

The third contribution of this work is the in vivo evaluation by nuclear and optical techniques of the natural behavior of labeled goat milk exosomes after exogenous administration in healthy mice. By means of SPECT/CT imaging and ex vivo evaluation, it was determined that the way of administering the exosome-based probe significantly alters their pharmacokinetic and biodistribution parameters. On the other hand, both optical and nuclear imaging revealed the high accumulation of the nanoprobes in liver after intravenous injection, due to its high uptake by hepatocytes and Kupffer cells. This finding could endorse their future used in the field of hepatic diseases.

Last contribution of this thesis deals with the evaluation of the exosome-based probes for diagnostic of inflammatory pathologies. Based on the literature, goat milk exosomes are involved in the immune response and inflammation. For this reason, a fluorescent exosome-based probe developed in this thesis was evaluated in vitro against cells related to the inflammatory process and in vivo in a peritonitis mouse model, by different optical imaging techniques. Fluorescent exosomes demonstrated their ability to detect the inflammatory process underlying the disease, presenting particular uptake by the proinflammatory population of macrophages.

In conclusion, this thesis provides novel methodologies to the labeling and characterization of milk exosomes for use as natural nanoprobes for molecular imaging. These approaches improve the current labeling protocols, enabling the development of stable molecular probes that do not alter the original properties of the exosomes. Pharmacokinetic and biodistribution evaluation of the developed nanoprobes highlight the importance of choosing the appropriate route of administration of exosomes according to their purpose, as well as their potential applicability in liver pathologies. Finally, studies performed in the in vivo model of peritonitis support their use as imaging probes for the detection of inflammatory response, enabling the evaluation of the process at cellular level as well as the in vivo localization of the inflammatory focus.

TABLE OF CONTENTS

CHAPTER 1 . GENERAL INTRODUCTION 1

1.1. Nanotechnology and biomedicine 1
1.2. Exosomes: natural nanoparticles manufactured by cells 2
1.3. Role of exosomes in disease progression 4
1.4. Molecular imaging 5
1.5. Milk exosomes as natural liposome-like nanoparticles for biomedical imaging .. 8
1.6. Bibliography 10

CHAPTER 2 . MOTIVATION AND OBJETIVES 15

2.1. Objectives 16
2.2. Scientific contributions 16
2.3. Outline of the document 17
2.4 Bibliography 17

CHAPTER 3 . ISOLATION OF GOAT MILK EXOSOMES BY NOVEL COMBINED BIOPHYSICAL METHODOLOGY 19

3.1. Introduction 19
3.2. Materials and Methods 20
3.3. Results 24
3.4. Discussion 29
3.5. Bibliography 31

CHAPTER 4 . RADIOACTIVE LABELING OF MILK-DERIVED EXOSOMES WITH ^{99M}TC AND IN VIVO TRACKING BY SPECT IMAGING 34

4.1. Introduction 34
4.2. Materials and Methods 35
4.3. Results 39
4.4. Discussion 44
4.5. Bibliography 47

CHAPTER 5 . COVALENTLY LABELED FLUORESCENT EXOSOMES FOR IN VITRO AND IN VIVO APPLICATIONS 51

5.1. Introduction 51
5.2. Materials and Methods 52
5.3. Results 57
5.4. Discussion 63
5.5. Bibliography 67

CHAPTER 6 . GOAT MILK EXOSOMES AS NATURAL NANOPARTICLES FOR DETECTING INFLAMMATORY PROCESSES BY OPTICAL IMAGING 70

6.1. Introduction 70
6.2. Materials and Methods 71

6.3. Results and Discussion 75
6.4. Conclusions 82
6.5. Bibliography 82
CHAPTER 7 . GENERAL DISCUSSION AND CONCLUSIONS 86
7.1 Conclusions 88
7.2 Future research lines derived from this thesis project 88
7.3 Bibliography 89
SCIENTIFIC OUTPUT DERIVED FROM THE THESIS: PUBLISHED AND SUBMITTED CONTENT 91
OTHER RESEARCH MERITS..... 95

LEGEND OF FIGURES AND TABLES

Figure 1.1 Comparative metric scale of nanotechnology, common biomolecules and macro-objects..... 1

Figure 1.2 Schematic representation of the different parts of a liposome. 2

Figure 1.3 Scheme of the biogenesis of exosomes inside a cell. 3

Figure 1.4 Image of a milk exosome by (A) Transmission Electron Microscopy and (B) example of the general molecular structure of an exosome, including some of its most relevant components. 4

Figure 1.5 Main imaging modalities for preclinical and clinical research. 6

Figure 1.6 Cows, goats and sheep are the main sources of animal milk for daily human consumption. 10

Figure 3.1 Qualitative results from *Biophysical procedure*. 25

Figure 3.2 Transmission Electron Microscopy (TEM) images of size exclusion chromatography fractions. 26

Figure 3.3 Transmission Electron Microscopy (TEM) of isolated vesicles. 27

Figure 3.4 Size and concentration evaluation of isolated nanovesicles. 27

Figure 3.5 Identification of exosome protein biomarkers by Western Blot analysis. 28

Figure 3.6 Biochemical profile of plasma samples from control (PBS) and treated (exosomes) mice. 29

Figure 4.1 Chemical optimization of goat milk exosome radiolabeling conditions..... 40

Figure 4.2 Physicochemical characterization of [^{99m}Tc]-Exo. 41

Figure 4.3 Assessment of intravenous administration. 42

Figure 4.4 Intraperitoneal administration. 43

Figure 4.5 Intranasal administration. 44

Figure 5.1 Optical labeling and physicochemical characterization of control and fluorescence-labeled milk exosomes (MiExo). 58

Figure 5.2 Physicochemical characterization of control and fluorescence-labeled cancer cell line-derived exosomes. 59

Figure 5.3 In vitro stability of Bodipy FL-labeled milk exosomes (BDP-MiExo) over time, evaluated with high performance liquid chromatography. 60

Figure 5.4 Confocal microscope imaging for assessing the uptake of sulfo-cyanine 7.5-labeled milk exosomes (SCy-MiExo) by hepatocytes. 61

Figure 6.1 Physicochemical characterization of fluorescent milk exosomes. 76

Figure 6.2 In vitro metabolic activity evaluation with RAW 264.7 cells. 77

Figure 6.3 Assessment of exosome uptake by RAW 264.7 macrophages. 78

Figure 6.4 In vitro evaluation of Exo-BDP uptake in macrophage populations. 79

Figure 6.5 Abdominal in vivo uptake in a mouse peritonitis model. 80

Figure 6.6 Flow cytometry of Exo-SCy5 in exudate neutrophils and macrophages. 81

Figure 6.7 Confocal imaging of cells obtained from FACS and immunostained with specific antibodies. 82

Table 4.1 Summary of pharmacokinetic properties of [^{99m}Tc]-Exo for the different administration routes. 44

Table 5.1 Ex vivo average radiant efficiencies (p/s/cm^2/sr)/(μW/cm^2) of sulfo-cyanine 7.5-labeled milk exosomes (SCy-MiExo) and free SCy 7.5 measured in organs excised at 24 h post-injection. Data are expressed as the mean ± standard deviation..... 63

FUNDING STATEMENT

The work developed in this PhD thesis was framed within several national and international research projects, supported by the following funding:

- Instituto de Salud Carlos III, through the project “PI16/02037”, co-funded by European Regional Development Fund (ERDF), “A way to make Europe”

- Comunidad de Madrid, project “Y2018/NMT-4949 (NanoLiver-CM)” and “S2017/BMD-3867 (RENIM-CM)”, co-funded by European Structural and Investment Fund

During part of the pre-doctoral period (2022 – 2023), the author of this thesis has been also funded by Instituto de Investigación Sanitaria Gregorio Marañón, Intramural Programme for the Promotion of R&D&I 2021, Sub-programme "Pre-doctoral training contract".

CHAPTER 1 . GENERAL INTRODUCTION

1.1. Nanotechnology and biomedicine

The concept of "nanotechnology" was first introduced by physicist and Nobel Laureate Richard Feynman in 1959 [1]. Since then, nanotechnology has been considered as a scientific field that conduces physics, chemistry, biology and technology to the nanometer scale (10^{-9} m), with the aim of producing new small-engineered devices. The underlying idea is to manipulate the structure of a wide variety of materials into new constructions with unique intrinsic properties, depending on their shape, surface, biocompatibility, etc. Thus, nanotechnology has potential applicability in diverse technologies.

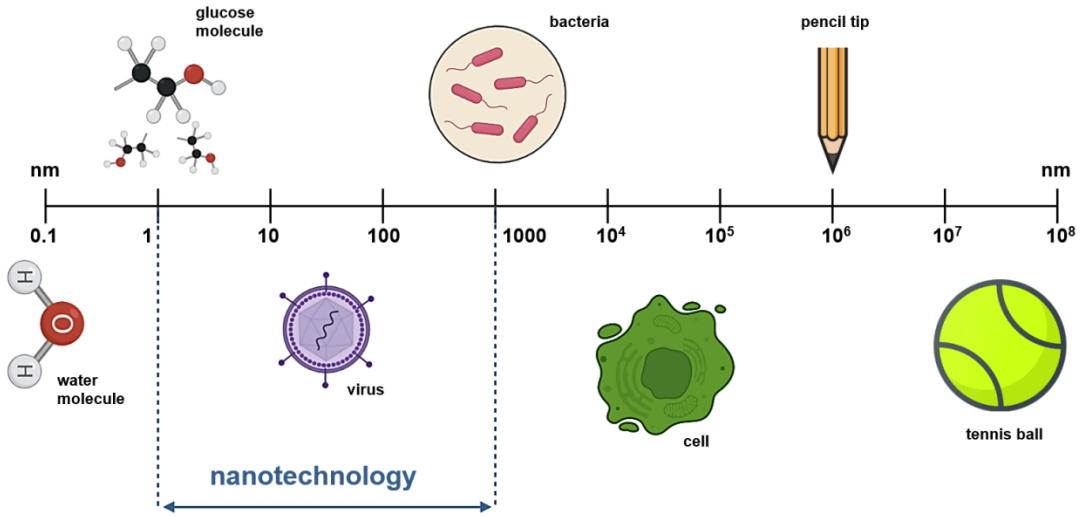

Figure 1.1 Comparative metric scale of nanotechnology, common biomolecules and macro-objects.

Renewable energy and electronics are two of the major beneficiaries of the development of nanotechnology. Nanostructures synthesized from metallic and semiconductor components are currently being exploited to replace some of the materials traditionally used in this field. In its structure, it is worth noting the arrangement of the items forming long surfaces that increase the area of energy conduction [2]. Interestingly, organic materials also have great applicability in electronics. This is the case of graphene, a two-dimensional carbon crystal with a promising future in the design of touch-screens and microchips due to its flexibility, transparency and high electron mobility [3].

Regarding the application of this nanotechnology in the field of biomedicine, researchers have focused their efforts on the development of biocompatible nanoparticles (NPs) for improving current drug delivery and molecular imaging strategies. This is due to the capability of this kind of NPs to incorporate into their structure therapeutic and/or imaging agents, enhancing their solubility, in vivo stability and accumulation in specific biological targets [4]. Even the current pandemic situation

that has taken place during the writing of this thesis (COVID-19) is benefiting from the use of NPs as alternative theranostic (therapeutic + diagnostic) agents [5].

Among the NPs developed, polymeric nanoformulations and lipid-based structures are particularly attractive for offering multiple functionalization possibilities, in addition to demonstrating the efficacy of loading therapeutic agents [4].

Lipid-based nanosystems include liposomes, which are spherical particles composed of self-enclosed lipid bilayers and an aqueous core [6]. This characteristic structure enables hydrophilic, hydrophobic and lipophilic compounds to be encapsulated within it [4]. In addition, size, stability, biocompatibility or ionic charge properties can be modified by surface engineering during or after chemical synthesis [4,6]. Together with the organic character of these NPs, all these features make liposomes excellent carriers of therapeutic compounds, such as anti-tumor drugs, and diagnostic agents, especially for magnetic resonance and nuclear imaging [6,7].

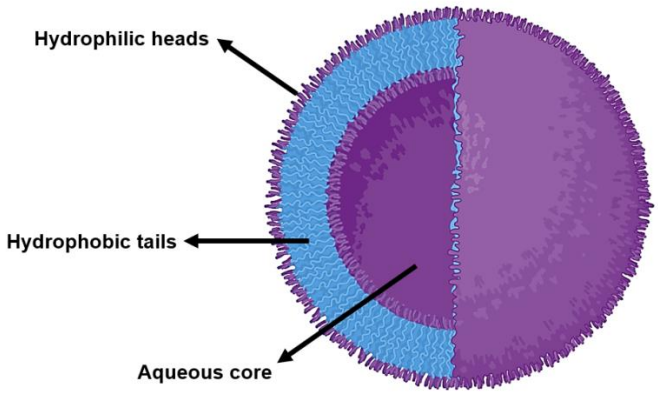

Figure 1.2 Schematic representation of the different parts of a liposome.

Despite the promising results achieved in preclinical research, several limitations hinder the translation of inorganic and lipid-based NPs from bench to clinic, highlighting: (i) low reproducibility, scalable and/or cost-effective production, (ii) poor stability in the bloodstream and (iii) limited biocompatibility and potential toxic profile [7]. In relation to the latter point, ecotoxicology of synthetic nanomaterials is gaining relevance due to the scarcity of information available about their impact in animal/human respiratory health or microenvironments such as seawater [8].

1.2. Exosomes: natural nanoparticles manufactured by cells

Charles Darwin's theory of Pangenesis was not very successful among his successors, but one of the concepts included therein has been rescued by the current literature related to bio-nanotechnology. Darwin hypothesized that cells shed microscopic particles (called “gemmules”) to the bloodstream for the transference of heritable information between generations through the interaction with reproductive cells [9,10]. Years later, scientist confirmed the existence of primitive small phospholipid vesicles released by cells, but categorized them as “platelet dust” [10]. From the mid-1990s to the early 2000s, the concept of phospholipid vesicles was revolutionized under the term

"extracellular vesicles" and several biological roles were associated with these particles [11-14], beyond being the dumpsters of the cells.

Nowadays, it has been established that extracellular vesicles (EVs) constitute a heterogeneous group of particles naturally secreted by most living cell types. The main purpose of the release of these vesicles is the intercellular communication through the encapsulation and transfer of biomolecules such as proteins, lipids, nucleic acids and sugars [15,16]. This process has been evolutionarily conserved not only in animal cells but also in plants and pathogenic and non-pathogenic bacteria [17-19].

The term EVs encompasses several types of vesicles whose specific nomenclature is open to controversy due to the difficulty of classifying them solely by their physicochemical characteristics, biogenesis pathway or biological role. Rose Johnstone established the term "exosomes" a few years after its first association with biological functions [20]. The "Minimal Information for Studies of Extracellular Vesicles (MISEV)" guide, published in 2018 by the International Society of Extracellular Vesicles [21], categorizes exosomes as small EVs originated from late endosomes inside cells.

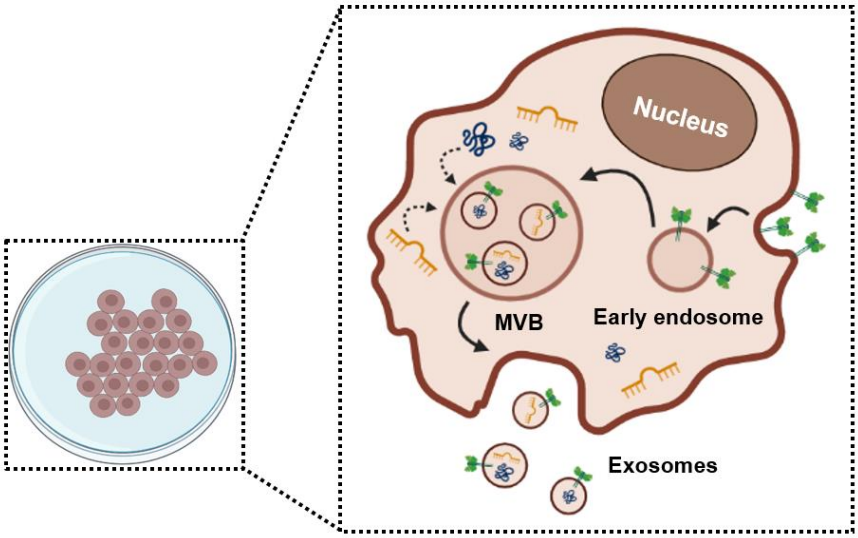

Figure 1.3 Scheme of the biogenesis of exosomes inside a cell.

Early endosomes are formed from the invagination of the cell membrane and accumulate different biological compounds until the mature into multivesicular bodies (MVB). When MVB fuse to the cell membrane, exosomes are released into the biological medium [22].

Other works also suggest that EVs should comply with the following general specifications for being considered as exosomes: size range from 20 to 200 nm [23], phospholipid bilayer membrane [24], cup-shape morphology under electron microscope [24,25], negative surface charge in buffer [26] and membrane biomarkers enriched in HSP70, HSP90, CD63, CD81 or TSG101, among others [17]. However, a consideration to bear in mind is that, due to their intracellular biogenesis, all exosomes have parent-

cell-specific signatures [18] which influence the composition of their surface and also some of their physicochemical properties.

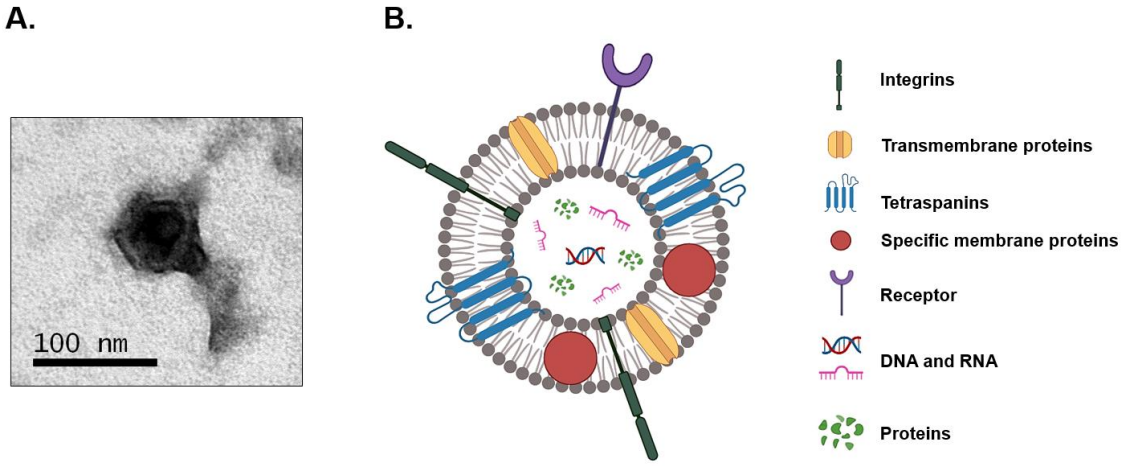

Figure 1.4 Image of a milk exosome by (A) Transmission Electron Microscopy and (B) example of the general molecular structure of an exosome, including some of its most relevant components.

The role of exosomes in cellular communication and bioactive compounds exchange appears to be crucial, contributing both in fundamental biological processes and in the development of some pathologies.

1.3. Role of exosomes in disease progression

Mammalian-derived exosomes are released by cells under normal physiological conditions to mediate several biological processes by the trafficking of bioactive material, from modulating the activity of the cells neighboring the parent cell to neuronal communication, pregnancy or the macrophage polarization during the immune response [24].

However, the role of these exosomes is not always beneficial for the organism, acting in the development and progression of many diseases. For example, exosomes can contribute to neurodegenerative disorders by the transmission of pathogenic proteins between cells [27,28]. The detection of misfolded proteins inside exosomes, associated with the development of Alzheimer's or Parkinson's diseases such as tau or α-synuclein, opens the door not only to study the inhibition of the biological pathway related to exosome secretion but also to the use of these vesicles as biomarkers of disease [29-31].

Exosomes may also promote the spread of infectious agents from virus/bacterial-infected cells [24,32], as result of evading the immune system response through the incorporation of infectious-specific components into the exosomes naturally secreted by infected cells [33]. Viruses such as human immunodeficiency virus (HIV-1) or varicella-zoster virus are capable of altering the protein content of exosomes, of loading histocompatibility complex into their structure, and also of incorporating their own DNA/RNA inside these vesicles [32,33]. Thus, exosomes work as “Trojan horses” in the transmission of infection to healthy host cells, which are unable to distinguish

between normal and pathogenic exosomes. These changes in exosome content are not accidental, as some studies describe that viruses are able to intervene in the endosomal pathway in order to alter the biogenesis of exosomes and thus their composition and secretion [34]. This also occurs in the case of bacterial infections, where a significant increase in exosome release after infection has been demonstrated [35].

However, one of the main lines of study in the area of exosomes is their involvement in oncological processes. The progression of primary tumors is not limited to the aberrant behavior of malignant cancer cells but also to their microenvironment and the cells that compose it, such as fibroblasts, endothelial and stromal cells, or tumor-associated macrophages. This is partly due to the dynamic transference of proteins, lipids and nucleic acids as RNA from tumor to surrounding cells by exosome secretion, at all stages of cancer progression [36]. By this pathway, tumor cells can promote the disruption of endothelial cell barriers, facilitating the angiogenesis and metastatic processes [36], or induce the conversion of healthy stromal cells into cancer-associated fibroblasts which support tumor growth, resistance and spread [36,37]. Modulation of immune response is also influenced by exosomes through the reprogramming of tumor-associated macrophages into its M2 anti-inflammatory and immunosuppressive phenotype [38,39]. Those are just few examples of the key role of exosomes in tumor development, but the underlining message is the strong ability of these vesicles to interact in many biological processes and with cells of different lineage than the parent one.

1.4. Molecular imaging

Imaging techniques are applied in the fields of biomedical research and clinical practice to test novel drugs, elucidate the cause of a disease, determine its stage and severity or follow the disease response to a treatment regimen. Each imaging modality has its own features, varying primarily in terms of sensitivity, spatial and temporal resolution, depth of penetration and imaging characteristics (e.g. dynamic/static, small region/whole subject) [40].

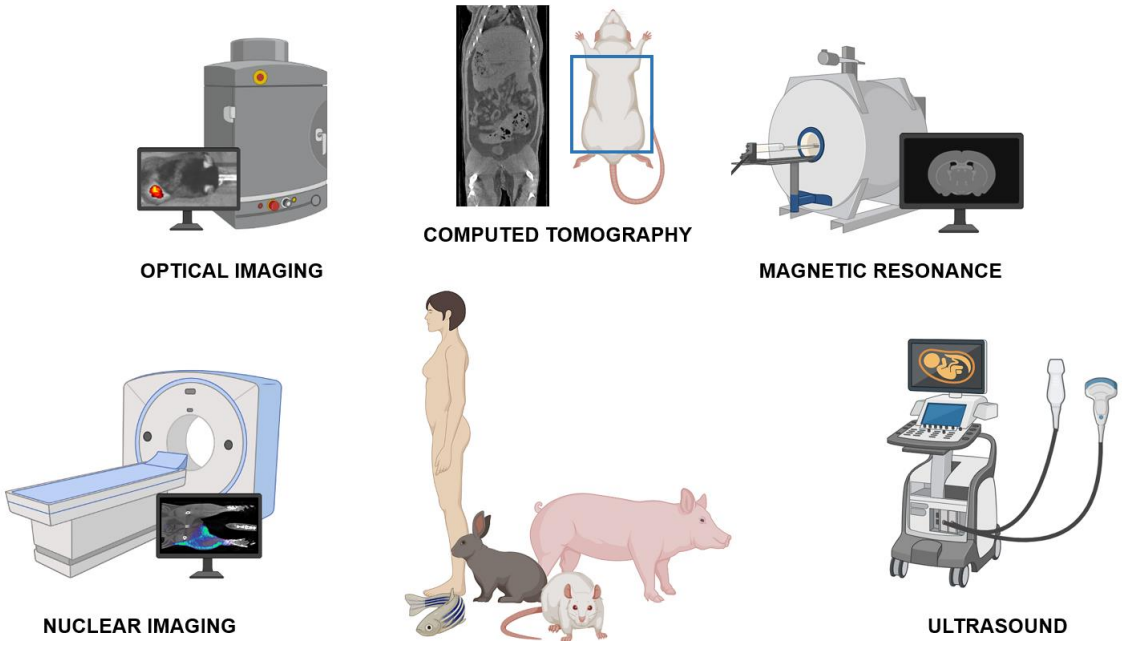

Figure 1.5 Main imaging modalities for preclinical and clinical research.

However, the choice of the most appropriate imaging technique is initially dependent on the data to be collected, in terms of anatomical or functional information.

Molecular (or functional) imaging is defined as the detection and visualization of certain biological processes and pathways in living organisms at the cellular and molecular level. Imaging techniques encompassed in this concept move into the chemical, metabolic, cellular and tissue level to provide functional information under non-invasive conditions, enabling the real-time evaluation of cellular and pathophysiological processes in living subjects [41]. Among the various imaging techniques included in this category, optical and nuclear imaging stand out as those with better preclinical application and clinical transfer.

1.4.1. Optical imaging

Optical imaging is widely used for cellular assays, but is also gaining relevance in small animal preclinical research. The advantages of optical imaging lie in its high sensitivity, cost-effectiveness and safety, due to the use of light instead of ionizing radiation for imaging molecular and cellular processes [42]. This modality includes bioluminescence and fluorescence.

In the case of bioluminescence, the light arises as a result of the oxidation reaction between a substrate (luciferin) and an enzyme (luciferase), which produces the emission of photons [40]. Cells and tissues do not emit endogenous bioluminescence, so the main advantage of this technique is the absence of background signal or "auto-bioluminiscence" [40]. Several pathological processes can be evaluated at molecular stages using bioluminescence imaging, including cancer biology. However, the use of bioluminescence has been limited to the preclinical field because of problems derived from light propagation in living tissues and the substrate-enzyme reaction requirements [40,42].

In the case of fluorescence, it is necessary to illuminate the sample under study with a laser, enabling the absorption of energy and the emission of light. Thus, image acquisition requires the use of a fluorescent probe, such as commercial fluorophores or dyes. These offer a wide variety of labeling possibilities, enabling us to improve the imaging resolution and depths. The main drawback of this modality is the natural in vivo absorption of light by some tissues and biomolecules, such as hemoglobin, which results in a significant background signal that may limit the detection of the process to be detected [40]. This phenomenon, called "autofluorescence", can be attenuated by the use of near-infrared (650 - 900 nm) fluorescent agents, which avoids the background signal of endogenous molecules and tissues [43] and provide deeper tissue penetration. The development of near-infrared fluorescence has enabled the transference of optical imaging from in vitro and preclinical assays to clinical applications, such as fluorescence-guided surgery [44].

1.4.2. Nuclear imaging

Nuclear imaging is based on the detection of the radiation emitted by a radioisotope or radionuclide, which enables imaging biochemical processes, molecular targets or pathogens in living subjects. This modality includes Positron Emission Tomography (PET) and Single-Photon Emission Computed Tomography (SPECT), and the choice between them depends mainly on the physics of the radiation emitter. Both techniques present limitless depth of tissue penetration and enable two- or three-dimensional imaging with high sensitivity, as well as the quantification of the registered radioactive signal [45,46]. These features have facilitated the successful translation of nuclear medicine to the clinic, although its ionizing nature limits the number of scans enabled per individual and year [40].

Both PET and SPECT require the administration to the subject of an imaging agent called radiotracer. A radiotracer is composed by a biological element and a radioisotope. The first is the active part of the tracer, able to bind or detect with high specificity and affinity the evaluated biological target. Thus, biocompounds selected are usually antibodies or small organic molecules, such as amino acids or peptides [45]. The radioisotope is the part which, thanks to the emission of ionizing radiation, can be detected by PET or SPECT. It is a prerequisite that it can be conjugated to the biological agent without altering its inherent functionality.

Since these nuclear imaging techniques only provide functional information regarding metabolic pathways and biochemical processes, the complementary use of structural techniques is necessary for the anatomical localization of the pathology or target. PET and SPECT are normally combined with X-Ray Computed Tomography (CT), which enables the precise correlation between the functional data achieved from nuclear imaging and the anatomical characteristics of the event under evaluation [40]. This approach is known as "multimodality imaging".

1.5. Milk exosomes as natural liposome-like nanoparticles for biomedical imaging

Molecular imaging techniques described above have in common the need to use imaging agents, either to obtain the desired functional information or to improve the image acquisition characteristics.

NPs have been widely used as contrast agents for the study of disease development at the preclinical level. Compared to traditional molecular probes, NPs offer intrinsic magnetic and optical properties which can be exploited in various imaging modalities. In addition, the controlled variation of their physicochemical and surface properties enables to easily improve their specificity and circulation time in blood, as well as the design of multifunctional nanostructures [47]. Iron oxide NPs as contrast agents for MRI or fluorescent quantum dots for optical imaging are two examples of NPs whose raw material enables them to be used in molecular imaging. However, several limitations mainly associated with their synthesis, toxicity and long-term stability hinder the NPs translation to clinical diagnostics [47].

As described up to this point of this thesis, the physicochemical features of exosomes together with their assumed biocompatibility and intrinsic biological role in disease development postulate them as candidates to replace synthetic liposomes and lipid-based NPs in biomedical imaging, both in preclinical and clinical applications. Although exosomes do not have any component with imaging properties in their composition, they can be labeled with fluorescent or radioactive agents, or encapsulate cores of optically/magnetically active materials in order to overcome their limitations, as was ideally intended with lipid-based NPs [48].

Because all cells produce exosomes, and their intrinsic characteristics and biological role strongly depend on the parental cell, the choice of the type of exosome as a therapeutic/diagnostic nanoplatform will vary depending on its specific application.

At the therapeutic level, there is a growing interest in the potential use of exosomes in regenerative medicine and modulation of the immune response, with at least 11 studies presently registered in the clinicaltrials.gov repository in recruitment or completed status. All of them have in common the election of mesenchymal cell-derived exosomes for different purposes, such as inflammatory modulation after viral infection, assessment of tumor response to exosome administration or tissue regeneration (lung or brain) after acute damage, including treatments for SARS-CoV-2 [49-51]. However, one of the main drawbacks of employing exosomes isolated from cell culture is their low production yield and scalability, hindering their translation to clinical use [52].

Thinking about cancer cell-derived exosomes for biomedical purposes due to their strong involvement in the development of the disease, controversy arises due to their potential applications as well as their possible secondary effects. Although their use as anti-tumor immune response stimulators has been suggested, it has also been demonstrated that cancer cell-derived exosomes can promote adverse effects that may favor tumor development [53]. Thus, it seems more interesting to design imaging tools

based on tumor exosomes to fully characterize their role in the development of cancer instead of considering their directly use as an imaging/therapeutic platform.

Focusing on the use of exosomes as medical imaging or therapeutic NPs, these vesicles should meet the following requirements: i) resistance to conditions different from those of their natural biological environment (necessary not to be destroyed during chemical treatments), ii) non-toxicity or immunogenicity and iii) high availability and the possibility of scalable isolation. Consequently, exosomes contained in food products, such as plants, fruits or milk, have attracted scientific interest because of accomplishing these characteristics. Research lines involving food-contained exosomes summarized that these vesicles can join the bloodstream of an individual after oral ingestion and deliver their cargo to distal organs, resisting to the harsh digestion conditions [54]. In addition, some natural therapeutic effects have been associated with food-derived exosomes, such as the modulation of the anti-inflammatory response by grape berry, curcumin and ginger derived exosomes [54].

One of the most studied populations of food-derived vesicles is milk exosomes due to the high consumption of milk from animal origin by adult humans and its proven fundamental role in the maturation of the infant immune system. Milk exosomes are secreted by some of the cells that compose the mammary glands, such as macrophages, lymphocytes, and epithelial and mammary stem cells [55,56]. Once included in milk, exosomes are incorporated into the circulatory system of the consuming organism after being orally ingested and absorbed in the intestine.

Depending on the origin of the milk (human or animal), the health of the producing organism and the lactation period, the milk exosomes cargo and functionality may vary [55]. Nevertheless, the biological role of milk exosomes is mainly related to the maturation and growth of digestive system [57], and the regulation of the inflammation response and infant immune system, including strong interaction with cells from these biological environments [54,57]. In this regard, several publications have also reported the protective and anti-inflammatory effect of milk extracellular vesicles in pathologies such as colitis or osteoarthritis [58,59].

Among the different milk sources, human and bovine milks are the most exploited in the field of the extracellular vesicles research [60]. However, goat milk is also one of the most consumed milks by humans and is gaining relevance in recent years due to the demonstrated enrichment of its exosomes in immunomodulatory metabolites [61], as well as the excellent capacity of these nanovesicles to encapsulate chemotherapeutic drugs compared to other milk exosomes [62]. Nevertheless, these findings have been reported so recently and few literature about goat milk exosomes has been reported to date.

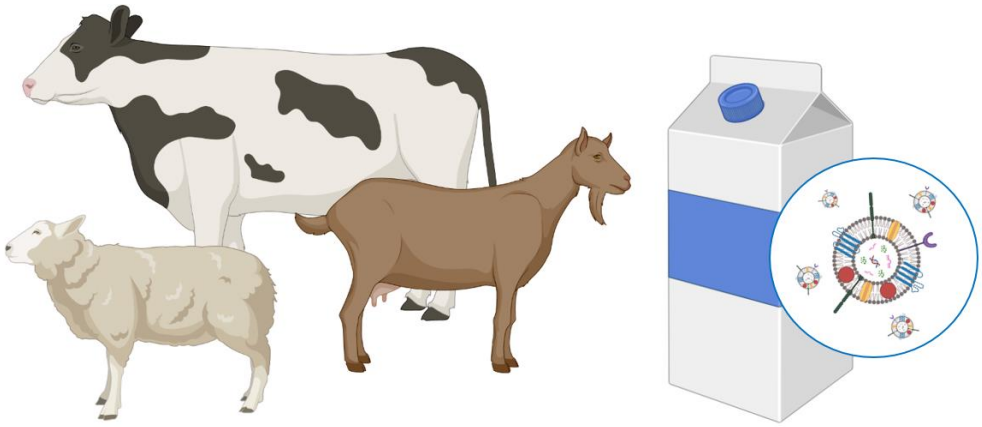

Figure 1.6 Cows, goats and sheep are the main sources of animal milk for daily human consumption.

Altogether, the resistance of milk exosomes to harsh conditions such as low pH (in the digestive system [63]) or extreme temperature changes (in the pasteurization process in the case of commercial milk [64]), together with their cross-species tolerance, their high availability and their apparently non-pathogenic/protective biological role, support their potential use as substitutes of lipid-based NPs in the development of natural exosome-based probes for biomedical imaging.

1.6. Bibliography

1. Bayda, S.; Adeel, M.; Tuccinardi, T.; Cordani, M.; Rizzolio, F. The history of nanoscience and nanotechnology: from chemical–physical applications to nanomedicine. *Molecules* 2020, *25*, p 112.
2. Cheng, H.; Doemeny, L.J.; Geraci, C.L.; Grob Schmidt, D. Nanotechnology overview: Opportunities and challenges. In *Nanotechnology: Delivering on the Promise Volume 1*, *ACS Publications* 2016, pp. 1-12.
3. 15 years of graphene electronics. *Nature Electronics* 2019, *2*, pp 369-369.
4. Mitchell, M.J.; Billingsley, M.M.; Haley, R.M.; Wechsler, M.E.; Peppas, N.A.; Langer, R. Engineering precision nanoparticles for drug delivery. *Nature Reviews Drug Discovery* 2021, *20*, pp 101-124.
5. Peplow, M. Nanotechnology offers alternative ways to fight COVID-19 pandemic with antivirals. *Nature biotechnology* 2021, *39*, pp 1172-1174.
6. Torchilin, V.P. Recent advances with liposomes as pharmaceutical carriers. *Nature reviews Drug discovery* 2005, *4*, pp 145-160.
7. van der Meel, R.; Sulheim, E.; Shi, Y.; Kiessling, F.; Mulder, W.J.; Lammers, T. Smart cancer nanomedicine. *Nature nanotechnology* 2019, *14*, pp 1007-1017.
8. Handy, R.D.; Von der Kammer, F.; Lead, J.R.; Hassellöv, M.; Owen, R.; Crane, M. The ecotoxicology and chemistry of manufactured nanoparticles. *Ecotoxicology* 2008, *17*, pp 287-314.
9. Aucamp, J.; Bronkhorst, A.J.; Badenhorst, C.P.; Pretorius, P.J. A historical and evolutionary perspective on the biological significance of circulating DNA and extracellular vesicles. *Cellular and Molecular Life Sciences* 2016, *73*, pp 4355-4381.
10. Margolis, L.; Sadovsky, Y. The biology of extracellular vesicles: The known unknowns. *PLoS biology* 2019, *17*, p e3000363.

11. Bonucci, E. Fine structure and histochemistry of "calcifying globules" in epiphyseal cartilage. *Zeitschrift für Zellforschung und Mikroskopische Anatomie* 1970, *103*, pp 192-217.
12. Johnstone, R.M.; Adam, M.; Hammond, J.; Orr, L.; Turbide, C. Vesicle formation during reticulocyte maturation. Association of plasma membrane activities with released vesicles (exosomes). *Journal of Biological Chemistry* 1987, *262*, pp 9412-9420.
13. Raposo, G.; Nijman, H.W.; Stoorvogel, W.; Liejendekker, R.; Harding, C.V.; Melief, C.; Geuze, H.J. B lymphocytes secrete antigen-presenting vesicles. *Journal of Experimental Medicine* 1996, *183*, pp 1161-1172.
14. Ratajczak, J.; Wysoczynski, M.; Hayek, F.; Janowska-Wieczorek, A.; Ratajczak, M. Membrane-derived microvesicles: important and underappreciated mediators of cell-to-cell communication. *Leukemia* 2006, *20*, pp 1487-1495.
15. Yáñez-Mó, M.; Siljander, P.R.-M.; Andreu, Z.; Bedina Zavec, A.; Borràs, F.E.; Buzas, E.I.; Buzas, K.; Casal, E.; Cappello, F.; Carvalho, J. Biological properties of extracellular vesicles and their physiological functions. *Journal of extracellular vesicles* 2015, *4*, p 27066.
16. Soekmadji, C.; Li, B.; Huang, Y.; Wang, H.; An, T.; Liu, C.; Pan, W.; Chen, J.; Cheung, L.; Falcon-Perez, J.M. The future of Extracellular Vesicles as Theranostics–an ISEV meeting report. Taylor & Francis: 2020.
17. Zhang, Y.; Bi, J.; Huang, J.; Tang, Y.; Du, S.; Li, P. Exosome: a review of its classification, isolation techniques, storage, diagnostic and targeted therapy applications. *International journal of nanomedicine* 2020, *15*, p 6917.
18. Herrmann, I.K.; Wood, M.J.A.; Fuhrmann, G. Extracellular vesicles as a next-generation drug delivery platform. *Nature nanotechnology* 2021, *16*, pp 748-759.
19. Bose, S.; Aggarwal, S.; Singh, D.V.; Acharya, N. Extracellular vesicles: An emerging platform in gram-positive bacteria. *Microbial Cell* 2020, *7*, p 312.
20. Harding, C.V.; Heuser, J.E.; Stahl, P.D. Exosomes: looking back three decades and into the future. *The Journal of cell biology* 2013, *200*, p 367.
21. Théry, C.; Witwer, K.W.; Aikawa, E.; Alcaraz, M.J.; Anderson, J.D.; Andriantsitohaina, R.; Antoniou, A.; Arab, T.; Archer, F.; Atkin-Smith, G.K. Minimal information for studies of extracellular vesicles 2018 (MISEV2018): a position statement of the International Society for Extracellular Vesicles and update of the MISEV2014 guidelines. *Journal of extracellular vesicles* 2018, *7*, p 1535750.
22. Hessvik, N.P.; Llorente, A. Current knowledge on exosome biogenesis and release. *Cellular and Molecular Life Sciences* 2018, *75*, pp 193-208.
23. Abels, E.R.; Breakefield, X.O. Introduction to extracellular vesicles: biogenesis, RNA cargo selection, content, release, and uptake. *Cellular and molecular neurobiology* 2016, *36*, pp 301-312.
24. He, C.; Zheng, S.; Luo, Y.; Wang, B. Exosome theranostics: biology and translational medicine. *Theranostics* 2018, *8*, p 237.
25. Sedykh, S.E.; Burkova, E.E.; Purvinsh, L.V.; Klemeshova, D.A.; Ryabchikova, E.I.; Nevinsky, G.A. Milk exosomes: Isolation, biochemistry, morphology, and perspectives of use. *Extracellular Vesicles and Their Importance in Human Health* 2020, pp 1-28.
26. Beit-Yannai, E.; Tabak, S.; Stamer, W.D. Physical exosome: exosome interactions. *Journal of cellular and molecular medicine* 2018, *22*, pp 2001-2006.

27. Guo, J.L.; Lee, V.M. Cell-to-cell transmission of pathogenic proteins in neurodegenerative diseases. *Nature medicine* 2014, *20*, pp 130-138.
28. Bellingham, S.A.; Guo, B.; Coleman, B.; Hill, A.F. Exosomes: vehicles for the transfer of toxic proteins associated with neurodegenerative diseases? *Frontiers in physiology* 2012, *3*, p 124.
29. Asai, H.; Ikezu, S.; Tsunoda, S.; Medalla, M.; Luebke, J.; Haydar, T.; Wolozin, B.; Butovsky, O.; Kügler, S.; Ikezu, T. Depletion of microglia and inhibition of exosome synthesis halt tau propagation. *Nature neuroscience* 2015, *18*, pp 1584-1593.
30. Cerri, S.; Ghezzi, C.; Sampieri, M.; Siani, F.; Avenali, M.; Dornini, G.; Zangaglia, R.; Minafra, B.; Blandini, F. The exosomal/total α-synuclein ratio in plasma is associated with glucocerebrosidase activity and correlates with measures of disease severity in PD patients. *Frontiers in cellular neuroscience* 2018, *12*, p 125.
31. Danzer, K.M.; Kranich, L.R.; Ruf, W.P.; Cagsal-Getkin, O.; Winslow, A.R.; Zhu, L.; Vanderburg, C.R.; McLean, P.J. Exosomal cell-to-cell transmission of alpha synuclein oligomers. *Molecular neurodegeneration* 2012, *7*, pp 1-18.
32. Khan, G.; Ahmed, W.; Philip, P.S. Exosomes and their role in viral infections. *Novel Implications of Exosomes in Diagnosis and Treatment of Cancer and Infectious Diseases* 2017, pp 76-95.
33. Sampey, G.C.; Meyering, S.S.; Zadeh, M.A.; Saifuddin, M.; Hakami, R.M.; Kashanchi, F. Exosomes and their role in CNS viral infections. *Journal of neurovirology* 2014, *20*, pp 199-208.
34. Jia, X.; Yin, Y.; Chen, Y.; Mao, L. The Role of Viral Proteins in the Regulation of Exosomes Biogenesis. *Frontiers in Cellular and Infection Microbiology* 2021, *11*, p 422.
35. Zhang, W.; Jiang, X.; Bao, J.; Wang, Y.; Liu, H.; Tang, L. Exosomes in pathogen infections: a bridge to deliver molecules and link functions. *Frontiers in immunology* 2018, *9*, p 90.
36. Li, I.; Nabet, B.Y. Exosomes in the tumor microenvironment as mediators of cancer therapy resistance. *Molecular cancer* 2019, *18*, pp 1-10.
37. Tung, K.H.; Ernstoff, M.S.; Allen, C.; La Shu, S. A Review of Exosomes and their Role in The Tumor Microenvironment and Host–Tumor "Macroenvironment". *Journal of immunological sciences* 2019, *3*, p 4.
38. da Cunha, B.R.; Domingos, C.; Stefanini, A.C.B.; Henrique, T.; Polachini, G.M.; Castelo-Branco, P.; Tajara, E.H. Cellular interactions in the tumor microenvironment: the role of secretome. *Journal of Cancer* 2019, *10*, p 4574.
39. Su, M.-J.; Aldawsari, H.; Amiji, M. Pancreatic cancer cell exosome-mediated macrophage reprogramming and the role of microRNAs 155 and 125b2 transfection using nanoparticle delivery systems. *Scientific reports* 2016, *6*, pp 1-15.
40. James, M.L.; Gambhir, S.S. A molecular imaging primer: modalities, imaging agents, and applications. *Physiological reviews* 2012, *92*, pp 897-965.
41. Pysz, M.A.; Gambhir, S.S.; Willmann, J.K. Molecular imaging: current status and emerging strategies. *Clinical radiology* 2010, *65*, pp 500-516.
42. Arranz, A.; Ripoll, J. Advances in optical imaging for pharmacological studies. *Frontiers in pharmacology* 2015, *6*, p 189.
43. Jaffer, F.A.; Weissleder, R. Molecular imaging in the clinical arena. *Jama* 2005, *293*, pp 855-862.

44. Nagaya, T.; Nakamura, Y.A.; Choyke, P.L.; Kobayashi, H. Fluorescence-guided surgery. *Frontiers in oncology* 2017, *7*, p 314.
45. Graham, M.M. Clinical molecular imaging with radiotracers: current status. *Medical Principles and Practice* 2012, *21*, pp 197-208.
46. Chen, Z.-Y.; Wang, Y.-X.; Lin, Y.; Zhang, J.-S.; Yang, F.; Zhou, Q.-L.; Liao, Y.-Y. Advance of molecular imaging technology and targeted imaging agent in imaging and therapy. *BioMed research international* 2014, *2014*.
47. Kim, J.; Lee, N.; Hyeon, T. Recent development of nanoparticles for molecular imaging. *Philosophical Transactions of the Royal Society A: Mathematical, Physical and Engineering Sciences* 2017, *375*, p 20170022.
48. Mirahadi, M.; Ghanbarzadeh, S.; Ghorbani, M.; Gholizadeh, A.; Hamishehkar, H. A review on the role of lipid-based nanoparticles in medical diagnosis and imaging. *Therapeutic delivery* 2018, *9*, pp 557-569.
49. Sarvar, D.P.; Shamsasenjan, K.; Akbarzadehlaleh, P. Mesenchymal stem cell-derived exosomes: new opportunity in cell-free therapy. *Advanced pharmaceutical bulletin* 2016, *6*, p 293.
50. Shi, L.; Huang, H.; Lu, X.; Yan, X.; Jiang, X.; Xu, R.; Wang, S.; Zhang, C.; Yuan, X.; Xu, Z. Effect of human umbilical cord-derived mesenchymal stem cells on lung damage in severe COVID-19 patients: a randomized, double-blind, placebo-controlled phase 2 trial. *Signal transduction and targeted therapy* 2021, *6*, pp 1-9.
51. Sengupta, V.; Sengupta, S.; Lazo, A.; Woods, P.; Nolan, A.; Bremer, N. Exosomes derived from bone marrow mesenchymal stem cells as treatment for severe COVID-19. *Stem cells and development* 2020, *29*, pp 747-754.
52. Gowen, A.; Shahjin, F.; Chand, S.; Odegaard, K.E.; Yelamanchili, S.V. Mesenchymal stem cell-derived extracellular vesicles: challenges in clinical applications. *Frontiers in cell and developmental biology* 2020, *8*, p 149.
53. Batrakova, E.V.; Kim, M.S. Using exosomes, naturally-equipped nanocarriers, for drug delivery. *Journal of Controlled Release* 2015, *219*, pp 396-405.
54. Munir, J.; Lee, M.; Ryu, S. Exosomes in food: Health benefits and clinical relevance in diseases. *Advances in Nutrition* 2020, *11*, pp 687-696.
55. Sanwlani, R.; Fonseka, P.; Chitti, S.V.; Mathivanan, S. Milk-derived extracellular vesicles in inter-organism, cross-species communication and drug delivery. *Proteomes* 2020, *8*, p 11.
56. Admyre, C.; Johansson, S.M.; Qazi, K.R.; Filén, J.-J.; Lahesmaa, R.; Norman, M.; Neve, E.P.; Scheynius, A.; Gabrielsson, S. Exosomes with immune modulatory features are present in human breast milk. *The Journal of immunology* 2007, *179*, pp 1969-1978.
57. de la Torre Gomez, C.; Goreham, R.V.; Bech Serra, J.J.; Nann, T.; Kussmann, M. "Exosomics"—A review of biophysics, biology and biochemistry of exosomes with a focus on human breast milk. *Frontiers in genetics* 2018, *9*, p 92.
58. Du, C.; Wang, K.; Zhao, Y.; Nan, X.; Chen, R.; Quan, S.; Xiong, B. Supplementation with Milk-Derived Extracellular Vesicles Shapes the Gut Microbiota and Regulates the Transcriptomic Landscape in Experimental Colitis. *Nutrients* 2022, *14*, p 1808.
59. Pieters, B.C.; Arntz, O.J.; Aarts, J.; Feitsma, A.L.; van Neerven, R.J.; van der Kraan, P.M.; Oliveira, M.C.; van de Loo, F.A. Bovine milk-derived extracellular vesicles inhibit catabolic and inflammatory processes in cartilage from

osteoarthritis patients. *Molecular Nutrition & Food Research* 2022, *66*, p 2100764.

60. Adriano, B.; Cotto, N.M.; Chauhan, N.; Jaggi, M.; Chauhan, S.C.; Yallapu, M.M. Milk exosomes: nature's abundant nanoplatform for theranostic applications. *Bioactive materials* 2021, *6*, pp 2479-2490.
61. Mecocci, S.; Gevi, F.; Pietrucci, D.; Cavinato, L.; Luly, F.R.; Pascucci, L.; Petrini, S.; Ascenzioni, F.; Zolla, L.; Chillemi, G. Anti-Inflammatory Potential of Cow, Donkey and Goat Milk Extracellular Vesicles as Revealed by Metabolomic Profile. *Nutrients* 2020, *12*, p 2908.
62. Ahmed, F.; Tamma, M.; Pathigadapa, U.; Reddanna, P.; Yenuganti, V.R. Drug Loading and Functional Efficacy of Cow, Buffalo, and Goat Milk-Derived Exosomes: A Comparative Study. *Molecular Pharmaceutics* 2022, *19*, pp 763-774.
63. Liao, Y.; Du, X.; Li, J.; Lönnerdal, B. Human milk exosomes and their microRNAs survive digestion in vitro and are taken up by human intestinal cells. *Molecular nutrition & food research* 2017, *61*, p 1700082.
64. Golan-Gerstl, R.; Elbaum Shiff, Y.; Moshayoff, V.; Schecter, D.; Leshkowitz, D.; Reif, S. Characterization and biological function of milk-derived miRNAs. *Molecular nutrition & food research* 2017, *61*, p 1700009.

CHAPTER 2 . MOTIVATION AND OBJECTIVES

The unique physicochemical and optical properties of synthetic nanoparticles as well as their multiple functionalization options have significantly increased their applicability in the field of biomedicine in recent years. Lipid-based nanoparticles, such as liposomes, are of particular interest as diagnostic agents and drug transporters. However, the limitations associated with these nanoformulations, such as low biocompatibility, lack of batch-to-batch reproducibility and potential toxicity, among others, hinder their translation to the clinic.

Milk exosomes are presented as a potential alternative to lipid-based nanoparticles due to their natural origin, expected non-toxicity and similar physicochemical properties. In this sense, their lipid bilayer composition enables the loading of several molecules within their structure [1] and the nanometric size facilitates their passive accumulation in biological targets with associated angiogenic development, based on the enhanced permeability and retention (EPR) effect, especially in tumor tissues [2]. In addition, the relationship between exosomes derived from different milk sources and the immune response has been established at a preclinical level, concluding the preventive and immunomodulatory effect of these nanovesicles against inflammatory processes [3-5]. This could support the natural vectorization of milk exosomes towards inflammatory foci or biological sites where immune response has been activated.

Based on the properties described above, exosomes are postulated as promising platforms for the development of imaging agents, with particular interest in the areas of inflammation/immunology and cancer. Goat milk was selected in this thesis because of the limited information on its exosomes compared to other milk sources, thus bringing an additional novelty character to this project. Although characterization techniques such as immunoblot analysis, RNA content evaluation, mass spectrometry or metabolomics are necessary to establish the basis of the biological behavior of exosomas before their clinical translation [6-8], the invasive nature of all of them implies the destruction of the nanovesicles, limiting the number of samples to be analyzed. Thus, biomedical imaging techniques emerge as a highly useful tool, enabling not only a more in-depth study of the pharmacokinetic properties of exosomes in a non-invasive manner, but also to evaluate their promising applications in the diagnosis of inflammation-related processes.

Optical imaging, especially in the near-infrared range, is very useful for the real-time tracking of exosomes in small mice [9] and the in vitro uptake assessment of these nanovesicles by different cell populations, supported by the cost-effectiveness and the usual availability of equipment in laboratory facilities [10,11]. However, current labeling methods, based on genetic engineering or the incorporation of fluorescent probes to the exosomes structure by encapsulation or membrane integration, assume an uncontrolled labeling of the vesicles, a modification of the exosome surface and an unintended release of the fluorescent agent due to the low stability of the probe [11,12].

As an alternative to optical imaging, especially for in vivo applications, several publications have also assessed the labeling of exosomes with radioactive isotopes for both PET and SPECT imaging. Technetium-99, ^{99m}Tc, is one of the most employed, and its incorporation into the exosome structure involves the binding of ^{99m}Tc complexes to surface proteins [13,14] or the intraluminal entrapment of ^{99m}Tc after crossing the exosome lipid membrane [15]. These approaches imply sensitive chemical conditions, the modification of membrane proteins (in case of surface radiolabeling) and the low stable incorporation of the isotope in the exosomal nucleus (in case of intraluminal radiolabeling) [10].

2.1. Objectives

The main objective of this PhD thesis is to develop milk exosome-based probes and evaluate their potential application as natural nanoplatforms for the diagnosis of several pathologies by medical imaging. To achieve this aim, the thesis project is divided into the following specific objectives:

1. To define an optimal protocol for the isolation and purification exosomes from goat milk exosomes, presenting a complete characterization of the collected nanovesicles.
2. To design radioactive and fluorescent labeling strategies for developing exosome-based nanoprobes, solving the drawbacks associated to current protocols.
3. To evaluate the in vivo pharmacokinetics and biodistribution properties of the exosome-based probes in healthy mice, for assessing their natural behavior.
4. To investigate the ability of the exosome-based probes for detecting inflammatory processes underlying pathologies, as potential diagnostic tools.

2.2. Scientific contributions

This thesis is part of the research line focused on the development of molecular probes of the Biomedical Imaging and Instrumentation Group (BiiG) of the Instituto de Investigación Sanitaria Gregorio Marañón (IiSGM).The results achieved from this thesis may establish the basis of the natural behavior of goat milk exosomes as probes for medical imaging, facilitating future research lines based on their evaluation in other pathologies related to inflammatory processes and on the customization of the exosome surface to improve their pharmacokinetic properties and their directionality towards certain therapeutic targets.

At the overall level, this thesis aims to offer exosome labeling alternatives to those currently employed, which will enhance their research as diagnostic tools for medical imaging but also for improving the knowledge on their pharmacokinetics, cell interaction and effectiveness for future clinical applications.

2.3. Outline of the document

This PhD thesis is based on four research articles, already published or under preparation. In case of published works, they have been included in this thesis as they were published, with minor modifications.

Chapter 1 compiles an overview of the state of the art in the field of nanotechnology applied to biomedicine as well as a general description of exosomes and their potential use as natural nanoparticles for molecular imaging. **Chapter 2** summarizes the motivation and objectives of this thesis. **Chapter 3** presents an innovative methodology for the isolation of exosomes from commercial goat milk and contents a complete physicochemical and biological characterization of these nanovesicles, based on the paper M.I. González, A. Santos-Coquillat, et al. *Goat Milk Exosomes As Natural Nanoparticles for Detecting Inflammatory Processes By Optical Imaging* (Small, 2021). **Chapter 4** describes a novel strategy for the labeling of exosomes with the radioisotope Technetium-99, ^{99m}Tc, based on the paper M.I. González et al. *Radioactive Labeling of Milk-Derived Exosomes with ^{99m}Tc and In Vivo Tracking by SPECT Imaging* (Nanomaterials, 2020). This approach has enabled us to evaluate the pharmacokinetics and biodistribution of exosomes in healthy mice by SPECT/CT imaging, comparing three different routes of administration. **Chapter 5** proposes an easy and straightforward approach for the fluorescent labeling of exosomes by the covalent biding between the nanovesicle surface and commercial fluorophores, based on the paper M.I. González et al. *Covalently Labeled Fluorescent Exosomes for In Vitro and In Vivo Applications (*Biomedicines, 2021). The resultant nanoprobes were validated both in vitro and in vivo. **Chapter 6** evaluates the applicability of the fluorescent nanoprobe developed in the previous chapter as diagnostic tool, based on the paper M.I. González, A. Santos-Coquillat, et al. *Goat Milk Exosomes As Natural Nanoparticles for Detecting Inflammatory Processes By Optical Imaging* (Small, 2021). To this end, the ability of fluorescent milk exosomes to detect inflammatory processes underlying disease was assessed in vitro in macrophages populations and in vivo in a peritonitis mouse model. Finally, **Chapter 7** summarizes a general discussion and conclusions of the thesis project.

Additionally, scientific output derived from this thesis and other research merits have been detailed at the end of the document.

Regarding the design of the figures presented in this thesis, the following ones from Chapter 1 have been totally or partially created with BioRender.com: Figure 1.1, Figure 1.2, Figure 1.3, Figure 1.4, Figure 1.5 and Figure 1.6.

2.4 Bibliography

1. Munagala, R.; Aqil, F.; Jeyabalan, J.; Gupta, R.C. Bovine milk-derived exosomes for drug delivery. *Cancer letters* 2016, *371*, pp 48-61.
2. Bazak, R.; Houri, M.; El Achy, S.; Hussein, W.; Refaat, T. Passive targeting of nanoparticles to cancer: A comprehensive review of the literature. *Molecular and clinical oncology* 2014, *2*, pp 904-908.

3. Benmoussa, A.; Diallo, I.; Salem, M.; Michel, S.; Gilbert, C.; Sévigny, J.; Provost, P. Concentrates of two subsets of extracellular vesicles from cow's milk modulate symptoms and inflammation in experimental colitis. *Scientific reports* 2019, *9*, pp 1-16.
4. Stremmel, W.; Weiskirchen, R.; Melnik, B.C. Milk exosomes prevent intestinal inflammation in a genetic mouse model of ulcerative colitis: A pilot experiment. *Inflammatory Intestinal Diseases* 2020, *5*, pp 117-123.
5. El-Kattawy, A.M.; Algezawy, O.; Alfaifi, M.Y.; Noseer, E.A.; Hawsawi, Y.M.; Alzahrani, O.R.; Algarni, A.; Kahilo, K.A.; El-Magd, M.A. Therapeutic potential of camel milk exosomes against HepaRG cells with potent apoptotic, anti-inflammatory, and anti-angiogenesis effects for colostrum exosomes. *Biomedicine & Pharmacotherapy* 2021, *143*, p 112220.
6. Ahmed, F.; Tamma, M.; Pathigadapa, U.; Reddanna, P.; Yenuganti, V.R. Drug Loading and Functional Efficacy of Cow, Buffalo, and Goat Milk-Derived Exosomes: A Comparative Study. *Molecular Pharmaceutics* 2022, *19*, pp 763-774.
7. Admyre, C.; Johansson, S.M.; Qazi, K.R.; Filén, J.-J.; Lahesmaa, R.; Norman, M.; Neve, E.P.; Scheynius, A.; Gabrielsson, S. Exosomes with immune modulatory features are present in human breast milk. *The Journal of immunology* 2007, *179*, pp 1969-1978.
8. Mecocci, S.; Gevi, F.; Pietrucci, D.; Cavinato, L.; Luly, F.R.; Pascucci, L.; Petrini, S.; Ascenzioni, F.; Zolla, L.; Chillemi, G. Anti-Inflammatory Potential of Cow, Donkey and Goat Milk Extracellular Vesicles as Revealed by Metabolomic Profile. *Nutrients* 2020, *12*, p 2908.
9. Gangadaran, P.; Hong, C.M.; Ahn, B.-C. An update on in vivo imaging of extracellular vesicles as drug delivery vehicles. *Frontiers in pharmacology* 2018, *9*, p 169.
10. Khan, A.A.; de Rosales, R.T. Radiolabelling of Extracellular Vesicles for PET and SPECT imaging. *Nanotheranostics* 2021, *5*, p 256.
11. Yi, Y.W.; Lee, J.H.; Kim, S.-Y.; Pack, C.-G.; Ha, D.H.; Park, S.R.; Youn, J.; Cho, B.S. Advances in analysis of biodistribution of exosomes by molecular imaging. *International journal of molecular sciences* 2020, *21*, p 665.
12. Rufino-Ramos, D.; Lule, S.; Mahjoum, S.; Ughetto, S.; Bragg, D.C.; de Almeida, L.P.; Breakefield, X.O.; Breyne, K. Using genetically modified extracellular vesicles as a non-invasive strategy to evaluate brain-specific cargo. *Biomaterials* 2022, *281*, p 121366.
13. Varga, Z.; Gyurkó, I.; Pálóczi, K.; Buzás, E.I.; Horváth, I.; Hegedűs, N.; Máthé, D.; Szigeti, K. Radiolabeling of extracellular vesicles with 99mTc for quantitative in vivo imaging studies. *Cancer Biotherapy and Radiopharmaceuticals* 2016, *31*, pp 168-173.
14. Molavipordanjani, S.; Khodashenas, S.; Abedi, S.M.; Moghadam, M.F.; Mardanshahi, A.; Hosseinimehr, S.J. 99mTc-radiolabeled HER2 targeted exosome for tumor imaging. *European Journal of Pharmaceutical Sciences* 2020, *148*, p 105312.
15. Hwang, D.W.; Choi, H.; Jang, S.C.; Yoo, M.Y.; Park, J.Y.; Choi, N.E.; Oh, H.J.; Ha, S.; Lee, Y.-S.; Jeong, J.M. Noninvasive imaging of radiolabeled exosome-mimetic nanovesicle using 99mTc-HMPAO. *Scientific reports* 2015, *5*, pp 1-10.

CHAPTER 3 . ISOLATION OF GOAT MILK EXOSOMES BY NOVEL COMBINED BIOPHYSICAL METHODOLOGY

Part of the content of this chapter has been already published as follows: González, M.I.*, Santos-Coquillat, A.*, Clemente-Moragón, A., González-Arjona, M., Albaladejo-García, V., Peinado, H., Muñoz, J., Ximénez-Embún, P., Ibañez, B., Oliver, E., Desco, M., Salinas, B. *Goat Milk Exosomes As Natural Nanoparticles for Detecting Inflammatory Processes By Optical Imaging* Small 2021, 2105421.

Authors signaled by an asterisk (*) have contributed equally to the research article.

3.1. Introduction

The term 'exosome' can be applied to bilayer membrane vesicles with nanometric size (20-200 nm) and cup-shape morphology [1,2], naturally secreted by cells as mediators of cell-cell communication. These nanovesicles have an endosomal origin and their cargo is composed by lipids, metabolites and nucleic acids (mainly miRNA) [3]. There are also several biomarkers which characterize them, including tetraspanins (e.g. CD63, CD81) and membrane molecules (e.g. TSG101) [4]. Several publications stand out the use of exosomes in biomedical applications; the lipid bilayer structure of these nanovesicles enables both hydrophilic and hydrophobic drugs to be loaded within their structure, supporting their use as drug delivery systems (DDS) [5]. Additionally, natural origin of exosomes ensures their in vivo biocompatibility, also exhibiting an intrinsic ability to target specific cells and tissues [6].

Despite all these promising properties, not all exosomes are available for biomedical purposes. The cellular origin determines not only the composition of the nanovesicle but also its biological function. Foodstuff and plants have been purposed as attractive sources of EVs for involving scalability, accessibility and cost-effectiveness, and ensuring biocompatibility and cross-species tolerance [7]. Specifically, milk represents the only EVs-enriched fluid commercially available and widely consumed by humans.

Exosomes presented in milk are of particular interest because of their remarkable robustness under degradation conditions, necessary to be incorporated into the organism through the intestine after oral ingestion [3]. In addition, their inherent biological functionality supports a promising role as therapeutic tools; milk exosomes are involved in the regulation of inflammatory processes and immune response as well as providing a vehicle for miRNA transmission from mothers to infants [1]. Several publications have demonstrated efficient encapsulation of therapeutic agents in these vesicles, including antitumor drugs [8]. Furthermore, the successful labeling of these nanovesicles with both fluorescent probes and radioisotopes also supports their potential use as novel diagnostic agents for nuclear or near-infrared (NIR) fluorescence imaging [9-11].

Among the different mammalian milk sources, goat milk is one of the most consumed milks by humans, although the vesicles contained therein have been not widely investigated. In addition, it has been reported that goat milk exosomes have a significant

role on inflammatory biological pathways compared to exosomes derived from other milk sources [11,12]. However, one of the drawback in the goat milk exosomes research is the high fat content compared to other human consumption milks and the significant casein composition [13], which could hinder its isolation and limit the efficiency of well-stablished extraction protocols.

The improvement of the purity and specificity of isolated goat milk exosomes is crucial due to their direct influence on their biophysical features. For example, co-precipitation of milk proteins misrepresents the quantification of the total protein amount in the collected sample [14] and may induce vesicle aggregation, altering its size and morphology. In addition, residual proteins bound to exosomes can change its surface charge, modifying the vesicle's in vivo stability and natural tropism [15,16]. Nowadays, different approaches are employed in the isolation of milk exosomes, including sequential centrifugation, size exclusion chromatography, density gradient centrifugation or immunomagnetic beads precipitation [3,17,18]. Among them, differential ultracentrifugation is one of the most widely employed [14]. This physical separation technique enables treating large milk volume, increasing the amount of exosomes that can be recovered per isolation round. This fact support the cost-effectiveness and scalability of the technique, despite the initial investment in the equipment. Nevertheless, the co-precipitation of 'contaminants' with nanovesicle-like physicochemical properties, such as proteins, casein or fat-containing globules [14] may limit the purity of the isolated vesicles.

Previous publications have evaluated the effect of combining differential ultracentrifugation with other isolation techniques in order to improve the purity of the exosome sample. For example, size exclusion chromatography (SEC) after differential ultracentrifugation can reduce the aggregation status of isolated exosomes as well as increase the elimination of residual elements [19,20]. The acidification of milk samples with acetic or hydrochloric acid can also avoid the co-precipitation of non-exosomal components during differential ultracentrifugation, although it can affect the surface composition of the nanovesicles [21].

We propose an innovative protocol which combines typical steps from differential ultracentrifugation with SEC to improve the purity of isolated goat milk exosomes, minimize their aggregation and collect a nanovesicle population as homogeneous as possible. Additionally, we have implemented the use of microbial rennet as biological agent to enhance the removal of casein and non-exosomal proteins. Isolated exosomes have been fully characterized not only to determine the efficacy of this methodology but also to present for the first time the physicochemical and biochemical properties of these nanovesicles.

3.2. Materials and Methods

Commercial organic semi-skimmed goat milk (El Cantero de Letur, Albacete, Spain) was acquired from the supermarket and storage at 4 ºC until use. All centrifugation steps were performed at 4 ºC employing an AVANTI J-30I centrifuge, a Ja 30,50 Ti

fixed-angle rotor (k factor = 280) and 30-mL polycarbonate tubes. This equipment was purchased from Beckman Coulter Instruments (Brea, CA, USA).

Unless otherwise noted, all reagents were purchased from Merck Life Science (Darmstadt, Germany) and used without further purification.

3.2.1. *Biophysical procedure* for the isolation of goat milk exosomes

60 mL of commercial goat milk were divided into two 30-mL centrifuge tubes and centrifuged for 10 min at 5,000 x g in order to remove milk fat and fat-containing vesicles, which are macrostructures commonly present in this biological fluid. Defatted supernatants were tempered and treated for 20 min at 37 ºC with 150 µL of microbial rennet per centrifuged tube (Postres Ultzama, Navarra, Spain). Milk samples were centrifuged for 10 min at 5,000 x g after the coagulation step. Resultant supernatants were successively centrifuged first 35 min at 13,000 x g and then 15 min at 35,000 x g for ensuring the removal of mammary gland-derived cell debris, somatic cells and large extracellular vesicles (e.g. microvesicles). Exosomes were precipitated by ultracentrifugation at 100,000 x g for 65 min. The whitish pellets were washed twice with 5 mL of phosphate-buffered saline (1X PBS) and ultracentrifuged at 100,000 x g for 95 min. Resultant pellets were pooled, filled up to 2.5 mL of 1X PBS and purified by size exclusion chromatography (SEC) using PD-10 columns (GE Healthcare Bio-Sciences AB, Chicago, IL, USA). Briefly, exosomes were collected in 7 fractions of 500 µL of 1X PBS and analyzed by Transmission Electron Microscopy (TEM). Exosome enriched fractions were mixed, raised up to 5 mL with 1X PBS and ultracentrifuged at 100,000 x g for 95 min. The resultant exosome pellet was dispersed in 100 - 200 µL of 1X PBS.

3.2.2. Physicochemical characterization

The isolated vesicles were fully characterized by physicochemical assays, following the Minimal Information for Studies of Extracellular Vesicles (MISEV) 2018 recommendations [14]. Triplicates of the samples per technique were employed.

3.2.2.1. Protein content determination

Total protein amount in isolated samples was quantified by Bradford-Coomassie colorimetric assay. Aliquots of 10 µL, previously diluted by 5-fold in 1X PBS, were loaded in a flat-bottom 96-well plate (Thermo Fischer Scientific, USA) and quantified against a Bovine Serum Albumin (BSA) standard curve. All samples were incubated for 10 min with 200 µL of ready-to-use Coomassie staining reagent. Absorbance per sample was measured at 540 nm using a 680 XR Microplate Reader (BIO-RAD Laboratories, Hercules, CA, USA).

3.2.2.2. Transmission Electron Microscopy

Shape, size and homogeneity of vesicle samples were assessed by Transmission Electron Microscopy (TEM) at ICTS Centro Nacional de Microscopía Electrónica (Universidad Complutense de Madrid, Madrid, Spain). This technique also enabled the detection of impurities and aggregates. Aliquots of 30 µg of isolated vesicles were

placed over formvar carbon coated copper grinds and negatively stained at room temperature with uranyl acetate. Samples were imaged using a JEOL JEM-1010 microscope, operating at 100 kV.

3.2.2.3. Dynamic Light Scattering

Dynamic Light Scattering (DLS) was selected for the analysis of the hydrodynamic size distribution of the isolated vesicles. Aliquots of 5 µL were 200-fold diluted in 1X PBS and placed in DTS0012 disposable cuvettes for their measurement in a Zetasizer Nano ZS90 (Malvern Panalytical, Malvern, UK). Three replicates were recorded under the following parameters: 25 ºC, 9 runs and 10 seconds/run.

3.2.2.4. Nanoparticle Tracking Analysis

Real-time concentration (particle/mL) as well as the core size of isolated vesicles were determined using a NanoSight NS300 instrument (Malvern Panalytical, Malvern, UK), equipped with a high sensitivity metal-oxide semiconductor (sCMOS) camera, a 532 nm laser and the NTA 3.4 Build software. Aliquots of 5 µL were 200-fold diluted with 1X PBS and filtered by 0.45 µm PES membrane filters for technical requirement. Then, samples were charged into the NanoSight chamber with a syringe pump module, stablishing an infusion speed of 40. Three dynamic videos of 60 seconds were recorded per sample, setting the camera level to 12, the detection threshold to 5 and temperature to 25 ºC. Replicated histograms were averaged to determine the modal size and particle concentration.

3.2.2.5. Zeta Potential

Superficial charge of isolated vesicles was evaluated by the measurement of the zeta potential (Z-Potential) in a Zetasizer Nano ZS90 (Malvern Panalytical, Malvern, UK). Same samples used for DLS were placed in DTS1070 cuvettes and measurements were run at 25 ºC, recording three replicates per sample.

3.2.3. Western Blot analysis

The detection of the exosome protein markers TSG101 and CD81 in the samples obtained by the *Biophysical procedure* was carried out by Western Blot assay. Isolated suspensions were homogenized 1:1 in RIPA buffer (PBS with 1 % Nonidet P-40, 0.5 % sodium deoxycholate, 0.1 % SDS), and protease inhibitor cocktail (Roche, Basel, Switzerland). The homogenates were centrifuged at 10,000 x g and 4 ºC for 10 minutes, and supernatants were transferred to different tubes. The amount of soluble protein was quantified with a Bicinchoninic Acid kit for protein determination, following manufacturer´s instructions (ThermoFisher Scientific, Rockford, IL, USA). Proteins were resuspended in reducing Sodium Dodecyl Sulfate (SDS) loading buffer and heated at 95 ºC for 5 min. 15 µg of nanovesicle proteins were run on a 10 % polyacrylamide gel under reducing conditions and transferred to a polyvinylidene fluoride membrane (Immobilon-P, Merck, Darmstadt, Germany). Circulating extracellular vesicles isolated from human WM64 melanoma cells as previously described [22] were run in parallel as positive control. Membranes were blocked with 3 % BSA, then incubated with a rabbit polyclonal anti-TSG101 antibody or a mouse monoclonal anti-CD81 antibody

(ThermoFisher Scientific, Waltham, MA, USA), both at a concentration of 1:1000 in blocking buffer, and finally incubated with the corresponding horseradish peroxidase-conjugated secondary antibodies (Agilent Dako, Santa Clara, CA, USA). Direct digital images were acquired with the Image Quant LAS 4000 mini (GE Healthcare, Chicago, IL, USA).

3.2.4. Proteomic evaluation

The protein content of goat's milk exosomes was solubilized using 8 m urea in 100 mM Tris-HCl (pH 8.0). Samples (20 μg) were digested using the standard FASP protocol. Briefly, proteins were simultaneously reduced (15 mm TCEP) and alkylated (30 mm CAA) for 30 min in the dark at room temperature, and sequentially digested with Lys-C (protein:enzyme ratio 1:50, overnight at room temperature; Wako) and with trypsin (protein:enzyme ratio 1:100, 6 h at 37 °C; Promega, WI, USA). Resulting peptides were desalted using C18 stage-tips.

3.2.4.1. Mass spectrometry

For the proteomic analysis of goat milk-derived exosomes we used liquid chromatography with tandem mass spectrometry (LC-MS/MS) by coupling an Ultimate 3000 RSLCnano System (Dionex) with a Q-Exactive Plus mass spectrometer (Thermo Fisher Scientific, CA, USA). Peptides were loaded into a trap column (Acclaim PepMapTM 100, 100 μm x 2 cm, Thermo Fisher Scientific, CA, USA) over 3 min at a flow rate of 10 μL/min in 0.1 % FA. Then peptides were transferred to an analytical column (PepMapTM RSLC C18, 2 μm, 75 μm x 50 cm, Thermo Fisher Scientific, CA, USA) and separated using a 90 min effective linear gradient (buffer A: 0.1 % FA; buffer B: 100 % ACN, 0.1 % FA) at a flow rate of 250 nL/min. The gradient used was: 0–5 min 4 % B, 5–7 min 6 % B 7–60 min 17.5 % B, 60–72.5 min 21.5 % B, 72.5-80 min 25 % B, 80–94 min 42.5 % B, 94–100 min 98 % B, 100–110 min 4 % B. The peptides were electrosprayed (2.1 kV) into the mass spectrometer through a heated capillary at 320 °C and a S-Lens RF level of 50 %. The mass spectrometer was operated in a data-dependent mode, with an automatic switch between the MS and MS/MS scans using a top 15 method (minimum AGC target 3E3) and a dynamic exclusion time of 26 s. MS (350–1500 m/z) and MS/MS spectra were acquired with a resolution of 70000 and 17500 FWHM (200 m/z), respectively. Peptides were isolated using a 2 Th window and fragmented using higher-energy collisional dissociation (HCD) at 27 % normalized collision energy. The ion target values were 3E6 for MS (25 ms maximum injection time) and 1E5 for MS/MS (45 ms maximum injection time). Samples were analyzed twice.

3.2.4.2. Proteomic data analysis

Raw files were processed with MaxQuant (v 1.6.1.0) using the standard settings against a *Bovidae* protein database (UniProtKB/Swiss-Prot/TrEMBL October 2018, 92, 108 sequences) supplemented with contaminants. Label-free quantification was done with match between runs (match window of 0.7 min and alignment window of 20 min). Carbamidomethylation of cysteines was set as a fixed modification whereas methionine

oxidation and N-term acetylation were variable protein modifications. The minimal peptide length was set to 7 amino acids and a maximum of two tryptic missed-cleavages were enabled. The results were filtered at 0.01 FDR (peptide and protein level) and subsequently the "proteinGroup.txt" file was loaded in Perseus (v1.6.0.7) for further analysis. Statistical overrepresentation of GO Terms, Reactome and Panther pathways were performed using Panther v15.0. The Bos taurus database was considered as the reference list and a Fisher's Exact test with FDR correction (5 %) was applied. The MS proteomic data have been deposited to the ProteomeXchange Consortium via the PRIDE partner repository with the dataset identifier PXD025026. For peer reviewing purposes, the data set can be accessible under the username reviewer_pxd025026@ebi.ac.uk and password: W8uD0thG.

3.2.5. Biochemical Assessment of Milk Exosomes in Plasma of Healthy Mice

Possible toxic effects of goat milk exosomes were evaluated in vivo on CD1 mice (13 weeks old; Charles River Laboratories International Inc., MA, USA) employing the same concentrations as in the in vivo imaging studies. Animals were randomized into two groups, control (n = 7) and treated (n = 8), which were intravenously injected through the lateral tail vein with either PBS (100 µL) or goat milk exosomes (20 µg, 100 µL in PBS), respectively. Blood samples were collected 24 h post-injection by cardiac puncture and plasma was separated from whole blood by centrifuging 5 min at 84 000 rpm. Complete biochemical analysis of blood plasma was carried out by Comparative Medicine Department of Centro Nacional de Investigaciones Cardiovasculares (CNIC) Carlos III (Spain), including basic, hepatic and inflammatory profiles.

3.3. Results

3.3.1. Qualitative evaluation of isolated goat milk exosomes

Biophysical procedure optimized for the isolation of goat milk exosomes (Figure 3.1A) combine the removal of fat milk, cell debris and large vesicles through the physical method of differential ultracentrifugation with the biological precipitation of casein and residual proteins by the enzymatic activity of microbial rennet.

Milk fat and fat-containing vesicles were mainly separated from the milk whey in the first centrifugation step, applying low speed (Figure 3.1B). Then, coagulation of milk by microbial rennet enabled precipitating a large quantity of casein along with other residual proteins (Figure 3.1C). The resultant supernatants were transparent and without turbidity (Figure 3.1D). Cell debris and large EVs were collected after centrifuging at higher speeds (Figure 3.1E) and milk exosomes were finally precipitated at 100,000 x g. The washing steps enabled the elimination of co-isolated milk residues, clarifying the exosomes pellet, which presented a whitish aspect (Figure 3.1F).

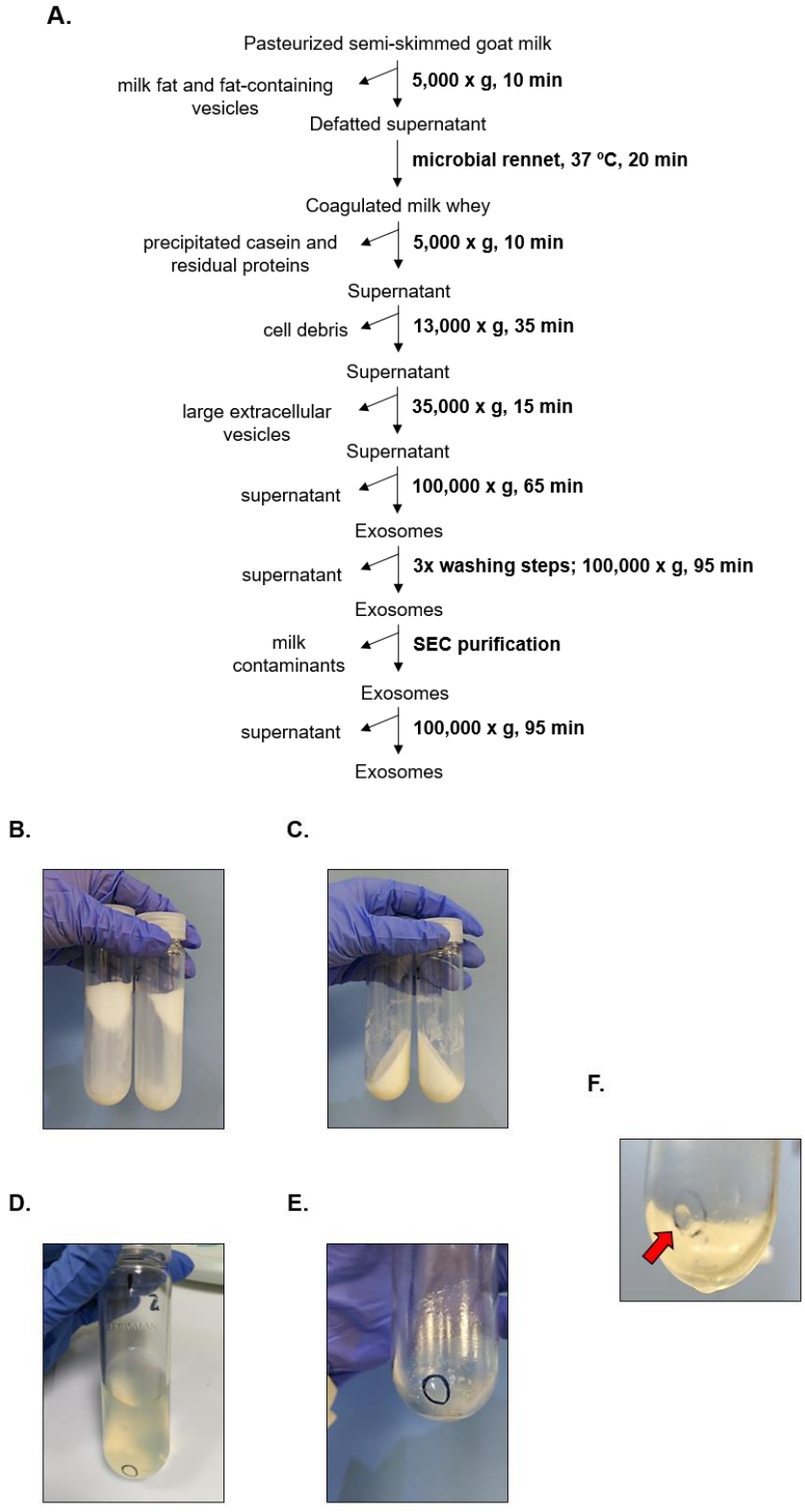

Figure 3.1 Qualitative results from *Biophysical procedure*.

(A) Scheme of goat milk exosomes *Biophysical* isolation protocol. (B) Milk fat stuck to the walls of the centrifuge tube after first centrifuge step. (C) Coagulated casein by microbial rennet. (D) Appearance of supernatants prior to the precipitation of goat milk exosomes. (E) Cell debris and large extracellular vesicles pellet. (F) Exosomes pellet (red arrow).

To assess the effect of incorporating size exclusion chromatography in the exosomes isolation protocol, eluted fractions were analyzed by TEM (Figure 3.2). Large extracellular vesicles were detected in the first elution fraction (500 µL), without presence of exosome-like particles (Figure 3.2A). Intermediate elution fractions (2.5 mL) were clearly enriched in exosome-like nanovesicles (Figure 3.2B), and the last elution fraction (500 µL) mainly presented residual proteins (Figure 3.2C). Once the first and last fractions were discarded, exosomes were precipitated again, forming a gelatinous pellet that was less whitish than before passing through the size exclusion column (Figure 3.1F).

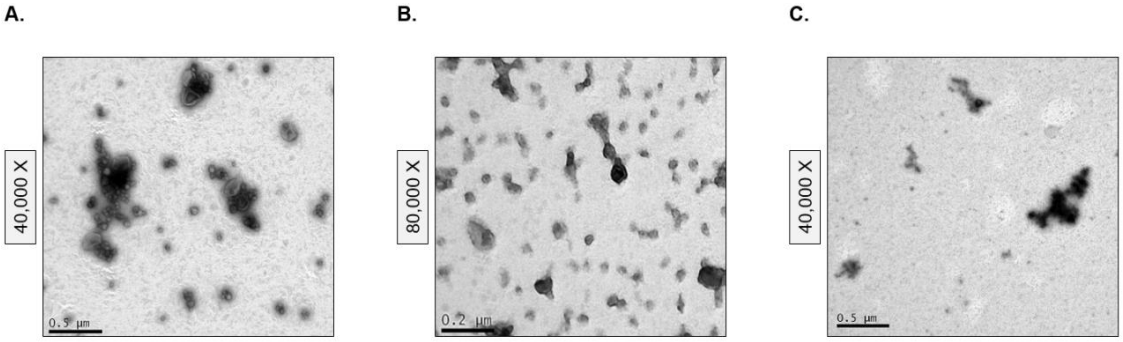

Figure 3.2 Transmission Electron Microscopy (TEM) images of size exclusion chromatography fractions.

(A) First elution fraction with large extracellular vesicles content. (B) Intermediate elution fractions containing exosome-type vesicles. (C) Last elution fraction with residual proteins content.

3.3.2. Physicochemical characterization

Following the optimized *Biophysical procedure*, a 3.77 ± 0.81 mg/mL total protein concentration was quantified by colorimetric assay.

TEM images confirmed morphological and size features of the isolated exosomes as well as their homogeneity or lack thereof. Nanovesicles isolated by the *Biophysical procedure* presented exosome-like characteristics, such as spherical shape with lipid bilayer and 'cup-shape' appearance (Figure 3.3A). This protocol provided a highly concentrated and homogeneous suspension, without aggregates or protein cluster (Figure 3.2B), although a small amount of milk lipoproteins (low density, < 60 nm [18,23]) were detected. However, most of the vesicle population presented a size in the range cataloged for exosomes (Figure 3.3B).

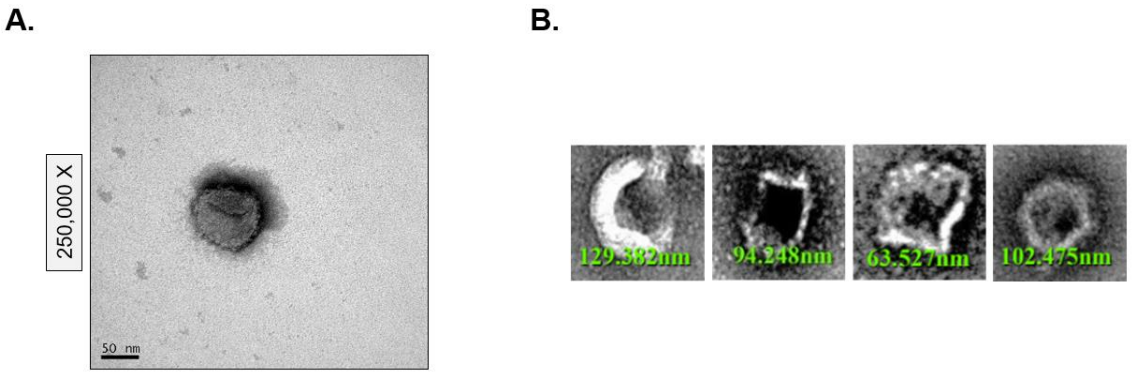

Figure 3.3 Transmission Electron Microscopy (TEM) of isolated vesicles.

(A) Magnified image of a single goat milk exosome. (B) Size measurements of isolated exosomes.

Size profile of the isolated nanovesicles was determined by DLS and NTA. First, the measurement of the hydrodynamic size of the unfiltered samples by DLS revealed that those nanovesicles were in the size range of exosomes (128.14 ± 4.13 nm) (Figure 3.4A). Moreover, the polydispersity index (PdI) confirmed the homogeneity of the sample (PdI: 0.08 ± 0.02). Once nanovesicles were passed through 0.45 µm syringe filters for their analysis by NTA, size changes were not observed (125.30 ± 5.60 nm) (Figure 3.4A), supporting results achieved by TEM in relation to the homogeneity and low aggregation status of the suspension.

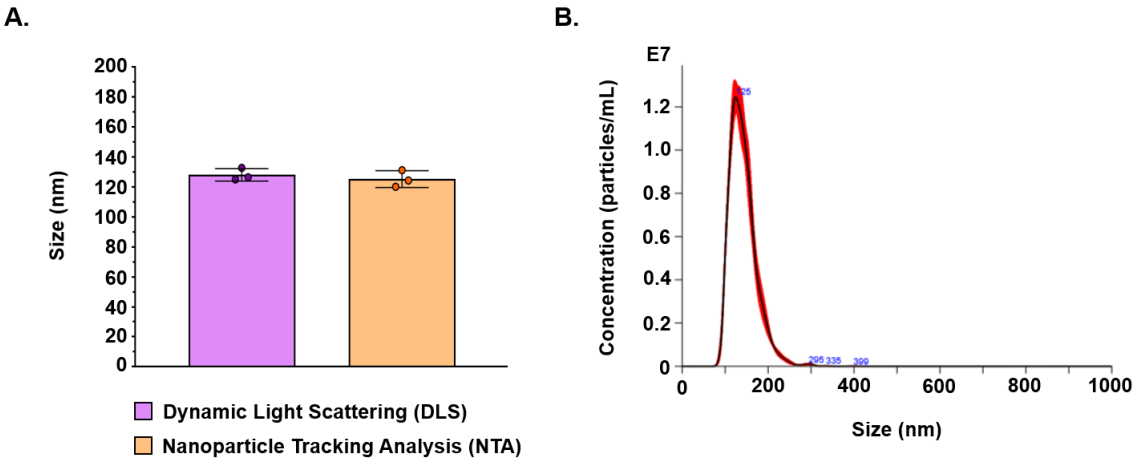

Figure 3.4 Size and concentration evaluation of isolated nanovesicles.

(A) Comparison of size measurements registered by Dynamic Light Scattering (DLS; purple) and Nanoparticle Tracking Analysis (NTA; orange). (B) Size distribution profile measured by Nanoparticle Tracking Analysis (NTA).

NTA also confirmed the higher content of goat milk exosomes in the sample isolated by the *Biophysical procedure* ($6.56 \cdot 10^{11} \pm 2.25 \cdot 10^{11}$ particles/mL) (Figure 3.4B). Finally, the colloidal stability of the sample was assessed by measuring the Z-potential. Exosomes suspension presented negative charge, showing values of -23.93 ± 2.10 mV.

3.3.3. Analysis of exosomal nature of isolated nanovesicles

Western Blot confirmed the presence of TSG-101 (44 kDa) and CD81 (26 kDa) exosomal biomarkers in samples isolated following the *Biophysical procedure* proposed on this work (Figure 3.5).

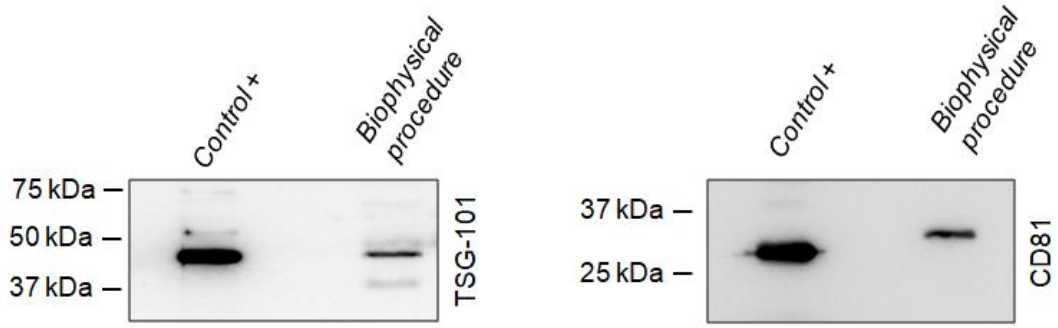

Figure 3.5 Identification of exosome protein biomarkers by Western Blot analysis.

Detection of biomarkers TSG-101 and CD81 in milk nanovesicles was compared to small extracellular vesicles derived from melanoma cells, as positive control.

To determine the composition of milk exosomes, extensive LC-MS/MS proteomic analyses were performed. A total of ~900 proteins (derived from ~4500 peptides) were identified in all three independent isolations of goat milk exosomes. GO analyses using the top 100 most abundant proteins revealed enrichment in terms such as extracellular exosome, extracellular region part, vesicle, and membrane-bounded vesicle, confirming the identity of the samples as extracellular vesicles. In addition, PANTHER overrepresentation analyses showed that the identified proteins were involved in processes such as neutrophil degranulation, the innate immune system, the immune system, hemostasis, and platelet activation.

A 15-fold or greater enrichment was observed for the ECRT (endosomal sorting complex required for transport), endosomal/vacuole pathway, and regulation of the complement cascade, among others. Similarly, proteins were involved in several molecular functions including membrane transport and binding activity, protein transport, vesicle-mediated transport, adhesion, or metabolic processes, related to general cell function and growth or to the endocytic pathway of the vesicles themselves. Other processes such as endosomal transport via the multivesicular body sorting pathway, that pathway itself, late endosome-to-vacuole transport, and response to reactive oxygen species were enriched more than tenfold.

Cellular compartment results showed an over-representation of “endosome”; this fact is of great importance, as exosomes differ from EVs in their cellular origin, which is the endocytic pathway [24].

Among the identified proteins, butyrophilin, β-lactoglobulin, CD36, α-lactalbumin, albumin, and xanthine oxidoreductase were highly abundant, as they are in milk exosomes from cow, horse, and human [18]. To further confirm the exosomal nature of

the nanoparticles, we compared our proteomic data with Exo-Carta and found many of the main exosome markers. These include tetraspanins such as CD9, CD63, and CD81, and other classical markers like TSG101, HSP90AA1, HSP90AB1, and annexins.

3.3.4. Plasma analysis of healthy mice treated with goat milk exosomes

Biochemical analysis of plasma did not show alterations in basic, hepatic, or inflammatory markers compared with those of control mice (Figure 3.6).

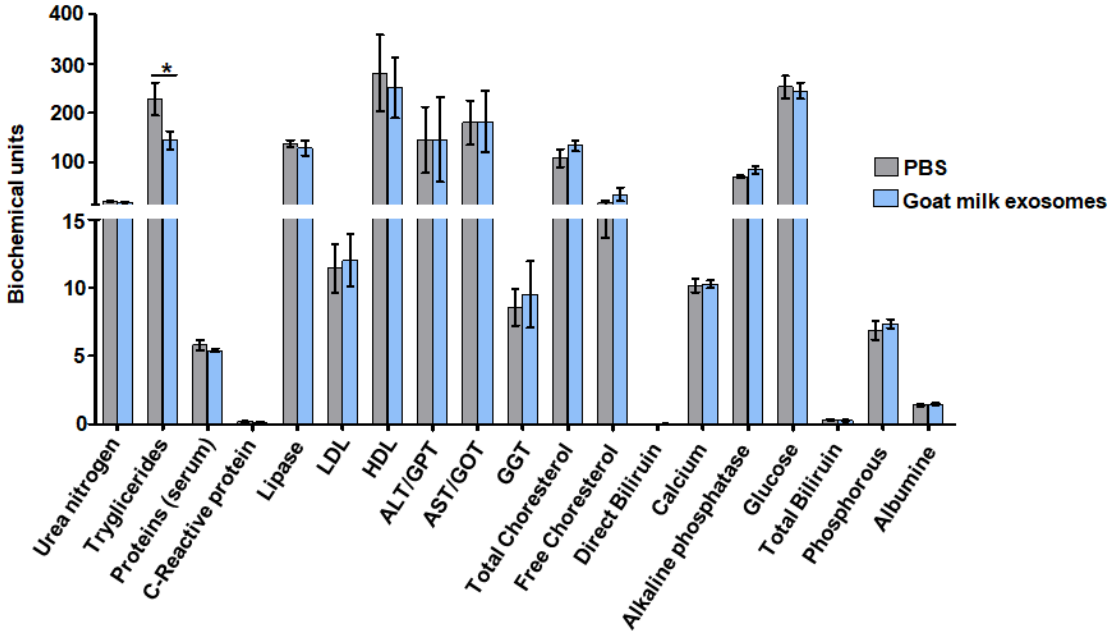

Figure 3.6 Biochemical profile of plasma samples from control (PBS) and treated (exosomes) mice.

Samples were collected 24 h after dose administration. Asterisks (*) indicate statistically significant differences ($p < 0.05$), observed only for triglycerides.

Although previous publications confirmed the high accumulation of milk exosomes in liver after intravenous administration [10,25], markers of hepatic damage, such as alanine aminotransferase and aspartate aminotransferase, did not differ between treated mice and controls (Figure 3.6) [26].

The evaluation of blood markers related to the immune system and inflammatory activity, such as C-reactive protein, high and low-density lipoprotein (HDL and LDL), albumin, and cholesterol, also suggested that goat milk exosomes did not significantly alter the inflammatory and immune profile of treated mice after 24 h (Figure 3.6). Only triglyceride values were reduced in treated mice compared with untreated mice (144.13 ± 52.43 mg/dL in treated mice and 228.14 ± 86.85 mg/dL in controls). This effect was previously described for bovine milk exosomes orally administered to rats [8].

3.4. Discussion

The potential use of goat milk exosomes for biomedical purposes is supported by their inherent characteristics, namely non-toxicity, robustness, lipid bilayer structure and intrinsic biological functionality related to inflammatory response. Translation of these

nanovesicles into clinic requires a cost-efficient and scalable isolation protocol, which ensures adequate purity and high extraction yields.

In this work, we present an optimized methodology for the isolation of exosomes extracted from commercial goat milk by combining traditional physical techniques with an innovative biological approach to obtain highly pure and enriched exosomes suspensions. Thus, isolation of goat milk exosomes was achieved by combining the gold standard physical isolations by differential ultracentrifugation and SEC with a biological treatment of milk using microbial rennet.

There are several differential ultracentrifugation protocols already established, which vary in the time and speed values applied at each sequential centrifugation step, with the only common grounds that the centrifugation temperature should be maintained at 4 °C and that sEVs precipitate at 100,000 x g and above [8,27,28]. As there is no standardized protocol for the collection of exosomes from milk, and considering the characteristics of goat milk in terms of high fat and casein content [29], our protocol has been designed to include enough centrifugation steps for removing as many milk "contaminants" as possible before the nanovesicles precipitation. These centrifugation steps follow a pattern similar to that previously described in the literature, regarding centrifugation speeds [27,28].

On the other hand, this is the first time that milk samples for exosome isolation have been treated with microbial rennet. This biological agent triggers the coagulation of casein at the natural pH of milk. First, enzymatic activity of rennet hydrolyses casein, which is restructured into insoluble micelles. Ca^{2+} ions present in rennet formulation cause the aggregation of the micelles, forming a gel-like structure which can be precipitated by centrifugation [30,31].

Following this proposed strategy, fat-containing vesicles, cell debris and large EVs were precipitated by serial centrifugations and casein was mainly removed along with other milk proteins through the coagulation step. The biological treatment with rennet seems essential in the case of goat milk, due to its high casein content [29] and the similarity of the colloidal characteristics of casein micelles with extracellular vesicles [32]. Precipitated exosomes were additionally purified by SEC in order to separate co-isolated non-exosomal residues from the final nanovesicle suspension. The need to carry out this complementary purification step was demonstrated by the analysis of the elution fractions using TEM.

After the complete physicochemical characterization of the isolated nanovesicles, we conclude that particles with exosome-like features can be successfully collected following our optimized approach. TEM images showed vesicles with appropriated size and 'cup-shaped' morphology. This appearance can be typically detected when negatively stained exosomes are analyzed under TEM microscopes, while large EVs usually present irregular round shape and electron-dense appearance [33]. Nanovesicles visualized were non-aggregated and the presence of protein residues or clusters was ruled out. The size range of the nanovesicles was established by DLS and NTA, which also confirmed the homogeneity of the population and the non-aggregated status,

because no size differences were found before (DLS) and after (NTA) filtering the samples.

Protein quantification proved the protein enrichment of the suspension as well as the reproducibility of the optimized methodology. These two facts were also demonstrated by NTA through the detection of high amounts of vesicles in all measurements. This high isolation yield emphasizes the use of goat milk as economic and scalable source of exosomes, compare to other biological fluids and cell culture media [34].

Western Blot analysis revealed the exosomal nature of the fraction isolated by demonstrating the presence of common biomarkers which define a unique composition that differs from other non-vesicular milk components [4]. This results were also supported by the proteomic analysis of the samples, which also confirmed the endosomal origin of the nanovesicles. Moreover, this assessment identified proteins related to the immune system as has been previously described for milk-derived exosomes [12]. Finally, the biochemical analysis confirmed the in vivo biocompatibility and non-toxicity of isolated exosomes. Nevertheless, this evidence is still insufficient to rule out the existence of mild or late immunogenic effects. Further research in this direction is warranted.

Thus, we have proposed a novel protocol for the isolation of exosomes from goat milk, through the combination of physical (differential ultracentrifugation and SEC) and biological (microbial rennet) approaches. Its efficiency is corroborated by the results presented on this work, which demonstrate the high purity, stability and homogeneity of the exosomes isolated following this procedure. Moreover, biochemical results achieved support the absence of toxic and inflammatory effects, as expected for goat milk exosomes.

3.5. Bibliography

1. de la Torre Gomez, C.; Goreham, R.V.; Bech Serra, J.J.; Nann, T.; Kussmann, M. “Exosomics”—A review of biophysics, biology and biochemistry of exosomes with a focus on human breast milk. *Frontiers in genetics* 2018, *9*, p 92.
2. Abels, E.R.; Breakefield, X.O. Introduction to extracellular vesicles: biogenesis, RNA cargo selection, content, release, and uptake. *Cellular and molecular neurobiology* 2016, *36*, pp 301-312.
3. Sanwlani, R.; Fonseka, P.; Chitti, S.V.; Mathivanan, S. Milk-derived extracellular vesicles in inter-organism, cross-species communication and drug delivery. *Proteomes* 2020, *8*, p 11.
4. Zhang, Y.; Bi, J.; Huang, J.; Tang, Y.; Du, S.; Li, P. Exosome: a review of its classification, isolation techniques, storage, diagnostic and targeted therapy applications. *International journal of nanomedicine* 2020, *15*, p 6917.
5. van der Meel, R.; Fens, M.H.; Vader, P.; Van Solinge, W.W.; Eniola-Adefeso, O.; Schiffelers, R.M. Extracellular vesicles as drug delivery systems: lessons from the liposome field. *Journal of controlled release* 2014, *195*, pp 72-85.
6. Tschuschke, M.; Kocherova, I.; Bryja, A.; Mozdziak, P.; Angelova Volponi, A.; Janowicz, K.; Sibiak, R.; Piotrowska-Kempisty, H.; Iżycki, D.; Bukowska, D.

Inclusion biogenesis, methods of isolation and clinical application of human cellular exosomes. *Journal of clinical medicine* 2020, *9*, p 436.

7. Chen, C.; Sun, M.; Liu, X.; Wu, W.; Su, L.; Li, Y.; Liu, G.; Yan, X. General and mild modification of food-derived extracellular vesicles for enhanced cell targeting. *Nanoscale* 2021, *13*, pp 3061-3069.
8. Munagala, R.; Aqil, F.; Jeyabalan, J.; Gupta, R.C. Bovine milk-derived exosomes for drug delivery. *Cancer letters* 2016, *371*, pp 48-61.
9. Adriano, B.; Cotto, N.M.; Chauhan, N.; Jaggi, M.; Chauhan, S.C.; Yallapu, M.M. Milk exosomes: nature's abundant nanoplatform for theranostic applications. *Bioactive materials* 2021, *6*, pp 2479-2490.
10. González, M.I.; Martín-Duque, P.; Desco, M.; Salinas, B. Radioactive labeling of milk-derived exosomes with 99mTc and in vivo tracking by SPECT imaging. *Nanomaterials* 2020, *10*, p 1062.
11. Santos-Coquillat, A.; González, M.I.; Clemente-Moragón, A.; González-Arjona, M.; Albaladejo-García, V.; Peinado, H.; Muñoz, J.; Ximénez Embún, P.; Ibañez, B.; Oliver, E. Goat milk exosomes as natural nanoparticles for detecting inflammatory processes by optical imaging. *Small* 2022, *18*, p 2105421.
12. Mecocci, S.; Gevi, F.; Pietrucci, D.; Cavinato, L.; Luly, F.R.; Pascucci, L.; Petrini, S.; Ascenzioni, F.; Zolla, L.; Chillemi, G. Anti-Inflammatory Potential of Cow, Donkey and Goat Milk Extracellular Vesicles as Revealed by Metabolomic Profile. *Nutrients* 2020, *12*, p 2908.
13. Izumi, H.; Kosaka, N.; Shimizu, T.; Sekine, K.; Ochiya, T.; Takase, M. Purification of RNA from milk whey. In *Circulating MicroRNAs*, *Springer* 2013, pp. 191-201.
14. Théry, C.; Witwer, K.W.; Aikawa, E.; Alcaraz, M.J.; Anderson, J.D.; Andriantsitohaina, R.; Antoniou, A.; Arab, T.; Archer, F.; Atkin-Smith, G.K. Minimal information for studies of extracellular vesicles 2018 (MISEV2018): a position statement of the International Society for Extracellular Vesicles and update of the MISEV2014 guidelines. *Journal of extracellular vesicles* 2018, *7*, p 1535750.
15. Beit-Yannai, E.; Tabak, S.; Stamer, W.D. Physical exosome: exosome interactions. *Journal of cellular and molecular medicine* 2018, *22*, pp 2001-2006.
16. Midekessa, G.; Godakumara, K.; Ord, J.; Viil, J.; Lättekivi, F.; Dissanayake, K.; Kopanchuk, S.; Rinken, A.; Andronowska, A.; Bhattacharjee, S. Zeta potential of extracellular vesicles: toward understanding the attributes that determine colloidal stability. *Acs Omega* 2020, *5*, pp 16701-16710.
17. Yu, L.-L.; Zhu, J.; Liu, J.-X.; Jiang, F.; Ni, W.-K.; Qu, L.-S.; Ni, R.-Z.; Lu, C.-H.; Xiao, M.-B. A comparison of traditional and novel methods for the separation of exosomes from human samples. *BioMed research international* 2018, *2018*.
18. Sedykh, S.E.; Burkova, E.E.; Purvinsh, L.V.; Klemeshova, D.A.; Ryabchikova, E.I.; Nevinsky, G.A. Milk exosomes: Isolation, biochemistry, morphology, and perspectives of use. *Extracellular Vesicles and Their Importance in Human Health* 2020, pp 1-28.
19. Sidhom, K.; Obi, P.O.; Saleem, A. A review of exosomal isolation methods: is size exclusion chromatography the best option? *International Journal of Molecular Sciences* 2020, *21*, p 6466.
20. Yang, D.; Zhang, W.; Zhang, H.; Zhang, F.; Chen, L.; Ma, L.; Larcher, L.M.; Chen, S.; Liu, N.; Zhao, Q. Progress, opportunity, and perspective on exosome

isolation-efforts for efficient exosome-based theranostics. *Theranostics* 2020, *10*, p 3684.

21. Rahman, M.M.; Shimizu, K.; Yamauchi, M.; Takase, H.; Ugawa, S.; Okada, A.; Inoshima, Y. Acidification effects on isolation of extracellular vesicles from bovine milk. *PLoS One* 2019, *14*, p e0222613.
22. Peinado, H.; Alečković, M.; Lavotshkin, S.; Matei, I.; Costa-Silva, B.; Moreno-Bueno, G.; Hergueta-Redondo, M.; Williams, C.; García-Santos, G.; Ghajar, C.M. Melanoma exosomes educate bone marrow progenitor cells toward a pro-metastatic phenotype through MET. *Nature medicine* 2012, *18*, pp 883-891.
23. Brennan, K.; Martin, K.; FitzGerald, S.; O'sullivan, J.; Wu, Y.; Blanco, A.; Richardson, C.; Mc Gee, M. A comparison of methods for the isolation and separation of extracellular vesicles from protein and lipid particles in human serum. *Scientific reports* 2020, *10*, pp 1-13.
24. Kowal, J.; Tkach, M.; Théry, C. Biogenesis and secretion of exosomes. *Current opinion in cell biology* 2014, *29*, pp 116-125.
25. González, M.I.; González-Arjona, M.; Santos-Coquillat, A.; Vaquero, J.; Vázquez-Ogando, E.; de Molina, A.; Peinado, H.; Desco, M.; Salinas, B. Covalently Labeled Fluorescent Exosomes for In Vitro and In Vivo Applications. *Biomedicines* 2021, *9*, p 81.
26. Fox, J.G.; Barthold, S.; Davisson, M.; Newcomer, C.E.; Quimby, F.W.; Smith, A. The mouse in biomedical research: history, wild mice, and genetics; Elsevier: 2006, Vol. 1.
27. Vaswani, K.; Koh, Y.Q.; Almughlliq, F.B.; Peiris, H.N.; Mitchell, M.D. A method for the isolation and enrichment of purified bovine milk exosomes. *Reproductive biology* 2017, *17*, pp 341-348.
28. Yamauchi, M.; Shimizu, K.; Rahman, M.; Ishikawa, H.; Takase, H.; Ugawa, S.; Okada, A.; Inoshima, Y. Efficient method for isolation of exosomes from raw bovine milk. *Drug development and industrial pharmacy* 2019, *45*, pp 359-364.
29. Gao, R.; Zhang, R.; Qian, T.; Peng, X.; He, W.; Zheng, S.; Cao, Y.; Pierro, A.; Shen, C. A comparison of exosomes derived from different periods breast milk on protecting against intestinal organoid injury. *Pediatric Surgery International* 2019, *35*, pp 1363-1368.
30. University of Guelph. Enzymic Coagulation of Milk. Availabe online: https://www.uoguelph.ca/foodscience/book-page/enzymic-coagulation-milk (accessed on 27 July, 2021).
31. Abada, E.A. Application of microbial enzymes in the dairy industry. In *Enzymes in food biotechnology*, *Elsevier* 2019, pp. 61-72.
32. Somiya, M.; Yoshioka, Y.; Ochiya, T. Biocompatibility of highly purified bovine milk-derived extracellular vesicles. *Journal of extracellular vesicles* 2018, *7*, p 1440132.
33. Théry, C.; Ostrowski, M.; Segura, E. Membrane vesicles as conveyors of immune responses. *Nature reviews immunology* 2009, *9*, pp 581-593.
34. Théry, C.; Amigorena, S.; Raposo, G.; Clayton, A. Isolation and characterization of exosomes from cell culture supernatants and biological fluids. *Current protocols in cell biology* 2006, *30*, pp 3.22. 21-23.22. 29.

CHAPTER 4 . RADIOACTIVE LABELING OF MILK-DERIVED EXOSOMES WITH ^{99m}Tc AND IN VIVO TRACKING BY SPECT IMAGING

The content of this chapter has been published as follows: González, M.I., Martín-Duque, P., Desco, M., Salinas, B. *Radioactive Labeling of Milk-Derived Exosomes with ^{99m}Tc and In Vivo Tracking by SPECT Imaging*. Nanomaterials 2020, 10, 1062.

4.1. Introduction

The emerging field of nanomedicine holds great promise in the development of drug delivery systems (DDS) with targeted treatment based on controlled release, especially in the field of oncology [1-3]. One of the most favored nanosystems is liposomes, which are spherical vesicles consisting of one or more lipid bilayer membrane(s) encapsulating an aqueous medium. While there is extensive literature on the use of liposomes as DDS in the preclinical field, translation to clinical practice is limited, mainly owing to their inability to evade the host immune system, instability, and toxicity [4]. Natural exosomes and exosome-like systems, on the other hand, are emerging as promising new structures based on the fact that they are similar to liposomes in terms of morphology and size. In addition, they are involved in cell–cell communication, immune response, and tumor progression [5-7]. These nanostructures are the smallest cellular vesicles reported to date. They range in size from 50 to 150 nm and are cup-shaped [8]. The lipid bilayer structure present in exosomes enables self-assembly of both hydrophilic and lipophilic substances such as doxorubicin, paclitaxel, antifungal drugs, and analgesics [9-13]. Moreover, depending on their characteristics and origin, their specific tropism can be exploited to steer them towards diseased tissues or organs [14,15]. These biological and physicochemical properties enable exosomes to act as “Trojan horses” for therapeutic agents, thus enhancing their transport to target tissue and increasing their effectiveness. In addition, the biocompatibility and minimal-to-no inherent toxicity of exosomes overcome the limitations observed with most synthetic DDS, thus making them an ideal nanoplatform in the development of new DDS [16].

Use of natural exosomes of non-human origin (such as milk) as nanocarriers has been widely tested in preclinical studies owing to their suitability, scalability, lack of toxicity, and low cost [17-19]. However, several limitations still need to be addressed before their translation to clinical practice. These include their largely unexplored natural behavior after exogenous administration and the lack of knowledge about their pharmacokinetic properties as DDS. Such properties are crucial for optimization of dosimetry, where the administration route plays a fundamental role, especially in tissue selectivity and biodistribution [14,20].

Molecular imaging is a well-known, non-invasive technique that enables in vivo assessment of cells, biomolecules, and new therapeutic approaches [21,22] and obviates the removal of tissue samples or organs from their natural environment, thus reducing animal sacrifice and tedious histological assays [23].

Consequently, this technique is extremely useful for the in vivo tracking of exosomes, which is oriented towards the evaluation of pharmacokinetic properties and optimization of dosimetry. Previous studies have assessed in vivo administration routes based on optical imaging after labeling exosomes using fluorescent dyes or genetic engineering techniques [20,24]. Nevertheless, this approach is limited by the inherent background generated by natural biomolecules, such as hemoglobin [25-27], or the instability of the probe which leads to incorrect data resulting from the non-specific signal of the free dyes [23]. Furthermore, translation of optical imaging to humans is largely hampered by the limited penetration of light [28]. Nuclear imaging techniques (positron emission tomography (PET) and single photon emission computed tomography (SPECT) may overcome some of these difficulties and seem to be promising approaches owing to their high sensitivity, easy quantification, and wide availability of different radionuclides [23].

This study was the first to evaluate in vivo tracking of natural milk exosomes by nuclear imaging (SPECT) based on labeling with radioactive technetium (^{99m}Tc (IV)). The methodology applied enabled us to carry out a complete pharmacokinetic assessment of the radioactive tracer, [^{99m}Tc]-Exo, in healthy mice in order to optimize its dosimetry as a DDS. We also studied differences in the natural behavior of the exosomes as a function of the more usual administration routes in the preclinical field (intravenous and intraperitoneal injection and intranasal instillation).

4.2. Materials and Methods

4.2.1. Isolation of Milk-Derived Exosomes

Exosomes were isolated from commercial fresh pasteurized semi-skimmed goat milk (El Cantero de Letur, Albacete, Spain) by successive centrifugations at 4 ºC in 30 mL polycarbonate centrifuge tubes, using a Ja 30,50 Ti rotor (Beckman Coulter Instruments, Brea, CA, USA). Briefly, milk was centrifuged for 10 min at 5,000 x g, 35 min at 13,000 x g, and 15 min at 35,000 x g in order to remove contaminants such as fat globules (MFGs) and cell debris. Additionally, microbial rennet was used to precipitate milk casein. The supernatant was ultracentrifuged at 100,000 x g and 4 ºC for 70 min to precipitate the exosomes (50–150 nm). The resultant pellet was washed three times with phosphate-buffered saline (1X PBS) and then purified by size exclusion chromatography (SEC) using PD-10 columns (GE Healthcare Bio-Sciences AB, Chicago, IL, USA). Pure exosomes were ultracentrifuged again at 100,000 x g for 90 min, and the exosome pellet was dispersed in 100 µL of 1X PBS. The protein content of the final sample was quantified using the Coomassie–Bradford assay and stored in aliquots at −20 ºC until use.

4.2.2. Protein Content

Protein content was quantified using the Bradford–Coomassie colorimetric assay. A standard calibration curve was obtained using known concentrations of bovine serum albumin (from 2000 µg/mL to 8 µg/mL) and fitting a third-order polynomial equation ($R^2 > 0.99$), employing MATLAB software (MathWorks Inc., Natick, MA, USA). This

standard calibration curve was used to determine the protein content of the exosome samples with 10 µL of exosome solution. Absorbance at 595 nm was measured using a Synergy™ HT Multi-Mode Microplate Reader (Biotek Instruments Inc., Winooski, VT, USA).

4.2.3. Radiolabeling of Goat Milk Exosomes with Reduced Technetium (^{99m}Tc (IV))

Unless otherwise stated, all reagents were purchased from Sigma–Aldrich (St. Louis, MO, USA) and used without further purification. Commercial sodium pertechnetate, [^{99m}Tc] $NaTcO_4$, was obtained from a TEKCIS™ Technetium ^{99m}Tc Generator (Curium Pharma, Madrid, Spain). For radiolabeling of exosomes, [^{99m}Tc] $NaTcO_4$ (30 µL, 5 mCi) was initially reduced in the presence of 20 µL $SnCl_2$ in HAc (10 %). To determine the optimal reaction conditions, several concentrations of $SnCl_2$ were tested (0.0004 M, 0.002 M, 0.004 M, 0.006 M, 0.008 M, and 0.01 M). The reduction reaction was carried out for 5 min at 37 ºC under an N_2 atmosphere and further neutralized with NaOH (10 µL, 2.8 N).

Exosomes isolated at different concentrations (10 µg, 30 µg, and 75 µg; 50 µL) were finally radiolabeled with a solution of ^{99m}Tc (IV) in a thermomixer at 37 ºC with shaking for 30 min. The resulting products were purified using exosome spin columns (Invitrogen, Carlsbad, CA, USA). The radiochemical yield of the reaction was evaluated by iTLC analysis (silica-gel; mobile phase = 90:10 MeOH:H_2O; Merck, Germany). The radiopurity of the nanotracer was measured using high-performance liquid chromatography (HPLC, Agilent 1200 series; 0.2 mL/min; 254 nm; mobile phase = 1X PBS; Agilent Technologies, Santa Clara, CA, USA).

Reaction yields were calculated by measuring the activity of purified radiolabeled exosomes using a Genesys LTI gamma counter (Laboratory Technologies Inc., Elburn, IL, USA).

4.2.4. Radiolabeling of Milk Exosomes with Commercial Pertechnetate (^{99m}Tc (VII))

The possibility of active labeling based on the iodide symporter (NIS) was assessed by radiolabeling milk exosomes with commercial pertechnetate (^{99m}Tc (VII)). Thirty microliters of sodium pertechnetate (5 mCi; Curium Pharma, Madrid, Spain) was mixed with 20 µL of HAc (10 %) for 5 min at 37 ºC and shaken under an N_2 atmosphere. Then, the solution was neutralized with NaOH (10 µL of 2.8 N), and over 30 µg of goat milk exosomes (50 µL) was added. The reaction was maintained at 37 ºC with shaking for 30 min. The final product was purified by exosome spin columns (Invitrogen, Carlsbad, CA, USA). The radiochemical yield of the reaction was evaluated by iTLC analysis (silica-gel; mobile phase = 90:10 MeOH:H_2O; Merck, Germany).

The reaction yield was calculated by measuring the activity of the purified product using a Genesys LTI gamma counter (Laboratory Technologies Inc., Elburn, IL, USA).

4.2.5. High-Performance Liquid Chromatography (HPLC)

High-performance liquid chromatography (HPLC) was performed using an Agilent 1200 series HPLC system. Radio-HPLC was performed using an identical Agilent

system which was also equipped with a Gina Scan-RAM Radio-TLC/HPLC detector (Microbeam, Spain). Analytic runs were performed on a Yarra SEC-3000 column (300 × 7.8 mm; Phenomenex Inc., Torrance, CA, USA). The solvent system was 1X PBS for the quality control of the radiotracers with a gradient of 100 % between 0 and 80 min and a flow of 0.2 mL/min. Data were processed using Gina Star (Microbeam S.A., Madrid, Spain).

4.2.6. Transmission Electron Microscopy (TEM)

Nanovesicles suspensions of both non-radioactive and radiolabeled exosomes were deposited onto a formvar carbon-coated copper grid and stained with uranyl acetate at room temperature. A JEOL JEM-1010 transmission electron microscope (JEOL USA Inc., Peabody, MA, USA) from ICTS Centro Nacional de Microscopía Electrónica (Universidad Complutense de Madrid, Spain) was employed to observe the samples.

4.2.7. Dynamic Light Scattering (DLS) Analysis

Aliquots of the corresponding exosomes were passed through a 0.44 µm filter, and the size distribution was analyzed using a Zetasizer Nano device (Malvern Panalytical, Malvern, UK). The parameters selected were protein as the sample material, 25 ºC, 120 seconds of equilibration time, and water as dispersant. Disposable cuvettes DTS0012 (Brand, Germany) were used as measurement cells.

4.2.8. In Vitro Stability Studies

The in vitro stability of radiolabeled exosomes was assessed by incubating 150 µCi of [^{99m}Tc]-Exo in 1X PBS from 1 h to 48 h at 37 ºC. Aliquots of 3 µl of solution were analyzed at each time point by iTLC on a silica-gel plate (Merck, Germany) and in a mobile phase of 90:10 MeOH:H_2O.

A Genesys gamma counter (Laboratory Technologies Inc., Elburn, IL, USA) was used to measure the activity of the iTLC regions.

4.2.9. Ethics Statement

The animal experiments complied with the ARRIVE guidelines and were in accordance with the EU Directive (2010/63/EU) for animal experiments. The Hospital General Universitario Gregorio Marañón Animal Care and Use Committee approved all the procedures (PROEX 097/16).

4.2.10. Blood Half-Life

Blood half-life was determined by measuring activity in serial blood samples. Specifically, [^{99m}Tc]-Exo tracer was administered to healthy female Balb/C mice (14–18 weeks old, 20–25 g in weight, n = 3) via intranasal instillation (30 µL in PBS, 110–190 µCi, 9 ± 2 µg), intraperitoneal injection (300 µL, 350–490 µCi, 24 ± 5 µg), or intravenous tail injection (300 µL, 100–170 µCi, 19 ± 8 µg). Except for the intranasal route, tracer was administered under 2 % sevoflurane anesthesia (O_2 100 %; 200–400 cc/min; Zoetis, Belgium). Blood samples were extracted from the saphenous vein in awake mice at several time points post-injection. This blood was weighed, and radioactivity was measured on a Wallac Wizard 1480-011 Automatic Gamma Counter

(Perkin Elmer, Waltham, MA, USA). Measurements in counts per minute were normalized to the mean % ID/g of tissue. Data were modeled as a two-compartmental kinetic model and analyzed by two-phase decay nonlinear regression with Prism 6.0c (GraphPad Software, La Jolla, CA, USA).

4.2.11. In Vivo SPECT/CT Imaging

The SPECT (single photon emission computed tomography) and CT (computed tomography) scans were acquired from healthy female Balb/C mice (14–18 weeks old, 20–25 g in weight, n = 6 per administration route) after administration of the [^{99m}Tc]-Exo tracer by intranasal instillation (30 µL in PBS, 140–170 µCi, 12 ± 4 µg), intraperitoneal injection (300 µL, 190–340 µCi, 19 ± 5 µg), or intravenous tail injection (300 µL, 310–350 µCi, 18 ± 9 µg). Images were acquired with the animals under 2 % sevoflurane anesthesia (O_2 100 %; 200–400 cc/min; Zoetis, Belgium).

Longitudinal in vivo tracking of the radiolabeled exosomes was carried out using SPECT (MiLabs USPECT II, Utrecht, The Netherlands) and CT (PET/CT SuperArgus, SEDECAL Molecular Imaging, Madrid, Spain) small animal imaging scanners. The animals were placed in the prone position and the field of view was adjusted to the area of interest. Once the radiotracer was administered, 18 frames of 5 min per animal were acquired and another 60 min scan was performed 24 h post-injection. A multi-pinhole 1.0 collimator was used for acquisition of the SPECT images, and, for the radionuclide ^{99m}Tc, an energy window ranging from 126 to 154 KeV was chosen. The number of counts acquired ranged between 1.5 M and 350 K in the worst cases (24 h studies). The OS-EM reconstruction was performed with a 0.75 mm^3 voxel size, 16 subsets, and 2 iterations using proprietary software (MiLabs, Utrecht, The Netherlands). For correcting disperse events, 2 windows of 20 % were applied to the left and right of the radioactive technetium peak, and reconstruction was completed under a Gaussian blurring postfilter with a FWHM of between 0.85 and 1 mm. For acquisition of anatomical images, the CT parameters selected were 40 KeV, 340 µA, 360 projections, and 2 × 2 binning. In addition, images (0.12 mm^3) were reconstructed using the software from the PET/CT system (SEDECAL Molecular Imaging, Madrid, Spain). No scatter or attenuation corrections were applied.

Both SPECT and CT images were co-registered with the MMWKS software package (SEDECAL Molecular Imaging, Madrid, Spain) [29] using 3 fiducial markers previously charged with contrast and radioactive agents.

4.2.12. Ex Vivo Biodistribution Studies

Biodistribution experiments were conducted on healthy female Balb/C mice (14–18 weeks old, 20–25 g in weight, n = 3 per administration route). The radioactive exosome [^{99m}Tc]-Exo preparation (250–300 µCi in 300 µL of a 1X PBS solution for the injections and 145–160 µCi in 30 µl of PBS for the intranasal instillation) was administered via the lateral tail vein, intraperitoneally, or intranasally, and the nanotracer was allowed to circulate for 24 h in the 3 groups. After this time, mice were sacrificed and their organs harvested (e.g., brain, trachea/thyroid, lungs, heart, stomach,

liver, spleen, kidneys, intestines, muscle, and skin, as well as feces). The activity (exosome content) in the tissue of interest was measured on a Wallac Wizard 1480-011 Automatic Gamma Counter (Perkin Elmer, Waltham, MA, USA) and expressed as mean % ID/g of tissue.

4.2.13. Autoradiography

Healthy female Balb/C mice (14–18 weeks old, 20–25 g in weight, n = 3 per administration route) received 16 ± 2 µg/100–210 µCi in 300 µL (1X PBS) of [^{99m}Tc]-Exo via intraperitoneal or intravenous injection, and 10 ± 4 µg/160–200 µCi in 30 µL of PBS via intranasal instillation. The mice were sacrificed after 24 h of circulation (90 min in the case of intranasal administration). Liver and brain tissue were excised, and series of 100–200 µm sections were sliced and mounted on plastic slides. Digital autoradiography was performed to determine radiotracer distribution by placing samples on the plate (BAS-MP 2025, Fujifilm, Tokyo, Japan) for 18 h at room temperature. Phosphor imaging plates were read at a pixel resolution of 200 µ with a Bio-Imaging Analyzer BAS-500 plate reader (Fujifilm, Tokyo, Japan). Tissue intensity was quantified using Fiji ImageJ Software (U.S. National Institutes of Health, Bethesda, MD, USA).

4.2.14. Data Analysis

Data were processed using Prism 6.0c (GraphPad Software, La Jolla, CA, USA).

4.3. Results

4.3.1. Protein Content

The most common method for estimating the number of exosomes per aliquot is currently quantification of protein content in the exosomal dispersion [30]. The Bradford–Coomassie colorimetric assay yielded 197 ± 64 µg of exosomes per 60 mL of goat milk.

4.3.2. Synthesis of Radioactive Exosomes ([^{99m}Tc]-Exo) and Optimization

Reducing conditions were optimized using a standard range of 4×10^{-4} M × 10^{-2} M of $SnCl_2$ as recommended in the literature [31]. We also tested several concentrations to achieve robust parameters for radiolabeling, reaching optimal conditions that generated the lowest degradation and aggregation effects in the sample (Figure 4.1A). Lower $SnCl_2$ concentrations were not sufficient to reduce the radioisotope and achieved low radiochemical yields (8.95 %). Conversely, higher concentrations led to degradation of the exosomes which was confirmed by the TEM image and resulted in a radiolabeling yield of 0.10 %. The $SnCl_2$ concentrations around 0.002 mM showed the highest radiochemical yield values (25.85 %) and the TEM image demonstrated that the initial exosome morphology remained unaltered. Moreover, we realized that the reaction yields also depended on the number of exosomes. The highest yields of radiolabeling (37.00 ± 9.00 %) were obtained for 75 µg of exosomes (Figure 4.1C, 1D).

Finally, we evaluated the effect of oxidation state using commercial ^{99m}Tc (VII) (pertechnetate) and reduced ^{99m}Tc (IV). Significant differences were observed (Figure 4.1B): the radio efficiency achieved using the reduced form of technetium was 99.5 %, as measured using iTLC analysis. However, exosomes did not incorporate ^{99m}Tc (VII) (radio efficiency of 0.4 %).

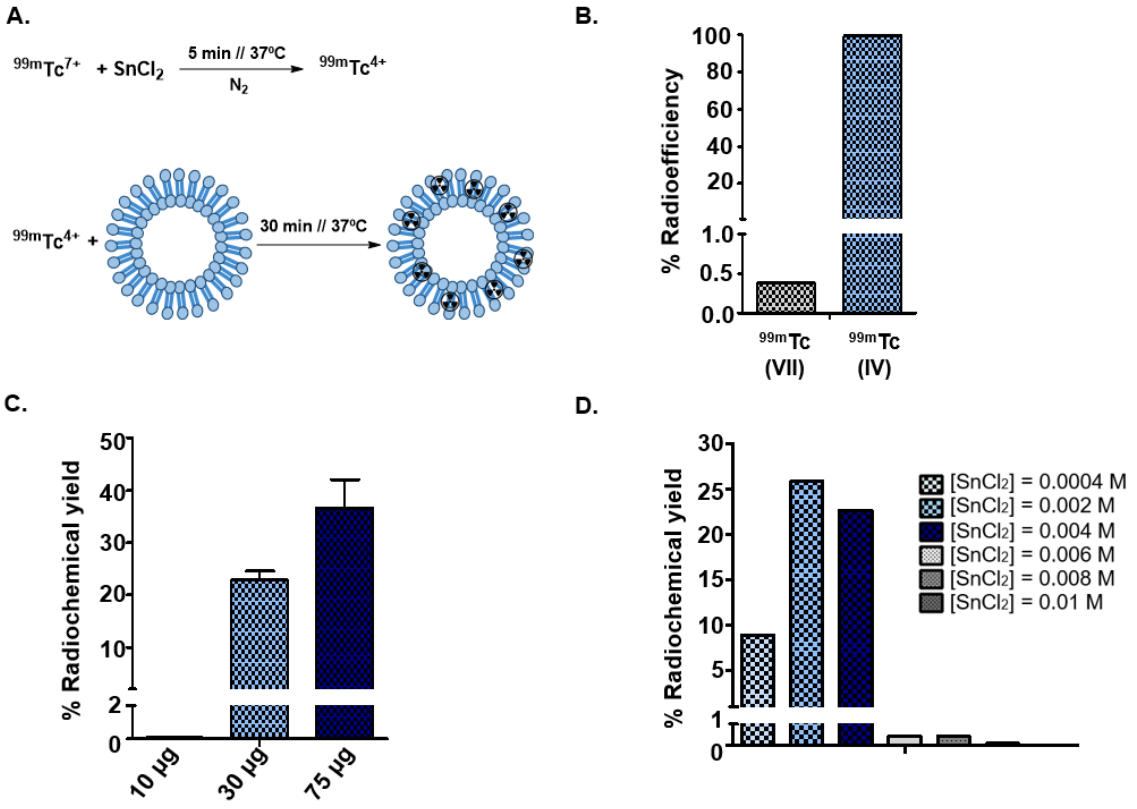

Figure 4.1 Chemical optimization of goat milk exosome radiolabeling conditions.

(A) Schematic representation of the reaction. (B) Radioefficiency of exosomes labeled with ^{99m}Tc (VII) vs. ^{99m}Tc (IV). (C) Effect of the exosome protein concentration in the radiochemical yield. (D) Determination of optimum concentration of $SnCl_2$ as a reducing agent.

4.3.3. Physicochemical Characterization

4.3.3.1. Size and Morphology

Assessment of exosome morphology using TEM showed a monodisperse population of the goat milk nanovesicles, with a common morphology consisting of a "cup-shaped" structure that was similar in both radiolabeled and control samples. These nanoparticles presented a core size of approximately 100 nm before and after labeling. Consistently, DLS analysis confirmed a hydrodynamic size of 122.00 ± 1.00 nm for non-labeled exosomes and 114.00 ± 8.00 nm for radiolabeled exosomes (Figure 4.2A, 2B).

4.3.3.2. Radiopurity of [^{99m}Tc]-Exo Tracer

The purity of the [^{99m}Tc]-Exo was determined by HPLC (Figure 4.2C), which confirmed a radiopurity > 95 %. The main peak in the radioactive chromatogram of

[^{99m}Tc]-Exo was observed at 24.9 min, matching the retention time of pure non-labeled exosomes in the UV chromatogram (254 nm) (Figure 4.2C).

4. 3.3.3. In Vitro Stability Studies

The high stability of the new radiotracer—95 % even after 48 h—was confirmed in vitro (Figure 4.2D).

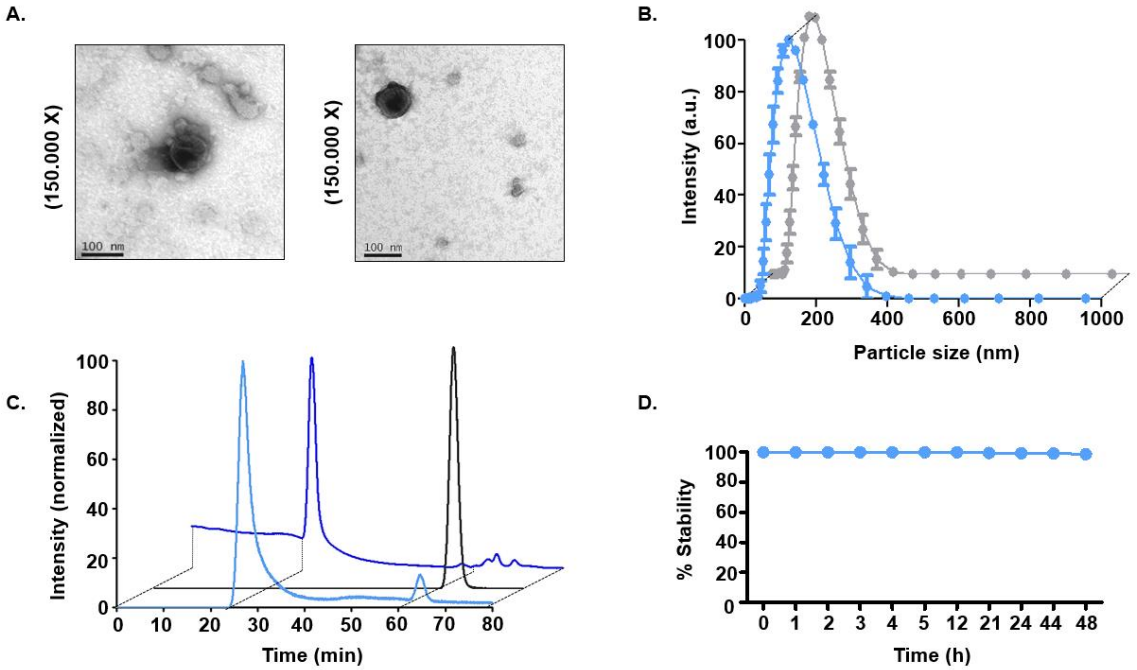

Figure 4.2 Physicochemical characterization of [^{99m}Tc]-Exo.

(A) Transmission electron microscopy images of non-labeled goat milk exosomes (left) and radiolabeled exosomes (right). (B) Hydrodynamic size measured using dynamic light scattering (non-labeled exosomes in blue and radiolabeled exosomes in grey). (C) Radioactive HPLC chromatogram of [^{99m}Tc]-Exo (light blue), free ^{99m}Tc (grey), and UV HPLC chromatogram of non-labeled goat milk exosomes (dark blue). (D) Longitudinal in vitro.

4.3.4. Pharmacokinetic Study and In Vivo Tracking

4.3.4.1. Intravenous Administration

Small animal SPECT/CT studies were carried out after administering radioactively labeled [^{99m}Tc]-Exo to healthy mice. Longitudinal tracking revealed fast blood clearance of these nanotracers. SPECT images at 5 min post-injection still showed circulation of the radioexosomes in the aorta and lungs, and images at 10 min indicated the beginning of accumulation in the liver. The high activity accumulation observed in bladder at 30 min and 60 min confirms a fast-urinary excretion. Spleen and liver uptake were confirmed after 1 h, and no significant changes in the exosome distribution were observed in further acquisitions at 3 h, 5 h, and 24 h (Figure 4.3A). The in vivo blood half-life study matched the results of SPECT imaging, showing quick blood clearance (Figure 4.3B) (Table 4.1). Ex vivo analysis of the biodistribution of [^{99m}Tc]-Exo 24 h after its administration also confirmed the data observed in vivo by SPECT (Figure

4.3C) (Table 4.1). These data are consistent with ex vivo autoradiography findings (Figure 4.3D). Histological sections of liver showed a clear delineation of hepatic tissue with [^{99m}Tc]-Exo which was not the case for brain tissue with a radioexosome signal in liver tissue that was 10X higher than in brain tissue (Figure 4.3D).

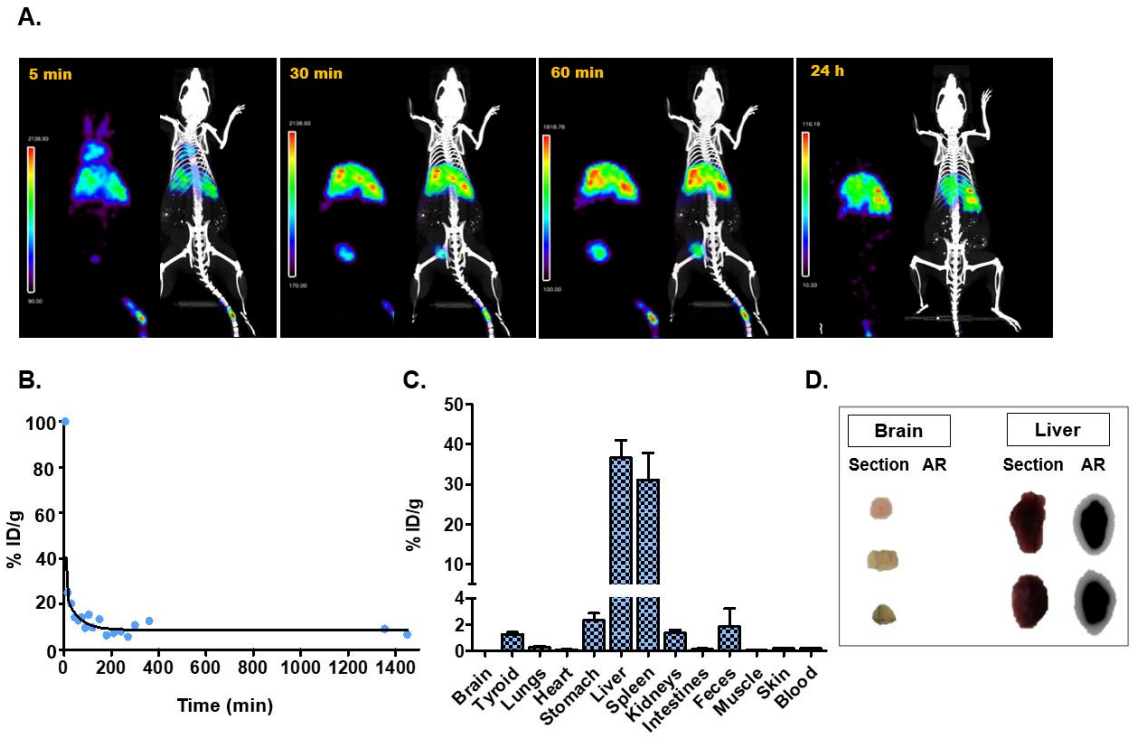

Figure 4.3 Assessment of intravenous administration.

(A) In vivo single photon emission computed tomography (SPECT) and computed tomography (CT) imaging of [^{99m}Tc]-Exo 5 min, 30 min, 60 min, and 24 h post-injection. (B) In vivo blood half-life. (C) Ex vivo biodistribution study 24 h after injection. (D) Histological evaluation by digital autoradiography (AR) and digital picture (section) of brain and liver.

4.3.4.2. Intraperitoneal Administration

The SPECT imaging acquired at 5 min post-injection of [^{99m}Tc]-Exo in healthy mice showed the main localization of the nanotracer in the abdominal cavity. Differences in the biodistribution of the radioactive exosomes were observed over time, with high accumulation in the spleen at 30 min post-injection and in the thyroid region at 3 h post-injection (Figure 4.4A). In vivo measurement of the blood circulation time of the radiotracer showed values 4 fold higher than those observed with intravenous administration (Figure 4.4B) (Table 4.1). Ex vivo biodistribution studies confirmed the accumulation of exosomes observed with SPECT imaging (Figure 4.4C) (Table 4.1), and autoradiography showed [^{99m}Tc]-Exo uptake in liver histological sections with no accumulation in brain. The activity of [^{99m}Tc]-Exo in liver was 2 fold higher than in brain tissue (Figure 4.4D).

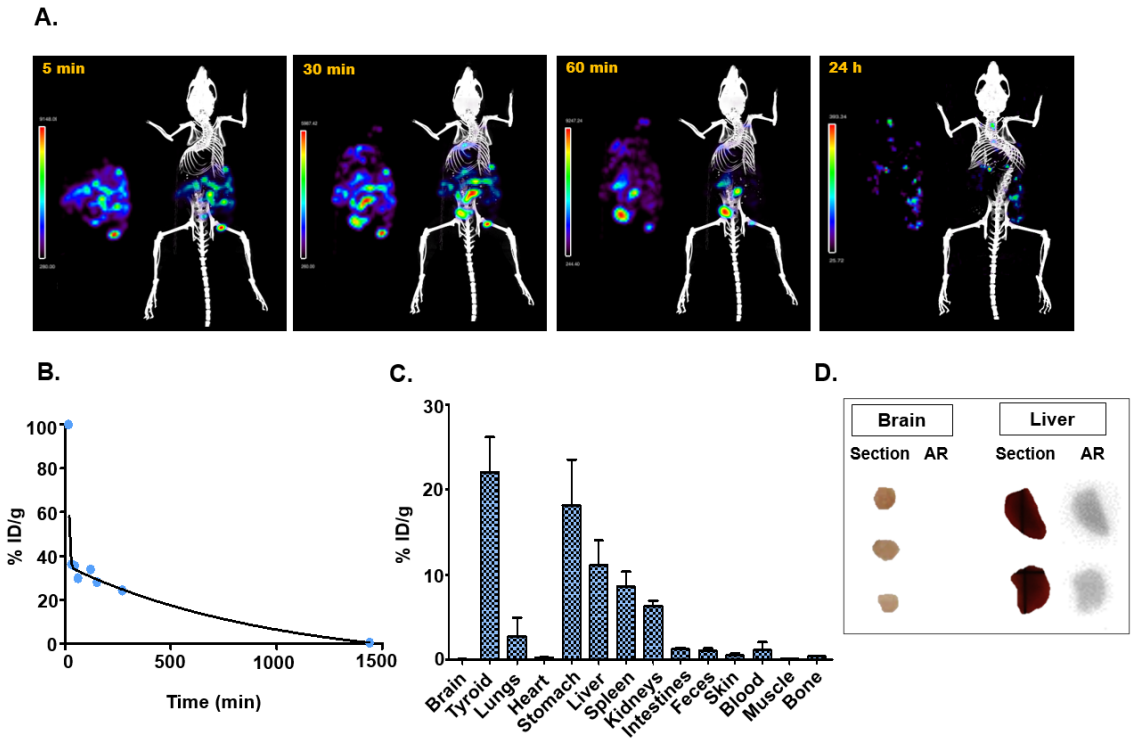

Figure 4.4 Intraperitoneal administration.

(A) In vivo SPECT/CT imaging of [^{99m}Tc]-Exo 5 min, 30 min, 60 min, and 24 h post-injection. (B) In vivo blood half-life. (C) Ex vivo biodistribution study 24 h after injection. (D) Histological evaluation by digital autoradiography (AR) and digital picture (section) of brain and liver.

4.3.4.3. Intranasal Instillation

The SPECT/CT and ex vivo studies were carried out 10 min, 90 min, and 24 h after administration of exosomes. The in vivo SPECT/CT image at 10 min post-injection showed the presence of activity in the nasal cavity and trachea, as well as in the lungs, with no significant changes at 24 h (Figure 4.5A). Measurements in blood samples confirmed a very short blood circulation half-life (Figure 4.5B) (Table 4.1), and ex vivo biodistribution supported the data observed in nuclear images, suggesting the elimination of the nanotracer through the digestive system (Figure 4.5C) (Table 4.1).

Although SPECT did not reveal brain uptake in vivo at any time point during the study, the higher sensitivity achieved with autoradiography enabled us to detect the presence of radioactive exosomes in the brain, specifically in the cerebellum. In this case, the signal intensity of [^{99m}Tc]-Exo in brain tissue was two-fold higher than in liver tissue (Figure 4.5D).

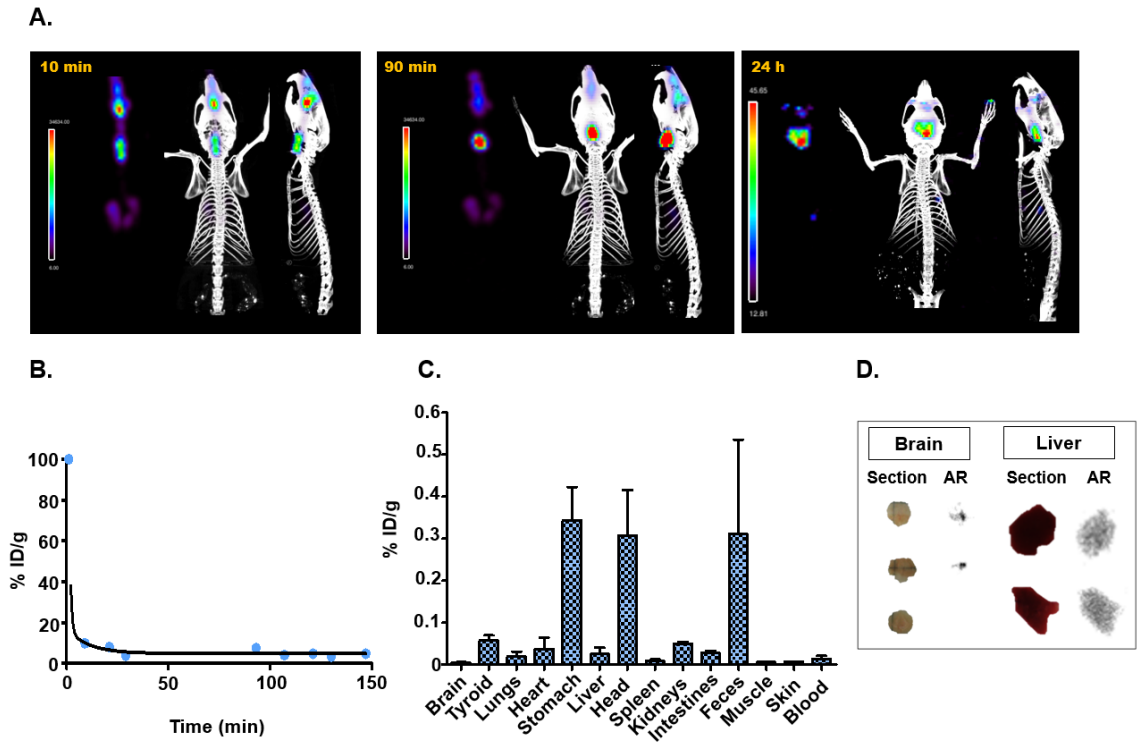

Figure 4.5 Intranasal administration.

(A) In vivo SPECT/CT imaging of [^{99m}Tc]-Exo 10 min, 90 min, and 24 h post-injection; (B) In vivo blood half-life; (C) Ex vivo biodistribution study 24 h after injection; (D) Histological evaluation by digital autoradiography (AR) and digital picture (section) of brain and liver.

Administration route	**$T_{1/2}$ (min)**	**Ex vivo biodistribution (main organs;% ID/g)**
Intravenous injection	3.84	Liver (36.6 ± 7.5); Spleen (31.1 ± 11.6); Stomach (2.1 ± 0.9)
Intraperitoneal injection	15.97	Thyroid (22.0 ± 7.2); Stomach (18.1 ± 9.3); Liver (11.1 ± 5.0)
Intranasal instillation	0.77	Stomach (0.34 ± 0.11); Head (0.31 ± 0.15); Feces (0.31 ± 0.39)

Table 4.1 Summary of pharmacokinetic properties of [^{99m}Tc]-Exo for the different administration routes.

4.4. Discussion

Over the last decade, extracellular vesicles, particularly exosomes, have emerged as new nanometric DDSs [10-12,15]. These are remarkably interesting because of their natural origin, which gives them an inherent cell/tissue targeting mechanism, as well as their lack of toxicity and suitable biocompatibility for possible translation to clinical practice. Although this promising application has been extensively verified, with some exosome-based therapy systems already being assessed in clinical trials [32,33], knowledge of the pharmacokinetic properties of the nanosystems remains incomplete.

In this context, molecular imaging is an ideal tool owing to its non-invasive character as well as its high sensitivity and specificity.

To our knowledge, ours is the first study to assess direct labeling of natural exosomes with the radioisotope ^{99m}Tc (IV) in an ionic salt form ($^{99m}TcCl_4$) using a novel and straightforward methodology. The radiolabeling procedure was optimized using goat milk exosomes because of their scalability and robustness. Previous studies [34,35] achieved radioactive labeling of exosome-like nanovesicles with radioactive technetium using the complex ^{99m}Tc-HMPAO or ^{99m}Tc-tricarbonyl. These approaches required commercial kits with more expensive and complex radioactive precursors that imply longer reaction times and more complex chemistry for the incorporation of the radionuclide. In contrast, our approach obviates the need for chelators and reduces the impact of the chemical reaction on the exosome structure while providing a suitable reaction yield, high purity, and long-term stability. In addition, the use of milk exosomes enabled us to obtain higher amounts of exosomes than with exosome-like vesicles. Furthermore, our reaction was carried out under mild conditions (pH 7, 37 ºC) so as to avoid non-biological conditions that could alter the properties of the exosomes.

The complete characterization of the radioactive exosomes obtained proved that our radiochemical approach did not change the physicochemical properties of the original exosomes such as size and morphology; this is essential for their further use as DDSs. With respect to the mechanism for incorporating the radioisotope into the exosomes, the absence of radiolabeling with ^{99m}Tc (VII) pertechnetate enabled us to rule out biological active transport based on a sodium-dependent iodide transporter, NIS [36]. In fact, the high reaction yields achieved using the ionic form of technetium, ^{99m}Tc (IV), point to passive surface labeling, as reported in previous studies on synthetic liposomes [37-39], where the radionuclide remained in the hydrophobic site by chelation with the phosphonate groups of the membrane [40,41]. Based on these data we interpret that the incorporation and retention of the ^{99m}Tc (IV) into the exosomal membrane is based on the coordination with the phosphonate groups that form the lipids present in the membrane. The high stability of this passive incorporation was confirmed by in vitro studies (in 1X PBS) of the degradation of radioactive exosomes, even after days. Due to the comparable molecular weight of plasma proteins and exosomes we did not attempt similar studies employing mouse plasma. This approach significantly outperformed previous exosome-labeling studies [20], where the instability of the modified exosome led to the release of the probe signaling component, in this case a dye, and produced high levels of unspecific signal in their in vivo application.

Although previous works have widely employed nuclear imaging for the evaluation of in vivo distribution of extracellular vesicles [42,43], this is the first time that this approach is employed in the evaluation of the effect of the administration route in the pharmacokinetic of the exosomes by means of SPECT/CT. The results obtained comparing three different administration routes (intravenous, intraperitoneal, and intranasal) showed noticeable differences, in agreement with previous ex vivo studies using similar exosomes with optical labeling [10].

Intravenous administration confirmed fast blood clearance (< 4 min) and predominantly hepatic uptake, probably due to active uptake by hepatocytes or Kupffer cells. This natural uptake of exosomes in liver and spleen observed in vivo by SPECT/CT imaging, as well as in ex vivo studies with autoradiography and a gamma counter, has been thoroughly reported in other ex vivo studies using exosomes of different origins [10,20,44], as well as with synthetic nanoparticles that are similar to liposomes in morphology and size [45].

In contrast, intraperitoneal administration led to circulation times three- to four-fold longer than those observed with the intravenous route, probably because of their slower incorporation into the bloodstream. In this case, our in vivo imaging and ex vivo biodistribution studies confirmed the existence of abdominal activity for at least 1 h, with lower liver uptake. This route also presented higher uptakes values of [^{99m}Tc]-Exo in lung tissue than the intravenous route, probably owing to aggregation of nanovesicles, as occurs with other synthetic nanoparticles [46]. A significant difference between these routes is the presence of thyroid uptake, which suggests the presence of free Tc, similar to previous studies that showed the natural uptake of other ionic technetium complexes (pertechnetate) in thyroid tissue due to NIS [47,48]. As the stability of [^{99m}Tc]-Exo was verified both in vitro and in vivo, the results point to possible exosome degradation related to their peritoneal absorption, which should be carefully considered before using this route for drug delivery, as the cargo could be released prematurely, e.g., before reaching the target.

Finally, intranasal instillation showed probe accumulation in the mouse head (nose), probably due to the retention of the radioactive [^{99m}Tc]-Exo during the breeding of the animal. In vivo SPECT imaging failed to detect radioactive exosomes in brain tissue. Nevertheless, the higher sensitivity of autoradiography enabled us to confirm the existence of uptake in brain tissue, similar to results previously reported with optical imaging [49].

Our study was subject to a series of limitations stemming from the use of goat milk exosomes. From a chemical standpoint, the synthesis conditions were optimized for the radiolabeling of these exosomes, although the methodology may need to be re-adjusted for other cell-derived exosomes in order to maintain or improve the radiochemical yield, purity, and stability achieved with milk-derived exosomes. From a biological standpoint, pharmacokinetic results can only be applicable to milk-derived exosomes, since it is well known that the exosomal origin induces molecular differences in membrane composition, which modulates their specific tissue tropism [38].

The complete assessment presented in our study confirms the success of our novel radioactive labeling method, which does not alter the original physicochemical properties of milk-derived exosomes and enables the in vivo study of their pharmacokinetic behavior by the non-invasive technique SPECT/CT. Our results also demonstrate the crucial role of the administration route in the biodistribution of the exosomes. In addition, our approach enabled us to confirm pharmacokinetic similarities

between goat milk exosomes and synthetic liposomes [16], thus supporting the use of milk-derived exosomes as a natural substitute for synthetic nanoparticles.

4.5. Bibliography

1. Tran, S.; DeGiovanni, P.J.; Piel, B.; Rai, P. Cancer nanomedicine: a review of recent success in drug delivery. *Clinical and translational medicine* 2017, *6*, p 44.
2. Jain, R.K.; Stylianopoulos, T. Delivering nanomedicine to solid tumors. *Nature Reviews Clinical Oncology* 2010, *7*, p 653.
3. Severino, P.; De Hollanda, L.M.; Santini, A.; Reis, L.V.; Souto, S.B.; Souto, E.B.; Silva, A.M. Advances in nanobiomaterials for oncology nanomedicine. In *Nanobiomaterials in Cancer Therapy*, *Elsevier* 2016, pp. 91-115.
4. Pérez-Herrero, E.; Fernández-Medarde, A. Advanced targeted therapies in cancer: Drug nanocarriers, the future of chemotherapy. *European journal of pharmaceutics and biopharmaceutics* 2015, *93*, pp 52-79.
5. Peinado, H.; Alečković, M.; Lavotshkin, S.; Matei, I.; Costa-Silva, B.; Moreno-Bueno, G.; Hergueta-Redondo, M.; Williams, C.; García-Santos, G.; Ghajar, C.M., et al. Melanoma exosomes educate bone marrow progenitor cells toward a pro-metastatic phenotype through MET. *Nature Medicine* 2012, *18*, p 883.
6. van Niel, G.; D'Angelo, G.; Raposo, G. Shedding light on the cell biology of extracellular vesicles. *Nature Reviews Molecular Cell Biology* 2018, *19*, p 213.
7. Maas, S.L.N.; Breakefield, X.O.; Weaver, A.M. Extracellular Vesicles: Unique Intercellular Delivery Vehicles. *Trends in cell biology* 2017, *27*, pp 172-188.
8. Gould, S.J.; Raposo, G. As we wait: coping with an imperfect nomenclature for extracellular vesicles. *Journal of extracellular vesicles* 2013, *2*.
9. S, E.L.A.; Mager, I.; Breakefield, X.O.; Wood, M.J. Extracellular vesicles: biology and emerging therapeutic opportunities. *Nature reviews. Drug discovery* 2013, *12*, pp 347-357.
10. Munagala, R.; Aqil, F.; Jeyabalan, J.; Gupta, R.C. Bovine milk-derived exosomes for drug delivery. *Cancer letters* 2016, *371*, pp 48-61.
11. Agrawal, A.K.; Aqil, F.; Jeyabalan, J.; Spencer, W.A.; Beck, J.; Gachuki, B.W.; Alhakeem, S.S.; Oben, K.; Munagala, R.; Bondada, S. Milk-derived exosomes for oral delivery of paclitaxel. *Nanomedicine: Nanotechnology, Biology and Medicine* 2017, *13*, pp 1627-1636.
12. Kim, M.S.; Haney, M.J.; Zhao, Y.; Yuan, D.; Deygen, I.; Klyachko, N.L.; Kabanov, A.V.; Batrakova, E.V. Engineering macrophage-derived exosomes for targeted paclitaxel delivery to pulmonary metastases: in vitro and in vivo evaluations. *Nanomedicine: Nanotechnology, Biology and Medicine* 2018, *14*, pp 195-204.
13. Tian, Y.; Li, S.; Song, J.; Ji, T.; Zhu, M.; Anderson, G.J.; Wei, J.; Nie, G. A doxorubicin delivery platform using engineered natural membrane vesicle exosomes for targeted tumor therapy. *Biomaterials* 2014, *35*, pp 2383-2390.
14. Yanez-Mo, M.; Siljander, P.R.; Andreu, Z.; Zavec, A.B.; Borras, F.E.; Buzas, E.I.; Buzas, K.; Casal, E.; Cappello, F.; Carvalho, J., et al. Biological properties of extracellular vesicles and their physiological functions. *Journal of extracellular vesicles* 2015, *4*, p 27066.
15. Thery, C.; Zitvogel, L.; Amigorena, S. Exosomes: composition, biogenesis and function. *Nat Rev Immunol* 2002, *2*, pp 569-579.

16. van der Meel, R.; Fens, M.H.; Vader, P.; Van Solinge, W.W.; Eniola-Adefeso, O.; Schiffelers, R.M. Extracellular vesicles as drug delivery systems: lessons from the liposome field. *Journal of controlled release* 2014, *195*, pp 72-85.
17. Ju, S.; Mu, J.; Dokland, T.; Zhuang, X.; Wang, Q.; Jiang, H.; Xiang, X.; Deng, Z.B.; Wang, B.; Zhang, L., et al. Grape exosome-like nanoparticles induce intestinal stem cells and protect mice from DSS-induced colitis. *Molecular therapy : the journal of the American Society of Gene Therapy* 2013, *21*, pp 1345-1357.
18. Zhang, M.; Viennois, E.; Xu, C.; Merlin, D. Plant derived edible nanoparticles as a new therapeutic approach against diseases. *Tissue barriers* 2016, *4*, p e1134415.
19. Samuel, M.; Chisanga, D.; Liem, M.; Keerthikumar, S.; Anand, S.; Ang, C.-S.; Adda, C.G.; Versteegen, E.; Jois, M.; Mathivanan, S. Bovine milk-derived exosomes from colostrum are enriched with proteins implicated in immune response and growth. *Scientific Reports* 2017, *7*, p 5933.
20. Wiklander, O.P.; Nordin, J.Z.; O'Loughlin, A.; Gustafsson, Y.; Corso, G.; Mager, I.; Vader, P.; Lee, Y.; Sork, H.; Seow, Y., et al. Extracellular vesicle in vivo biodistribution is determined by cell source, route of administration and targeting. *Journal of extracellular vesicles* 2015, *4*, p 26316.
21. Roberts-Dalton, H.; Cocks, A.; Falcon-Perez, J.M.; Sayers, E.J.; Webber, J.; Watson, P.; Clayton, A.; Jones, A.T. Fluorescence labelling of extracellular vesicles using a novel thiol-based strategy for quantitative analysis of cellular delivery and intracellular traffic. *Nanoscale* 2017, *9*, pp 13693-13706.
22. Hwang, J.Y.; Kim, S.T.; Kwon, J.; Lee, J.; Chun, Y.-O.; Han, J.S.; Han, H.-S. Ultrasensitive Fluorescence Monitoring and in Vivo Live Imaging of Circulating Tumor Cell-Derived miRNAs Using Molecular Beacon System. *ACS Sensors* 2018, *3*, pp 2651-2659.
23. Gangadaran, P.; Hong, C.M.; Ahn, B.-C. Current Perspectives on In Vivo Noninvasive Tracking of Extracellular Vesicles with Molecular Imaging. *BioMed Research International* 2017, *2017*, p 11.
24. Lai, C.P.; Mardini, O.; Ericsson, M.; Prabhakar, S.; Maguire, C.A.; Chen, J.W.; Tannous, B.A.; Breakefield, X.O. Dynamic Biodistribution of Extracellular Vesicles in Vivo Using a Multimodal Imaging Reporter. *ACS Nano* 2014, *8*, pp 483-494.
25. Bhaumik, S.; DePuy, J.; Klimash, J. Strategies to minimize background autofluorescence in live mice during noninvasive fluorescence optical imaging. *Lab Animal* 2007, *36*, p 40.
26. Monici, M. Cell and tissue autofluorescence research and diagnostic applications. *Biotechnology annual review* 2005, *11*, pp 227-256.
27. Jacques, S.L. Optical properties of biological tissues: a review. *Physics in Medicine & Biology* 2013, *58*, p R37.
28. van Leeuwen, F.W.; de Jong, M.; de Jong, M.; van Leeuwen, F.; Lahoutte, T.; Evangelista, L.; Barbet, J.; Del Vecchio, S.; Schibli, R.; Committee, E.T.M.I. Molecular imaging: the emerging role of optical imaging in nuclear medicine. Springer: 2014.
29. Pascau, J.; Vaquero, J.; Abella, M.; Cacho, R.; Lage, E.; Desco, M. Multimodality workstation for small animal image visualization and analysis. *Molecular Imaging and Biology* 2006, *8*, pp 97-98.

30. Théry, C.; Amigorena, S.; Raposo, G.; Clayton, A. Isolation and characterization of exosomes from cell culture supernatants and biological fluids. *Current protocols in cell biology* 2006, *30*, pp 3.22. 21-23.22. 29.
31. Owunwanne, A.; Church, L.B.; Blau, M. Effect of oxygen on the reduction of pertechnetate by stannous ion. *Journal of nuclear medicine: official publication, Society of Nuclear Medicine* 1977, *18*, pp 822-826.
32. Dai, S.; Wei, D.; Wu, Z.; Zhou, X.; Wei, X.; Huang, H.; Li, G. Phase I clinical trial of autologous ascites-derived exosomes combined with GM-CSF for colorectal cancer. *Molecular therapy* 2008, *16*, pp 782-790.
33. Escudier, B.; Dorval, T.; Chaput, N.; André, F.; Caby, M.-P.; Novault, S.; Flament, C.; Leboulaire, C.; Borg, C.; Amigorena, S., et al. Vaccination of metastatic melanoma patients with autologous dendritic cell (DC) derived-exosomes: results of thefirst phase I clinical trial. *Journal of translational medicine* 2005, *3*, pp 10-10.
34. Hwang, D.W.; Choi, H.; Jang, S.C.; Yoo, M.Y.; Park, J.Y.; Choi, N.E.; Oh, H.J.; Ha, S.; Lee, Y.S.; Jeong, J.M., et al. Noninvasive imaging of radiolabeled exosome-mimetic nanovesicle using (99m)Tc-HMPAO. *Sci Rep* 2015, *5*, p 15636.
35. Varga, Z.; Gyurkó, I.; Pálóczi, K.; Buzás, E.I.; Horváth, I.; Hegedűs, N.; Máthé, D.; Szigeti, K. Radiolabeling of Extracellular Vesicles with 99mTc for Quantitative In Vivo Imaging Studies. *Cancer Biotherapy and Radiopharmaceuticals* 2016, *31*, pp 168-173.
36. W. Seldin, D.; Simchon, S.; M Jan, K.; Chien, S.; Alderson, P. Dependence of Technetium-99m Red Blood Cell Labeling Efficiency on Red Cell Surface Charge; 1988, Vol. 29, pp. 1710-1713.
37. Jensen, A.T.I.; Rasmussen, P.; Andresen, T.L. Radiolabeling of liposomes and polymeric micelles with PET-isotopes. 2012.
38. Love, W.; Amos, N.; Williams, B.; Kellaway, I. Effect of liposome surface charge on the stability of technetium (99mTc) radiolabelled liposomes. *Journal of microencapsulation* 1989, *6*, pp 105-113.
39. Richardson, V.; Ryman, B.; Jewkes, R.; Jeyasingh, K.; Tattersall, M.; Newlands, E.; Kaye, S. Tissue distribution and tumour localization of 99m-technetium-labelled liposomes in cancer patients. *British journal of cancer* 1979, *40*, p 35.
40. Man, F.; Gawne, P.J.; de Rosales, R.T. Nuclear imaging of liposomal drug delivery systems: A critical review of radiolabelling methods and applications in nanomedicine. *Advanced drug delivery reviews* 2019.
41. Deliconstantinos, G.; Ramantanis, G.; Todorou, D.K. Interaction of 99mTc-labeled liposomes with Walker tumour cells in vitro. Liposome-mediated introduction of thaliblastine into resistant Walker tumour cells. *General pharmacology* 1983, *14*, pp 407-411.
42. Cheng, S.-H.; Yu, D.; Tsai, H.-M.; Morshed, R.A.; Kanojia, D.; Lo, L.-W.; Leoni, L.; Govind, Y.; Zhang, L.; Aboody, K.S., et al. Dynamic In Vivo SPECT Imaging of Neural Stem Cells Functionalized with Radiolabeled Nanoparticles for Tracking of Glioblastoma. *J Nucl Med* 2016, *57*, pp 279-284.
43. Rokka, J.; Snellman, A.; Kaasalainen, M.; Salonen, J.; Zona, C.; La Ferla, B.; Nicotra, F.; Re, F.; Masserini, M.; Forsback, S. 18F-labeling syntheses and preclinical evaluation of functionalized nanoliposomes for Alzheimer's disease. *European Journal of Pharmaceutical Sciences* 2016, *88*, pp 257-266.
44. Morishita, M.; Takahashi, Y.; Nishikawa, M.; Takakura, Y. Pharmacokinetics of exosomes an important factor for elucidating the biological roles of exosomes

and for the development of exosome-based therapeutics. *Journal of pharmaceutical sciences* 2017, *106*, pp 2265-2269.

45. Mirahmadi, N.; Babaei, M.; Vali, A.; Dadashzadeh, S. Effect of liposome size on peritoneal retention and organ distribution after intraperitoneal injection in mice. *International journal of pharmaceutics* 2010, *383*, pp 7-13.
46. Pérez-Campaña, C.; Gómez-Vallejo, V.; Puigivila, M.; Martín, A.; Calvo-Fernández, T.; Moya, S.E.; Ziolo, R.F.; Reese, T.; Llop, J. Biodistribution of Different Sized Nanoparticles Assessed by Positron Emission Tomography: A General Strategy for Direct Activation of Metal Oxide Particles. *ACS Nano* 2013, *7*, pp 3498-3505.
47. Ramos, C.D.; Wittmann, D.E.Z.; Etchebehere, E.C.S.d.C.; Tambascia, M.A.; Silva, C.A.M.; Camargo, E.E. Thyroid uptake and scintigraphy using 99mTc pertechnetate: standardization in normal individuals. *Sao Paulo Medical Journal* 2002, *120*, pp 45-48.
48. Anjos, D.A.; Etchebehere, E.C.; Santos, A.O.; Lima, M.C.; Ramos, C.D.; Paula, R.B.; Camargo, E.E. Normal values of [99mTc] pertechnetate uptake and excretion fraction by major salivary glands. *Nuclear medicine communications* 2006, *27*, pp 395-403.
49. Zhuang, X.; Xiang, X.; Grizzle, W.; Sun, D.; Zhang, S.; Axtell, R.C.; Ju, S.; Mu, J.; Zhang, L.; Steinman, L., et al. Treatment of brain inflammatory diseases by delivering exosome encapsulated anti-inflammatory drugs from the nasal region to the brain. *Molecular therapy : the journal of the American Society of Gene Therapy* 2011, *19*, pp 1769-1779.

CHAPTER 5 . COVALENTLY LABELED FLUORESCENT EXOSOMES FOR IN VITRO AND IN VIVO APPLICATIONS

The content of this chapter has been published as follows: González, M.I., González-Arjona, M., Santos-Coquillat, A., Vaquero, J., Vázquez-Ogando, E., de Molina, A., Peinado, H., Desco, M., Salinas, B. *Covalently Labeled Fluorescent Exosomes for In Vitro and In Vivo Applications*. Biomedicines 2021, 9(1), 81.

5.1. Introduction

Exosomes are considered the smallest extracellular vesicles (50–150 nm) of endosomal origin [1]; their structures consist of a lipid bilayer membrane derived from the parent cell membrane [2]. Based on their physicochemical and structural properties, exosomes constitute a natural alternative to synthetic nanoparticles for developing novel drug delivery systems (DDS). In particular, they are especially suited to substituting for liposomes, due to their similar size and morphology [3,4]. In addition, the roles of exosomes in neural communication and pathological states, such as inflammation, tumorigenesis, and pre-metastatic niche formation [5,6], suggest that they could serve as a natural bio-targeting agent, with better accumulation properties, compared to synthetic nanoparticles [7]. Among the different types of exosomes extracted from natural sources, those derived from plants or food (including milk exosomes) have been widely tested as natural nanoplatforms in therapy and diagnostics due to their low toxicity and lack of immunogenicity [8,9]. Milk exosomes are particularly interesting because their production is suitable, scalable, and economic, and their strength and stability are superior to those of other exosomes [10-12]. These properties support the further development of exosomes as a DDS for translation into the clinical field.

Although exosomes have shown promise as a DDS in preclinical research [11,13], the transfer of these nanovesicles into the clinical field for therapeutic applications requires a better understanding of their in vivo behavior, particularly their biodistribution and organ/tissue targeting capabilities. Non-invasive imaging techniques can provide accurate in vivo information about their pharmacokinetics and biodistribution. Among the different techniques applied in biomedical research, fluorescence confocal imaging is currently highly popular because it provides detailed microscopic images easily, cost-effectively, and rapidly. Optical imaging also offers a highly versatile platform for non-invasive in vivo imaging due to its high sensitivity and the possibility of using a wide variety of probes, based on proteins, enzymes, or antibodies. In addition, optical imaging does not require ionizing radiation, unlike other techniques, such as nuclear (e.g., single photon emission computed tomography or positron emission tomography) or X-ray imaging.

During the last few years, different approaches have been developed for the application of optical imaging to in vitro and in vivo evaluations of extracellular vesicles. These approaches vary from genetic engineering methods for incorporating bioluminescent

proteins [14] or green fluorescent protein (GFP) [15] into the exosome structure, to directly labeling exosomes with fluorescent lipophilic dyes [16]. Due to the complexity of the genetic engineering approach, the use of fluorescent dyes has become the gold standard for visualizing exosomes. Currently, the integration of lipophilic fluorophores, such as dialkylcarbocyanine or PKH dyes, into the exosomal membrane represents the most widely used labeling methodology, due to its simplicity and low cost [17]. Nevertheless, some drawbacks limit the use of labeled exosomes, such as excessive exosome aggregation, the weak bond between the exosome and the fluorophore, which can cause the release of the dye from the exosome to non-targeted cells/tissues, and the instability of the resulting probes, which can result in false signals in optical imaging [17-19].

Here, we describe a direct, straightforward, covalent method for labeling exosomes with commercial fluorescent dyes, which enables in vitro and in vivo assessments with optical imaging techniques.

5.2. Materials and Methods

5.2.1. Isolation of Milk Exosomes

Exosomes were isolated from commercial, fresh pasteurized, semi-skimmed goat milk (El Cantero de Letur, Albacete, Spain). Samples were centrifuged at 4 ºC in 30-mL polycarbonate tubes, in an AVANTI J-30I centrifuge equipped with a Ja 30,50 Ti fixed-angle rotor (Beckman Coulter Instruments, Brea, CA, USA). Briefly, milk was centrifuged 10 min at 5,000 x g and treated with microbial rennet to remove fat globules and milk casein. The resultant supernatant was successively centrifuged for 10 min at 5,000 x g, 35 min at 13,000 x g, and 15 min at 35,000 x g to exclude contaminants, such as cell debris and large vesicles. Then, the milk whey was ultracentrifuged at 100,000 x g for 70 min to precipitate the exosomes. The resultant pellet was washed three times with phosphate-buffered saline (1X PBS) and additionally purified in PD-10 size-exclusion columns (GE Healthcare Bio-Sciences, Uppsala, Sweden). The exosomes were concentrated to achieve the required volume by ultracentrifugation at 100,000 x g for 90 min. The nanovesicles pellet was dispersed in 100 µL 1X PBS and stored at -20 ºC until characterization and subsequent labeling. G values described on the isolation protocol refer to the average relative centrifugal force reached during the centrifugation step, after 5 min acceleration.

5.2.2. Cancer Cell Culture

Glioblastoma (U87) and mouse melanoma (B16F10) cell lines were kindly provided by the Cell Culture Unit of the Experimental Medicine and Surgery Unit at Hospital Universitario Gregorio Marañón (Madrid, Spain) and Centro Nacional de Investigaciones Oncológicas (CNIO) Carlos III (Madrid, Spain), respectively. These cell lines were cultured in Dulbecco's Modified Eagle Medium (DMEM; Gibco, ThermoFisher Scientific, Waltham, MA, USA) supplemented with 10 % fetal bovine serum (FBS; exosome-free, Gibco, ThermoFisher Scientific, Waltham, MA, USA) and 1 % L-glutamine, at 37 ºC, 5 % CO_2, and controlled humidity in 95 % air.

In order to remove extracellular vesicles present in serum, FBS was ultracentrifuged at 100,000 G and 4 ºC for 18 h.

5.2.3. Isolation of Cancer Cell Line-Derived Exosomes

Exosomes were isolated from cancer cell lines U87 and B16F10 according to previous protocols [20]. Briefly, once cells reached approximately 80 % confluence, the cell culture was placed in polycarbonate tubes, and exosomes were harvested in four successive centrifugations at 4 ºC, with an AVANTI J-30I centrifuge equipped with a Ja 30,50 Ti fixed angle rotor (Beckman Coulter Instruments, Brea, CA, USA). The centrifugation steps were: first 10 min at 300 G, then 10 min at 2000 G, then 30 min at 10,000 G, and finally 70 min at 100,000 G. The nanovesicles pellet obtained was washed with 1X PBS and re-isolated at 100,000 G for 70 min. The final pellet of exosomes was dispersed in 200 µL of 1X PBS and stored at −20 ºC until characterization and subsequent labeling. G values described on the isolation protocol refer to the average relative centrifugal force reached during the centrifugation step, after 5 min acceleration.

5.2.4. Protein Content Determination

The protein contents of unlabeled exosomes suspensions were quantified with the Bradford–Coomassie colorimetric assay. This assay employed a ready-to-use Coomassie staining reagent (Sigma-Aldrich, St. Louis, MO, USA), and the assay was performed according to the manufacturer's instructions. Absorbance was measured with a Synergy™ HT Multi-Mode Microplate Reader (Biotek Instruments Inc., Winooski, VT, USA).

5.2.5. Fluorescent Labeling of Exosomes

Unless otherwise noted, all reagents were purchased from Sigma-Aldrich (St. Louis, MO, USA) and used without further purification. Commercial SCy 7.5 and BDP-FL succinimidyl ester fluorophores were acquired from Lumiprobe (Hannover, Germany).

Synthesis of SCy-Exo: a solution of 75 µg exosomes (from goat milk, B16F10, or U87) in 100 µL 1X PBS was mixed with 10 µL SCy 7.5 (17 mM) at pH = 8.5 (with $NaHCO_3$ 0.1 M) and vortexed for 2 h at 4 ºC. The product was purified with Exosome Spin Columns (Invitrogen, Carlsbad, CA, USA).

Synthesis of BDP-Exo: a solution of 75 µg exosomes (from goat milk) in 100 µL 1X PBS was mixed with 10 µL BDP-FL (25 mM) at pH= 8.5 (with $NaHCO_3$ 0.1 M), and vortexed for 2 h at 4 ºC. The product was purified with Exosome Spin Columns (Invitrogen, Carlsbad, CA, USA).

5.2.6. Physicochemical Characterization

The morphology and size of exosomes were evaluated at ICTS Centro Nacional de Microscopía Electrónica (Universidad Complutense de Madrid, Spain). They employed TEM (JEOL JEM-1010, JEOL USA Inc., Peabody, MA, USA), which operated at 100 kV. Exosomes were negatively stained with uranyl acetate on formvar carbon-coated copper grids at room temperature. The hydrodynamic sizes of control and labeled

exosomes samples were measured with a Zetasizer Nano system (Malvern Panalytical, Malvern, UK). Concentrations (particles/mL) of exosomes in suspension as well as nanoparticles size were measured with a NanoSight NS500 (Malvern Panalytical, Malvern, UK), from Centro Nacional de Investigaciones Oncológicas (CNIO, Madrid, Spain), equipped with a high sensitivity sCMOS camera. Camera level and threshold were established in 11 and 10, respectively. Videos were recorded in static conditions and analyzed with NTA 3.1 Build software, and three replicate histograms were obtained for each sample.

5.2.7. Flow Cytometry Analysis

Unlabeled and fluorescently labeled exosomes were evaluated with a Gallios™ 10 color Flow Cytometer (Beckman Coulter Instruments, Brea, CA, USA). A blue-light laser (488 nm; BODIPY 550 SP filter) was employed for analyzing exosomes labeled with BDP-FL. A red-light laser (635 nm; 725/20 filter) was employed for analyzing exosomes labeled with SCy 7.5. The maximum number of events was not restricted during the measurement. For discriminating exosomes from other non-specific events and background, a delimited region was placed in the flow cytometry dot-plot; this gate was adjusted to the expected size range of exosomes.

Flow cytometry data were analyzed with Kaluza™ Acquisition Software (version 1.5; Beckman Coulter, Brea, CA, USA).

5.2.8. In Vitro Stability of Fluorescent Exosomes

In vitro stability was assessed by incubating 75 µg milk exosomes labeled with BDPFL (BDP-MiExo) in 1X PBS for 72 h at 37 ºC. At baseline (0 min), 12 h, 48 h and 72 h, the samples were collected and measured with a HPLC system (Agilent 1200 series; Agilent Technologies, Santa Clara, CA, USA), equipped with a UV absorbance detector and a Yarra SEC-3000 column (300 × 7.8 mm; Phenomenex Inc., Torrance, CA, USA). An isocratic gradient of 1X PBS with a flow rate of 0.2 mL/min was employed with a UV measurement at 503 nm. In addition, HPLC chromatogram of non-labeled milk exosomes was performed to confirm purity of the sample using same gradient and column but with a UV measurement at 254 nm.

5.2.9. Isolation of Primary Mouse Hepatocytes

Animal experiments conducted this project complied with the ARRIVE guidelines and were in accordance with the EU Directive (2010/63/EU) for animal experiments. The HGUGM Animal Care and Use Committee approved all procedures.

Hepatocytes were isolated from adult C57BL/6 mice (12–16 weeks old). These mice were genetically engineered to expressed enhanced green fluorescent protein EGFP on hepatocyte plasma membranes (mG) and Tomato-dye protein on the plasma membranes (mT) of other cell-types. Mice were generated with the Cre/LoxP system by crossing female mice that expressed Cre-recombinase under the control of the albumin promoter (AlbCre mice, B6.Cg-Speer6-ps1Tg(Alb-cre)21Mgn/J, stock# 3574, Jackson Lab, Farmington, CT, USA) and male mice that expressed the double-fluorescent Cre

reporter (mT/mG mice; B6.129(Cg)-Gt(ROSA)26Sortm4(ACTB-tdTomato, EGFP)Luo/J, stock# 7676, Jackson Lab, Farmington, CT, USA) [21].

Primary mouse hepatocytes were isolated with a two-step protocol for hepatic perfusion from the inferior cava vein, according to previously published protocols [22], with some modifications. Briefly, the liver was first perfused with Hank's Balanced Salt Solution (without calcium, magnesium, or phenol-red; Gibco, ThermoFisher Scientific, Waltham, MA, USA), containing 10 mM HEPES (pH 7.4), 0.2 mM EGTA, and 10 U/mL heparin. This was followed by perfusion with Williams E Medium (Gibco, ThermoFisher Scientific, Waltham, MA, USA), containing 10 mM HEPES (pH 7.4) and 0.4 mg/mL collagenase type IV from Clostridium histolyticum (Sigma-Aldrich, St. Louis, MO, USA). After filtering the digested liver through a 100 µm-pore cell strainer, cells were resuspended in attachment media (DMEM:F12 with 10 % FBS supplemented with 5 mM sodium pyruvate, 2 mM L-glutamine, 0.05 % $NaHCO_3$, 20 mM HEPES, 0.12 % glucose, 0.02 % BSA, 100 U/mL penicillin, and 100 µg/mL streptomycin). Next, the mixture was centrifuged at 50 x g, and purified with density gradient centrifugation in an isotonic solution of Percoll (GE Healthcare Bio-Sciences AB, Uppsala, Sweden). After a wash in attachment media with a 50 x g centrifugation, cell viability was checked with Trypan blue.

5.2.10. Confocal Studies of in Vitro Uptake

A 24-well cell culture plate (Corning, NY, USA) was pretreated with a 1:1000 solution of collagen type (I), and one round glass coverslip was added per well. Isolated primary mouse hepatocytes were seeded at a density of 20,000 cells per well and cultured overnight in attachment medium under controlled humidity conditions, in 95 % air and 5 % CO_2, at 37 ºC. Next, cells were incubated for 30 min, 60 min, 120 min, 240 min and 24 h with 5 µg/mL (2.5 µg/well) or 0.5 µg/mL (0.25 µg/well) milk exosomes labeled with SCy 7.5 (SCy-MiExo). Next, the hepatocytes were washed twice with PBS and fixed with 4 % paraformaldehyde (PFA) for 5 min. After removing the PFA and washing with PBS, the glass coverslips were placed on confocal slides and mounted with DAKO mounting medium (Agilent Technologies, Santa Clara, CA, USA), which contained DAPI fluorescent dye, for nuclei staining.

NIR fluorescent signals from SCy-MiExo were captured with a Leica-SPE microscope (Leica Microsystems Inc., Buffalo Grove, IL, USA) equipped with a 635 nm laser. Images were processed with Fiji ImageJ Software (U. S. National Institutes of Health, Bethesda, MD, USA). Exosome uptake was assessed by measuring the fluorescent signals in regions of interest (ROIs) in the perinuclear region of the cell.

5.2.11. In Vivo Optical Imaging

Fluorescent milk exosomes (SCy-MiExo) were administered to healthy CD1 female mice (n = 3 animals, weight 20–25 g). Mice were previously shaved in the abdominal region, and SCy-MiExo solutions were intravenously injected through the lateral tail vein (25 µg, 150 µL in 1X PBS). The in vivo biodistribution of SCy-MiExo was evaluated with an in vivo imaging system (IVIS Spectrum System; PerkinElmer Inc.,

Waltham, MA, USA) at 1 h, 4 h, and 24 h after injection. During image acquisition, mice were maintained under 1.5–2 % isofluorane. Fluorescent detection was performed with an indocyanine green filter set (excitation: 710/760 nm, emission: 810/875 nm), and the exposure time was under 0.5 s. To evaluate the natural behavior of the free SCy 7.5 dye, we conducted a control study with healthy CD1 female mice (n = 2, weight 20–25 g). Briefly, mice received an intravenous injection of commercial SCy 7.5 (17 mM, 150 µL, in 1X PBS). The imaging conditions were the same as those described above for SCy-MiExo imaging, except the exposure time was reduced to 0.2 s. All animals were sacrificed at 24 h post-injection, and the liver, spleen, kidneys, intestines, heart, lungs, brain, and skin were harvested and imaged with the same device.

Fluorescence images were quantified with Living Image Software provided with the IVIS Spectrum System (PerkinElmer Inc., Waltham, MA, USA). We measured the average radiant efficiency of the SCy-MiExo fluorescent signal from ROIs in all the excised organs. The average radiant efficiency was defined as the number of photons (p) that left a square centimeter of tissue per second and radiated into a solid angle of one steradian (sr). The resulting values, expressed in $(p/s/cm^2/sr)/(\mu W/cm^2)$, were normalized to the integration time, binning, f/stop, field of view, illumination intensity, and the ROI area, to ensure comparability between measurements.

5.2.12. Histological Analysis of Hepatic Tissue

At 24 h after the in vivo imaging, mice inoculated with SCy-MiExo, (intravenous administration, n = 3) were sacrificed, and livers were collected. Tissues were prepared for both confocal microscopy and histopathological analysis. Briefly, organs were fixed in 4 % PFA for 24 h, transferred to 70 % ethanol, and embedded in paraffin for routine hematoxylin and eosin histochemical staining.

For confocal imaging, liver tissues were fixed in 4 % PFA for 24 h, dehydrated in a sucrose solution, and embedded in optimal cutting temperature compound (OCT) for cutting into 10-µm sections. Images were acquired with a Leica SP5 microscope (Leica Microsystems Inc., Buffalo Grove, IL, USA) equipped with a 633-nm excitation laser, combined with a 10× dry-objective and a 20× oil-immersion objective. Image processing was carried out with LAS-AF 2.7.3. build 9723 Software incorporated into the microscope and with Fiji ImageJ Software (U. S. National Institutes of Health, Bethesda, MD, USA).

5.2.13. Data Analysis

Data processing and graph construction were performed with Prism 6.0c software (GraphPad Software, La Jolla, CA, USA). Data are expressed as the mean ± standard deviation.

Statistical analysis of the in vitro uptake was performed using one-way Analysis of Variance (ANOVA) and Tukey's multiple comparison test with Prism 8.4.3 software (GraphPad Software, La Jolla, CA, USA), after checking for normality. Significant differences stand for: * ($p \leq 0.05$), ** ($p \leq 0.01$), *** ($p \leq 0.001$), **** ($p \leq 0.0001$).

5.3. Results

The optimized labeling strategy we developed was successful and robust, based on a complete physicochemical characterization of fluorescent nanovesicles derived from milk and cancer cell lines. These novel nanoprobes displayed in vitro and in vivo stability. The applicability of these probes was evaluated by assessing uptake in primary hepatocytes and biodistribution in healthy mice, with confocal microscopy and in vivo optical imaging.

5.3.1. Characterization of Fluorescent Milk Exosomes

Purified milk exosomes (MiExo) labeled with bodipy FL (BDP-FL) and sulfo-cyanine 7.5 (SCy 7.5) showed bright orange and green colors, respectively (Figure 5.1A). To determine the successful attachment of the dye to the exosomes, we compared unlabeled exosomes to purified fluorescent exosomes with flow cytometry. For unlabeled milk exosomes, 0.44 % of events emitted a fluorescent signal at 503 nm and 0.05 % of events emitted a fluorescent signal at 778 nm. For BDP-MiExo and SCy-MiExo, we observed fluorescent signals in 99.56 % (at 503 nm) and 99.98 % (at 778 nm) of the events, respectively (Figure 5.1D).

Transmission electron microscopy (TEM) analyses of fluorescently labeled exosomes showed ‘cup-shaped’ structures typical of extracellular vesicles. The core size was similar to that of control unlabeled nanovesicles (Figure 5.1B), with no morphological alterations. A dynamic light scattering (DLS) analysis showed that the hydrodynamic sizes were 135.31 ± 13.10 nm for BDP-MiExo and 135.33 ± 9.43 nm for SCy-MiExo (Figure 5.1C). With both fluorescent labels, the exosomes slightly increased in hydrodynamic size, compared to the control exosomes (126.12 ± 2.94 nm). Size measurements obtained by Nanoparticle tracking analysis (NTA) for fluorescent labeled exosomes registered quite similar values for SCy-MiExo (134.30 ± 8.50 nm) and BDP-MiExo (140.40 ± 6.30 nm). This technique also reported concentrations of $1.02 \cdot 10^9 \pm 6.20 \cdot 10^7$ particles/mL for BDP-MiExo and $1.65 \cdot 10^9 \pm 1.18 \cdot 10^8$ particles/mL for SCy-MiExo, slightly lower values than those measured for the unlabeled exosome solution ($5.62 \cdot 10^9 \pm 2.29 \cdot 10^8$ particles/mL).

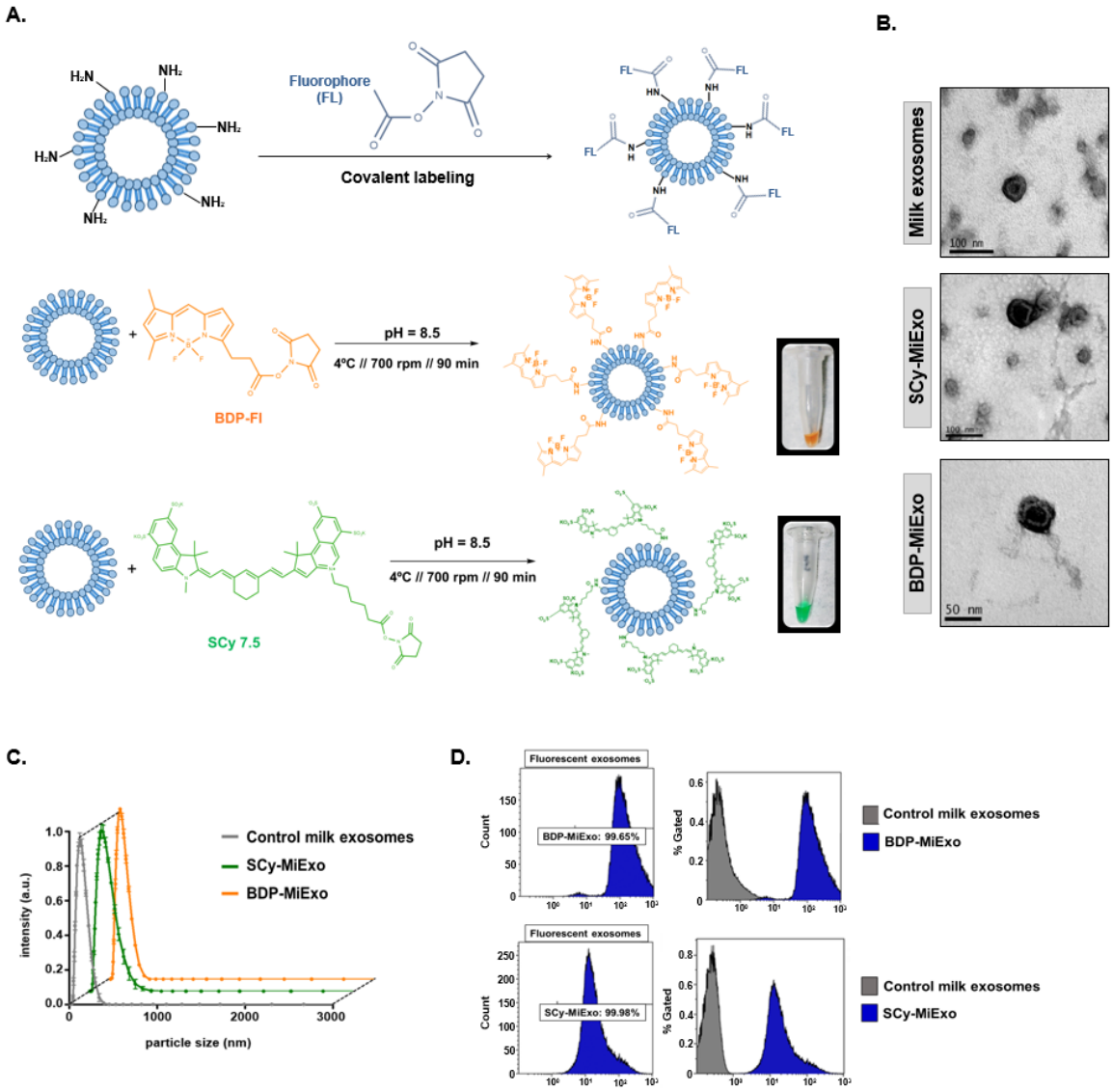

Figure 5.1 Optical labeling and physicochemical characterization of control and fluorescence-labeled milk exosomes (MiExo).

(A) Chemical strategies for labeling exosomes with Bodipy FL (BDP-FL, orange) and sulfo-cyanine 7.5 (SCy 7.5, green), and the resulting fluorescently labeled exosomes in dilution fluids. (B) Transmission electron microscope images for morphological evaluations of exosomes. (C) Size distributions of nanovesicles, evaluated with dynamic light scattering. Data are expressed as the mean ± standard deviation; (D) Flow cytometry results show the abundances of control exosomes (grey) and fluorescent nano-probes (blue). SCy MiExo: SCy 7.5-labeled milk exosomes; BDP-MiExo: BDP-FL-labeled milk exosomes.

5.3.2. Characterization of Fluorescent Cancer Cell Line-Derived Exosomes

Similar to milk exosomes, U87 and B16F10 exosome solutions exhibited a strong green color after labeling with SCy 7.5. Flow cytometry measurements in the size range of exosomes showed fluorescence signal emissions in 99.94 % of events with SCy-labeled U87 exosomes (SCy-U87Exo) and 99.67 % of events with SCy-labeled B16 exosomes (SCyB16Exo, Figure 5.2C). In unlabeled exosomes derived from U87 cells (U87Exo)

and B16F10 cells (B16Exo), 3.03 % and 4.95 % of events, respectively, exhibited fluorescent signals at 778 nm.

Physicochemical characterizations of control and labeled exosomes showed that labeling had minor effects on the morphological properties of these cancer cell line-derived exosomes. TEM imaging and DLS confirmed that SCy-U87Exo samples preserved the morphology and size of the non-labeled controls (Figure 5.2A); the hydrodynamic sizes were 132.00 ± 10.00 nm for control U87Exo and 135.32 ± 11.17 nm for the SCy-U87Exo (Figure 5.2B). Labeled U87Exo also exhibited a similar core size of 123.20 ± 7.00 nm after NTA analysis. However, the number of nanoparticles measured with NTA was slightly lower for SCy-U87Exo, after the chemical reaction ($2.25 \cdot 10^9 \pm 2.05 \cdot 10^8$ particles/mL), compared to control U87Exo ($3.35 \cdot 10^9 \pm 1.42 \cdot 10^8$ particles/mL).

TEM analyses confirmed that SCy-B16Exo showed typical exosome morphology. However, DLS showed a slight reduction in the size distribution, compared to controls (141.77 ± 1.00 for SCy-B16Exo nm vs. 177.00 ± 13.00 for control B16Exo; Figure 5.2B). The NTA analysis confirmed the size reduction of the nanovesicles (139.3 ± 10.2 nm) and revealed a slightly higher number of particles in the suspension of fluorescent SCy-B16Exo compared to unlabeled B16Exo ($5.91 \cdot 10^8 \pm 4.82 \cdot 10^7$ particles /mL vs. $9.59 \cdot 10^8 \pm 1.40 \cdot 10^8$ particles /mL).

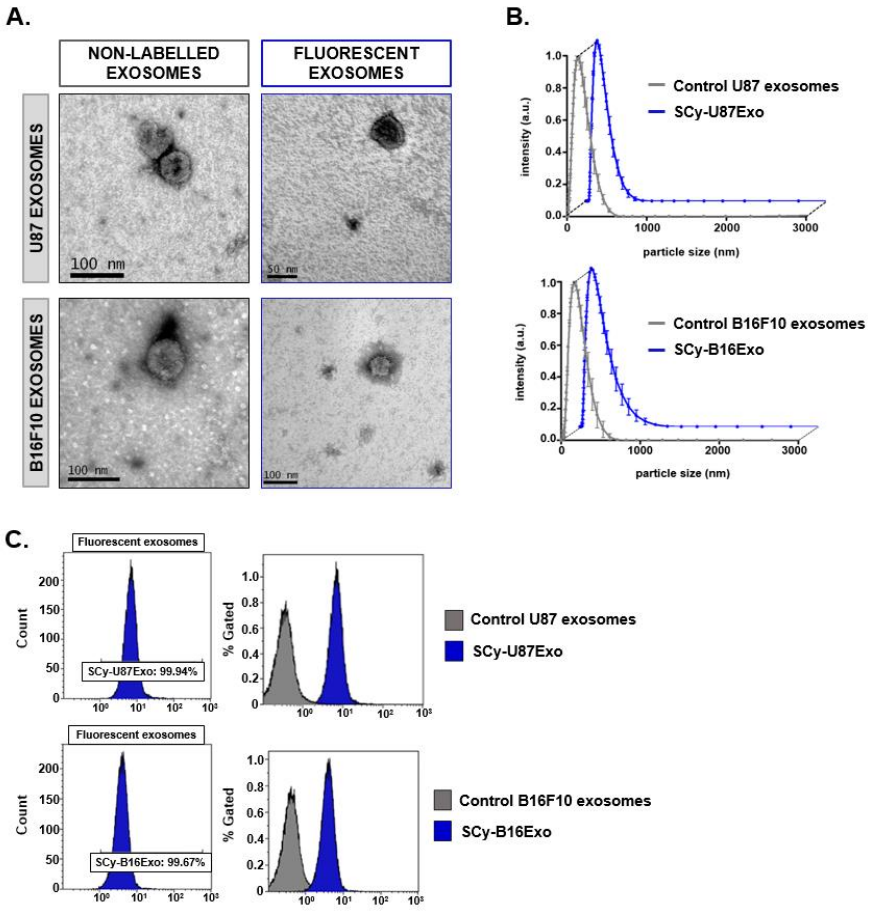

Figure 5.2 Physicochemical characterization of control and fluorescence-labeled cancer cell line-derived exosomes.

(A) Transmission electron microscope images show the nanovesicle morphology. (B) Size distributions of exosomes produced with dynamic light scattering. Data are expressed as the mean ± standard deviation. (C) Flow cytometry results show abundances of control exosomes and the fluorescent nano-probes. SCy: sulfo-cyanine 7.5; U87Exo: exosomes derived from U87 glioblastoma cells; B16Exo: exosomes derived from B16F10 mouse melanoma cells.

5.3.3. In vitro stability of fluorescent exosomes

The temporal stability of exosome labeling was confirmed in a longitudinal in vitro study with high performance liquid chromatography (HPLC). Fluorescent chromatograms of BDP-MiExo showed a single peak at 25.2 min (Figure 5.3), which corresponded to the retention time of pure unlabeled milk exosomes. No peak was registered at 38.3 min, which was the characteristic retention time for free BDP-FL.

A small peak was detected at a retention time of 3.8 min after 72 h of incubation, corresponding to events higher than exosomes, probably due to their aggregation at long time points.

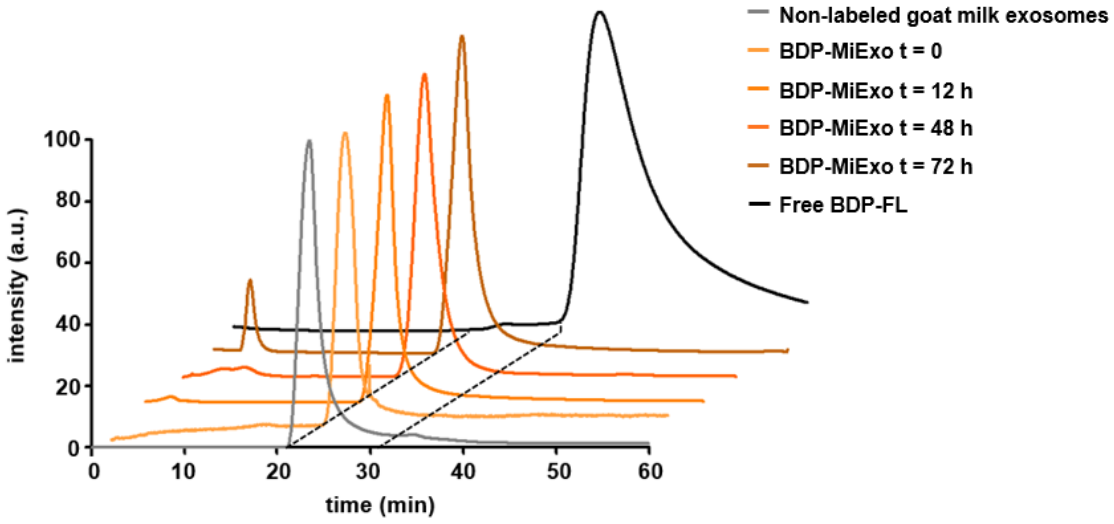

Figure 5.3 In vitro stability of Bodipy FL-labeled milk exosomes (BDP-MiExo) over time, evaluated with high performance liquid chromatography.

It was not possible to assess the stability of exosomes labeled with SCy 7.5 (at 778 nm), due to the limitations of the HPLC equipment. The upper limit of the absorbance detector was 600 nm.

5.3.4. In vitro study of SCy-MiExo

The ability of cells to internalize these natural nanovesicles was assessed with confocal imaging. Hepatocytes were exposed to both high (5 µg/mL) and low (0.5 µg/mL) doses of SCy-MiExo, and fluorescent signals were observed in the cytoplasm, even at short time points (1 h). The exosomes were distributed throughout the cytoplasm, especially in the perinuclear region (Figure 5.4A, 4B), and uptake was dose-dependent (Figure 5.4C). The time to the peak signal depended on the dose of exosomes added; in the near infra-red (NIR) channel, the brightest signals were observed after 24 h of incubation at

the high dose, and after 4 h for the low dose (Figure 5.4C). Values registered at the end point of the experiment (24 h) were statistically different if both dose. Moreover, exosome uptake registered at 24 h in case of 5 µg/mL is highly significant compare to the other time points for the same concentration (Figure 5.4D).

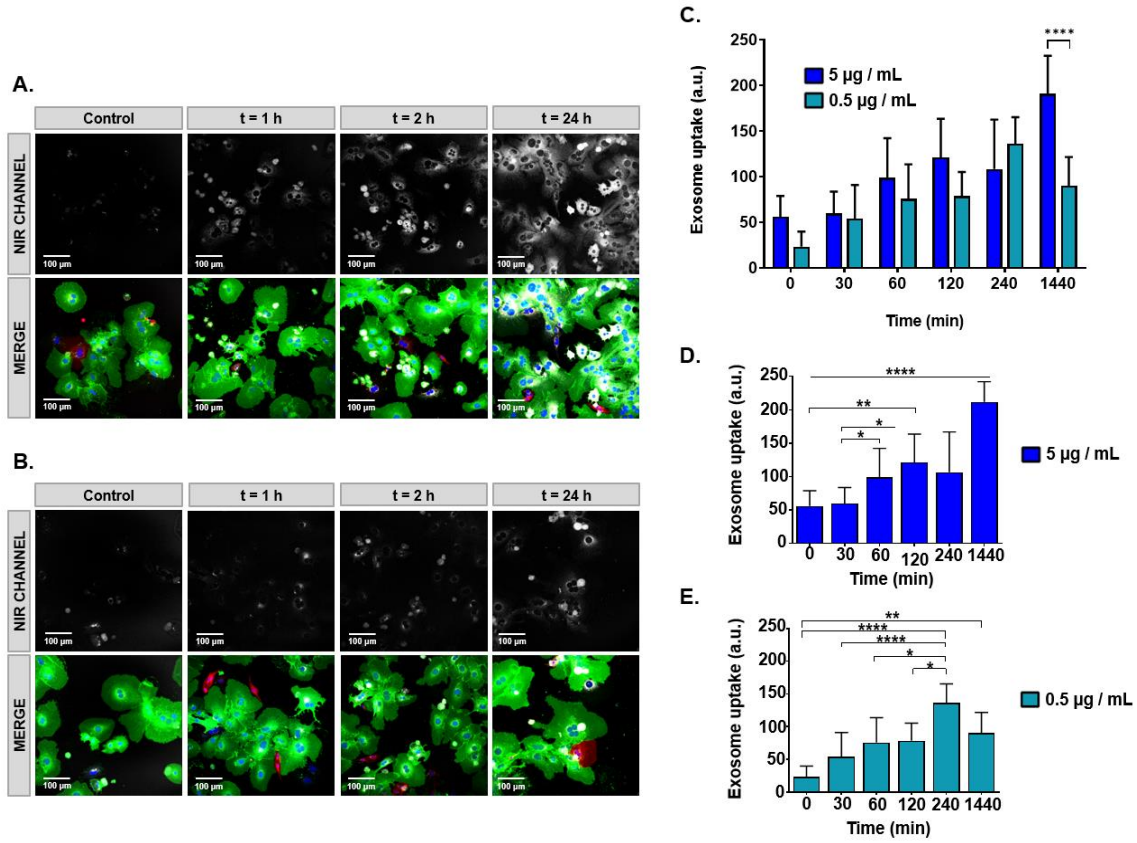

Figure 5.4 Confocal microscope imaging for assessing the uptake of sulfo-cyanine 7.5-labeled milk exosomes (SCy-MiExo) by hepatocytes.

(A, B) Near infrared (NIR, top) and fluorescence images (bottom) taken over time as hepatocytes internalized (A) 5 µg/mL and (B) 0.5 µg/mL of SCy-MiExo. (C) Quantification of the exosome uptake, at different SCy-MiExo concentrations, analyzed in regions of interest. Values were statistically significant between both concentration at 24 h; ****($p \leq 0.0001$). Data are expressed as the mean ± standard deviation. (D) Statistical analysis for the dose of 5 µg/mL: all values were significant compare to 24 h; *($p \leq 0.05$), **($p \leq 0.01$), ***($p \leq 0.001$), ****($p \leq 0.0001$). (E) Statistical analysis for the dose of 0.5 µg/mL; *($p \leq 0.05$), **($p \leq 0.01$), ***($p \leq 0.001$), ****($p \leq 0.0001$).

5.3.5. In vivo and ex vivo studies with SCy-MiExo

In vivo whole-body optical imaging showed that SCy-MiExo was mainly taken up in liver tissues (Figure 5.5A). The signal intensity in this organ increased over time, with maximum values at 24 h (Figure 5.5B). The biodistribution examined ex vivo, in the organs excised at 24 h, confirmed these results. Among all the organs studied, exosome uptake was highest in the liver (Table 5.1). We also detected fluorescent signals in the spleen and kidneys, but no significant uptake was detected in the other harvested organs (Figure 5.5C).

In contrast, in vivo imaging of the free dye showed a homogenous distribution throughout the entire body, and drastic reduction in the fluorescent intensity was observed after 4 h (Figure 5.5A). All of the excised organs evaluated ex vivo after 24 h post-injection showed the free fluorescent signal (Table 5.1). The biodistribution profile of free SCy 7.5 was absolutely different from that of SCy-MiExo (Figure 5.5C).

A histological study of the liver tissue (Figure 5.5D) showed high uptake and a homogeneous distribution of SCy-MiExo. Hematoxylin and eosin stained liver samples showed no significant alterations in liver tissue structure. We only detected some minor alterations related to the exposure to nanometric 'foreign bodies', such as large accumulations of Kupffer cells [23] or some vacuolization in hepatocytes, compared to the normal compartmentation of glycogen inside these hepatic cells (Figure 5.5E).

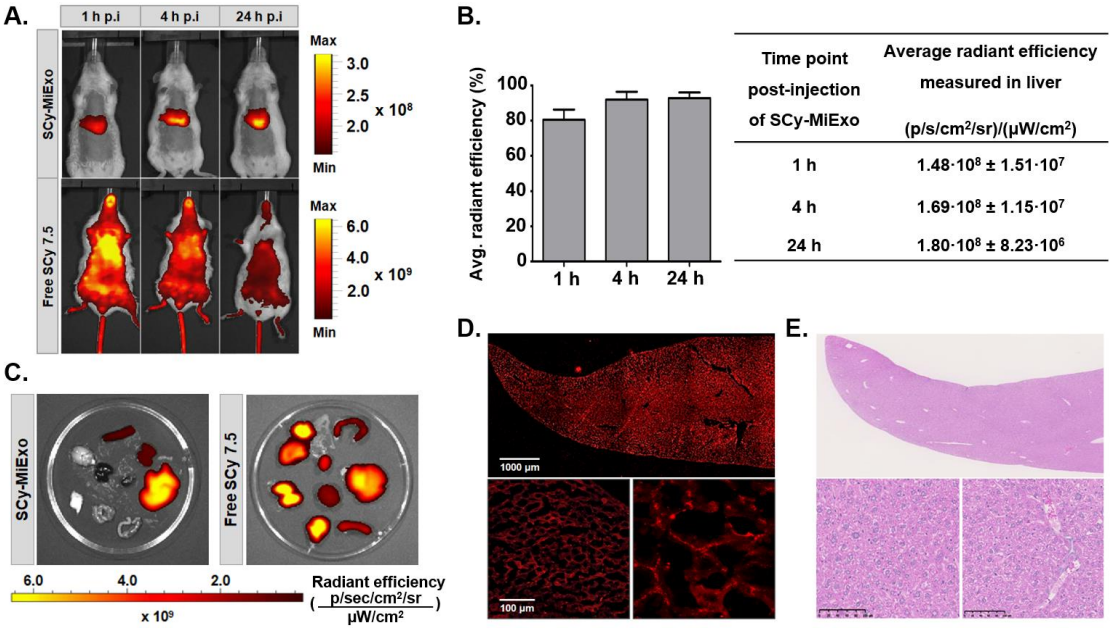

Figure 5. In vivo and ex vivo studies with SCy-MiExo.

(A) In vivo optical imaging of sulfo-cyanine 7.5-labeled milk exosomes (SCy-MiExo, top) and free SCy 7.5 (bottom) in healthy mice. (B) Time course of average radiant efficiency measured in vivo in livers of mice treated with SCy-MiExo. Data are expressed as the % (graph) and in units of p/s/cm^2/sr)/(µW/cm^2) (table), with the mean ± standard deviation. (C) Ex vivo biodistribution of SCy-MiExo (left) and free SCy 7.5 (right) in excised organs. (D) Confocal images of liver sections from mice treated with SCy-MiExo. Right down image presents a zoom of left right image. (E) H&E histological images of liver sections from mice treated with SCy-MiExo.

Organ	SCy-MiExo: ex vivo average radiant efficiency	Free SCy 7.5: ex vivo average radiant efficiency
Liver	$3.36 \cdot 10^8 \pm 5.84 \cdot 10^6$	$9.66 \cdot 10^8 \pm 2.20 \cdot 10^7$
Kidneys	$1.12 \cdot 10^8 \pm 4.72 \cdot 10^6$	$9.47 \cdot 10^8 \pm 7.72 \cdot 10^7$
Small intestine	-	$8.62 \cdot 10^8 \pm 3.50 \cdot 10^8$
Skin	-	$7.56 \cdot 10^8 \pm 3.53 \cdot 10^8$
Lungs	-	$5.35 \cdot 10^8 \pm 3.69 \cdot 10^8$
Intestines	-	$4.87 \cdot 10^8 \pm 2.03 \cdot 10^8$
Heart	-	$4.45 \cdot 10^8 \pm 1.13 \cdot 10^7$
Spleen	$9.94 \cdot 10^7 \pm 4.63 \cdot 10^6$	$3.48 \cdot 10^8 \pm 2.55 \cdot 10^7$
Brain	-	3.29·108 ± 1.05·107

Table 5.1 Ex vivo average radiant efficiencies (p/s/cm^2/sr)/(μW/cm^2) of sulfo-cyanine 7.5-labeled milk exosomes (SCy-MiExo) and free SCy 7.5 measured in organs excised at 24 h post-injection. Data are expressed as the mean ± standard deviation.

5.4. Discussion

Traditionally, the methodology employed in fluorescent exosome labeling for histological and cellular assessments has relied on the passive integration of lipophilic dyes into the exosome membrane [17,24]. However, passive integration implies a weak bond between the exosome structure and the dye, which could lead to the detachment and release of the fluorophore; the free fluorophore can produce false positives or increase the background signal [17]. To resolve these limitations, the present study described a straightforward methodology that ensured strong dye attachment to the exosome by creating covalent bonds between the ester groups of commercial fluorophores and the amine groups present in nanovesicles. This chemical methodology relied on the disposition of free amine groups from transmembrane proteins in the exosome membrane, and it was previously exploited in other protocols for exosome surface engineering with bio-orthogonal functional groups and radioisotopes [25,26]. To our knowledge, this study was the first to optimize this approach for labeling exosomes and to facilitate optical characterizations.

To demonstrate the versatility of our approach, we tested two widely different commercial fluorophores with different hydrophobicities, wavelengths, and chemical structures: BDP-FL and SCy 7.5. Moreover, we tested the approach in different types of exosomes, derived from goat milk and U87 and B16F10 cancer cells. The BDP-FL fluorophore (503 nm excitation) is typically used in preclinical studies of tissues and cells [27,28]. The SCy 7.5 fluorophore (778 nm excitation) is an ideal tool for in vivo applications; it can be detected in the NIR range, which provides relatively deep penetration and avoids the inconvenience of autofluorescence [29]. Moreover, SCy 7.5 is highly soluble in aqueous media, which provides an advantage over the more commonly used NHS ester dyes. For example, Cyanine 7 requires organic solvents for the labeling reaction, which might be toxic or otherwise harm these natural nanovesicles.

Exosomes isolated from goat milk were successfully labeled with both fluorophores. Visually, the intense colors emitted by the purified samples clearly showed that the dyes were incorporated into the exosome structures. Incorporation of the dye was confirmed and quantified with flow cytometry, which showed that 99 % of the exosome population was labeled. Although it is well known that these natural nanoparticles are sensitive to alterations in media conditions, our physicochemical characterization of labeled exosomes showed that the morphological structure of these nanoparticles was not significantly altered. We only observed a slight increase in the hydrodynamic size of fluorescently labeled exosomes compared to controls. This change in size was most likely due to the presence of the fluorophore on the exosome surface. Nevertheless, TEM analyses confirmed that the vesicles were round, with an intact lipid bilayer membrane. The slight reduction in the number of nanovesicles measured with NTA after the labeling reaction could be attributed to some sample loss during the purification step.

We also tested our procedure with two different cancer cell line-derived exosomes (U87 and B16F10). We employed SCy 7.5 for further in vivo experiments due to its convenient physicochemical properties (high solubility and appropriate emission wavelength). Moreover, BDP-Fl fluorophore requires organic media such as dimethyl sulfoxide (DMSO), which could compromise the integrity of the cancer cell line-derived exosomes, less robust than milk exosomes in degrading conditions [12,30].

Similar to the milk exosomes, both glioblastoma (SCy-U87Exo) and melanoma (SCyB16Exo) cell-derived exosomes showed an intense green color after dye binding. Moreover, both samples were efficiently labeled, based on flow cytometry measurements. Similar to the fluorescent milk exosomes, the physicochemical characterization of SCy-U87 exosomes showed that both size and morphology were preserved after the labeling reaction. The slight reduction in the number of nanovesicles detected with NTA could also be explained by a small loss of nanovesicles during the purification step. In contrast, although SCyB16Exo samples showed preserved morphological characteristics, the hydrodynamic size of these fluorescent exosomes was unexpectedly smaller than the size of unlabeled nanovesicles, unlike our findings with the milk and U87 exosomes. Previous studies showed that some exosomes tended to remain in an aggregated state after they are dispersed and stored in a saline solution, due to their surface composition [31]. NTA and DLS analyses could not distinguish between one big particle and two small, aggregated nanovesicles. Thus, exosome surface labeling with fluorophores could reduce their tendency to aggregate, which might lead to higher particle counts and more accurate size distribution measurements.

Large extracellular vesicles, which typically present electron-dense appearance and irregular shape in TEM images [32] were not located in any of the samples analyzed, supporting the exosome nature of the isolated nanovesicles from both milk and cancer cell lines. In addition, DLS and NTA registered homogeneous populations of nanovesicles in the size range of exosomes (30–150 nm) [33].

One of the key points in the development of our chemical approach was the strong attachment of the dye to the nanoparticle, which prevented detachment and release of the free fluorophore. The high stability of labeled exosomes over time was demonstrated with an in vitro longitudinal HPLC study. The absence of a secondary peak at 38.3 min, associated with the free fluorophore, confirmed the absence of free BDP-FL in the sample at all time points, even after 3 days. This finding highlighted the strength of the covalent link established between the fluorophore and the vesicle structure. A small peak at 3.8 min was only detected after long incubation times (72 h). That peak suggested that the milk nanovesicles were beginning to aggregate because our size exclusion columns enabled the larger molecules and nanoparticles to pass through first, and the smaller particles passed through later.

For in vitro and in vivo assessments of these novel optical nanoprobes, we decided to employ the SCy-MiExo vesicles because the milk exosomes showed promise as a DDS [11,34]. We performed in vitro evaluations of SCy-MiExo internalization into primary hepatocytes with confocal imaging. The reason for choosing this cell line was that it is well-known that the liver accumulates nanoparticles of 100–200 nm. We merged the green fluorescent images from the cells with the NIR images of the exosomes and we observed fluorescent exosome uptake even at short time points (30 min), which suggested rapid incorporation, as reported in previous studies of exosomes in tumors and inflammatory cells [35,36]. At all the studied time points, cytoplasmic accumulation was detected in the perinuclear area, similar to findings previously reported for synthetic liposomes of similar size [37]. This result indicated that these nanoparticles showed promise for use as drug delivery platforms. The cellular uptake time curve showed maximal uptake at different time points depending on the exosome dose. These time and dose effects were previously described for milk exosomes incubated with cancer cells [11]. In our case, a low dose (0.5 µg/mL) of SCy-MiExo showed the highest signal at 4 h, then it declined after 24 h. This pattern might reflect the fact that the total amount of exosomes was incorporated inside the hepatocytes after 4 h, then the exosomes were digested by the cells, which led to a decline in the fluorescent signal intensity at the latest time point (24 h). This behavior was previously observed with other cell-derived exosomes, which pointed to the possibility that nanovesicles were degraded after being engulfed by macrophages [35]. The high dose (5 µg/mL) of SCy-MiExo was clearly taken up at initial points (1 and 4 h), but the brightest signal intensity was recorded at 24 h. This result could be due to the high availability of exosomes; thus, after 4 h, exosomes remained available in the cell culture for internalization by hepatocytes at later time points.

The in vivo behavior of fluorescent SCy-MiExo was evaluated with optical imaging. The SCy dye was selected because it showed high hydrophilicity and high intensity emission in the NIR range, which is far from the autofluorescence range of natural biomolecules, such as hemoglobin [38]. We performed longitudinal in vivo imaging of the fluorescent nanovesicles in healthy mice to evaluate their biodistribution over time. Liver accumulation was observed at 1 h post-injection, which confirmed that these nanovesicles were cleared rapidly, primarily through hepatobiliary metabolism. This in

vivo biodistribution and mainly hepatobiliary metabolism was consistent with the pharmacokinetic profile observed in previous studies for small nanoparticles of similar size and shape, like synthetic liposomes or metallic nanoparticles [39]. As a control, we evaluated the in vivo biodistribution of the free dye. We observed high uptake of free SCy in the lungs, and a rapid decline in the fluorescent signal; this decline was linked to rapid renal excretion, evidenced by the high accumulation of free dye in the kidneys at 24 h post-injection. This behavior was typical of free fluorophores [40] and other small molecules [41]. This clear difference in the biodistribution profiles of free SCy 7.5 and fluorescent exosomes indicated that the nanovesicle labeling was robust and stable. A previous study from our group showed that the administration route affected the biodistribution of goat milk exosomes [42]. In that study, nuclear imaging showed the same in vivo biodistribution profile as that obtained in the present study with fluorescent SCy-MiExo, which implied that our approach did not modify the pharmacokinetic properties of the exosomes. Finally, our ex vivo imaging study of the organs confirmed that exosomes mainly accumulated in the liver, spleen, and kidneys, consistent with findings from previous studies that employed exogenous exosomes [17].

In conclusion, we developed a technique for readily determining the natural biodistribution of fluorescently labeled vesicles over time, without requiring the sacrifice of animals. We showed that milk exosomes were mainly taken up and retained in the liver and spleen, due to the phagocytic activity of Kupffer macrophages in these organs [43]. On the other hand, our histological evaluation confirmed that SCy-MiExo accumulation did not cause tissue damage or alterations in liver tissue structure. These observations opened up a novel avenue of approach for deep research on the potential role of milk exosomes in liver-targeting therapies.

This study presented a straightforward methodology for the covalent labeling of exosomes with commercial fluorophores. The reproducibility and robustness of the technique were assessed with two different dyes and several types of exosomes (derived from milk and two types of cancer cells). In all cases, we demonstrated the success of this chemical approach and the preservation of the physicochemical properties of the nanovesicles.

The applicability of this approach was validated with different optical imaging techniques. On the cellular scale, we demonstrated with confocal imaging that covalently labeled exosomes were internalized in hepatocytes. The results confirmed that labeled exosomes rapidly accumulated around the nucleus in a dose-dependent manner. Fluorescent exosomes were also successfully visualized in vivo, where they showed behavior similar to that observed for other synthetic nanoparticles, such as liposomes. These results suggested that our approach could be used for non-invasive in vivo applications, and that fluorescently labeled natural nanovesicles could serve as a substitute for synthetic nanoparticles in therapeutic applications.

5.5. Bibliography

1. Abels, E.R.; Breakefield, X.O. Introduction to extracellular vesicles: biogenesis, RNA cargo selection, content, release, and uptake. Springer: 2016.
2. Andaloussi, S.E.; Mäger, I.; Breakefield, X.O.; Wood, M.J. Extracellular vesicles: biology and emerging therapeutic opportunities. *Nature reviews Drug discovery* 2013, *12*, pp 347-357.
3. Kim, M.S.; Haney, M.J.; Zhao, Y.; Yuan, D.; Deygen, I.; Klyachko, N.L.; Kabanov, A.V.; Batrakova, E.V. Engineering macrophage-derived exosomes for targeted paclitaxel delivery to pulmonary metastases: in vitro and in vivo evaluations. *Nanomedicine: Nanotechnology, Biology and Medicine* 2018, *14*, pp 195-204.
4. Gangadaran, P.; Hong, C.M.; Ahn, B.-C. An update on in vivo imaging of extracellular vesicles as drug delivery vehicles. *Frontiers in pharmacology* 2018, *9*, p 169.
5. Van Niel, G.; d'Angelo, G.; Raposo, G. Shedding light on the cell biology of extracellular vesicles. *Nature reviews Molecular cell biology* 2018, *19*, p 213.
6. Tran, T.-H.; Mattheolabakis, G.; Aldawsari, H.; Amiji, M. Exosomes as nanocarriers for immunotherapy of cancer and inflammatory diseases. *Clinical Immunology* 2015, *160*, pp 46-58.
7. Ohno, S.-i.; Drummen, G.P.; Kuroda, M. Focus on extracellular vesicles: development of extracellular vesicle-based therapeutic systems. *International journal of molecular sciences* 2016, *17*, p 172.
8. Ju, S.; Mu, J.; Dokland, T.; Zhuang, X.; Wang, Q.; Jiang, H.; Xiang, X.; Deng, Z.-B.; Wang, B.; Zhang, L. Grape exosome-like nanoparticles induce intestinal stem cells and protect mice from DSS-induced colitis. *Molecular Therapy* 2013, *21*, pp 1345-1357.
9. Zhang, M.; Viennois, E.; Xu, C.; Merlin, D. Plant derived edible nanoparticles as a new therapeutic approach against diseases. *Tissue barriers* 2016, *4*, p e1134415.
10. Samuel, M.; Chisanga, D.; Liem, M.; Keerthikumar, S.; Anand, S.; Ang, C.-S.; Adda, C.G.; Versteegen, E.; Jois, M.; Mathivanan, S. Bovine milk-derived exosomes from colostrum are enriched with proteins implicated in immune response and growth. *Scientific Reports* 2017, *7*, p 5933.
11. Munagala, R.; Aqil, F.; Jeyabalan, J.; Gupta, R.C. Bovine milk-derived exosomes for drug delivery. *Cancer letters* 2016, *371*, pp 48-61.
12. Pieters, B.C.; Arntz, O.J.; Bennink, M.B.; Broeren, M.G.; van Caam, A.P.; Koenders, M.I.; van Lent, P.L.; van den Berg, W.B.; de Vries, M.; van der Kraan, P.M. Commercial cow milk contains physically stable extracellular vesicles expressing immunoregulatory TGF-β. *PLoS one* 2015, *10*, p e0121123.
13. Sun, D.; Zhuang, X.; Xiang, X.; Liu, Y.; Zhang, S.; Liu, C.; Barnes, S.; Grizzle, W.; Miller, D.; Zhang, H.-G. A novel nanoparticle drug delivery system: the anti-inflammatory activity of curcumin is enhanced when encapsulated in exosomes. *Molecular Therapy* 2010, *18*, pp 1606-1614.
14. Gangadaran, P.; Li, X.J.; Lee, H.W.; Oh, J.M.; Kalimuthu, S.; Rajendran, R.L.; Son, S.H.; Baek, S.H.; Singh, T.D.; Zhu, L. A new bioluminescent reporter system to study the biodistribution of systematically injected tumor-derived bioluminescent extracellular vesicles in mice. *Oncotarget* 2017, *8*, p 109894.
15. Suetsugu, A.; Honma, K.; Saji, S.; Moriwaki, H.; Ochiya, T.; Hoffman, R.M. Imaging exosome transfer from breast cancer cells to stroma at metastatic sites

in orthotopic nude-mouse models. *Advanced drug delivery reviews* 2013, *65*, pp 383-390.

16. Dominkuš, P.; Stenovec, M.; Sitar, S.; Lasič, E.; Zorec, R.; Plemenitaš, A.; Žagar, E.; Kreft, M.; Lenassi, M. PKH26 labeling of extracellular vesicles: characterization and cellular internalization of contaminating PKH26 nanoparticles. *Biochimica et Biophysica Acta (BBA)-Biomembranes* 2018, *1860*, pp 1350-1361.
17. Yi, Y.W.; Lee, J.H.; Kim, S.-Y.; Pack, C.-G.; Ha, D.H.; Park, S.R.; Youn, J.; Cho, B.S. Advances in analysis of biodistribution of exosomes by molecular imaging. *International journal of molecular sciences* 2020, *21*, p 665.
18. Jensen, E.C. Use of fluorescent probes: their effect on cell biology and limitations. *The Anatomical Record: Advances in Integrative Anatomy and Evolutionary Biology* 2012, *295*, pp 2031-2036.
19. Bertagna, F.; Bisleri, G.; Motta, F.; Merli, G.; Cossalter, E.; Lucchini, S.; Biasiotto, G.; Bosio, G.; Terzi, A.; Muneretto, C. Possible role of F18-FDG-PET/CT in the diagnosis of endocarditis: preliminary evidence from a review of the literature. *The international journal of cardiovascular imaging* 2012, *28*, pp 1417-1425.
20. Petersen, K.E.; Manangon, E.; Hood, J.L.; Wickline, S.A.; Fernandez, D.P.; Johnson, W.P.; Gale, B.K. A review of exosome separation techniques and characterization of B16-F10 mouse melanoma exosomes with AF4-UV-MALS-DLS-TEM. *Analytical and bioanalytical chemistry* 2014, *406*, pp 7855-7866.
21. Muzumdar, M.D.; Tasic, B.; Miyamichi, K.; Li, L.; Luo, L. A global double-fluorescent Cre reporter mouse. *genesis* 2007, *45*, pp 593-605.
22. Benveniste, R.; Danoff, T.M.; Ilekis, J.; Craig, H.R. Epidermal growth factor receptor numbers in male and female mouse primary hepatocyte cultures. *Cell Biochemistry and Function: Cellular biochemistry and its modulation by active agents or disease* 1988, *6*, pp 231-235.
23. Sadauskas, E.; Wallin, H.; Stoltenberg, M.; Vogel, U.; Doering, P.; Larsen, A.; Danscher, G. Kupffer cells are central in the removal of nanoparticles from the organism. *Particle and fibre toxicology* 2007, *4*, p 10.
24. Shen, L.-M.; Quan, L.; Liu, J. Tracking exosomes in vitro and in vivo to elucidate their physiological functions: implications for diagnostic and therapeutic nanocarriers. *ACS Applied Nano Materials* 2018, *1*, pp 2438-2448.
25. Smyth, T.; Petrova, K.; Payton, N.M.; Persaud, I.; Redzic, J.S.; Graner, M.W.; Smith-Jones, P.; Anchordoquy, T.J. Surface functionalization of exosomes using click chemistry. *Bioconjugate chemistry* 2014, *25*, pp 1777-1784.
26. Faruqu, F.N.; Wang, J.T.-W.; Xu, L.; McNickle, L.; Chong, E.M.-Y.; Walters, A.; Gurney, M.; Clayton, A.; Smyth, L.A.; Hider, R. Membrane Radiolabelling of Exosomes for Comparative Biodistribution Analysis in Immunocompetent and Immunodeficient Mice-A Novel and Universal Approach. *Theranostics* 2019, *9*, p 1666.
27. Irwin, C.P.; Portorreal, Y.; Brand, C.; Zhang, Y.; Desai, P.; Salinas, B.; Weber, W.A.; Reiner, T. PARPi-FL-a fluorescent PARP1 inhibitor for glioblastoma imaging. *Neoplasia* 2014, *16*, pp 432-440.
28. Carney, B.; Kossatz, S.; Reiner, T. Molecular imaging of PARP. *Journal of Nuclear Medicine* 2017, *58*, pp 1025-1030.
29. Mac, J.T.; Núñez, V.; Burns, J.M.; Guerrero, Y.A.; Vullev, V.I.; Anvari, B. Erythrocyte-derived nano-probes functionalized with antibodies for targeted

near infrared fluorescence imaging of cancer cells. *Biomedical optics express* 2016, *7*, pp 1311-1322.
30. Liao, Y.; Du, X.; Li, J.; Lönnerdal, B. Human milk exosomes and their microRNAs survive digestion in vitro and are taken up by human intestinal cells. *Molecular nutrition & food research* 2017, *61*, p 1700082.
31. Bosch, S.; De Beaurepaire, L.; Allard, M.; Mosser, M.; Heichette, C.; Chrétien, D.; Jegou, D.; Bach, J.-M. Trehalose prevents aggregation of exosomes and cryodamage. *Scientific reports* 2016, *6*, p 36162.
32. Théry, C.; Ostrowski, M.; Segura, E. Membrane vesicles as conveyors of immune responses. *Nature reviews immunology* 2009, *9*, pp 581-593.
33. Zocchi, M.R.; Tosetti, F.; Benelli, R.; Poggi, A. Cancer nanomedicine special issue review anticancer drug delivery with nanoparticles: Extracellular vesicles or synthetic nanobeads as therapeutic tools for conventional treatment or immunotherapy. *Cancers* 2020, *12*, p 1886.
34. Agrawal, A.K.; Aqil, F.; Jeyabalan, J.; Spencer, W.A.; Beck, J.; Gachuki, B.W.; Alhakeem, S.S.; Oben, K.; Munagala, R.; Bondada, S. Milk-derived exosomes for oral delivery of paclitaxel. *Nanomedicine: Nanotechnology, Biology and Medicine* 2017, *13*, pp 1627-1636.
35. Su, M.-J.; Aldawsari, H.; Amiji, M. Pancreatic cancer cell exosome-mediated macrophage reprogramming and the role of microRNAs 155 and 125b2 transfection using nanoparticle delivery systems. *Scientific reports* 2016, *6*, p 30110.
36. Roberts-Dalton, H.; Cocks, A.; Falcon-Perez, J.M.; Sayers, E.J.; Webber, J.; Watson, P.; Clayton, A.; Jones, A.T. Fluorescence labelling of extracellular vesicles using a novel thiol-based strategy for quantitative analysis of cellular delivery and intracellular traffic. *Nanoscale* 2017, *9*, pp 13693-13706.
37. Bellavance, M.-A.; Poirier, M.-B.; Fortin, D. Uptake and intracellular release kinetics of liposome formulations in glioma cells. *International journal of pharmaceutics* 2010, *395*, pp 251-259.
38. Yakimov, B.P.; Gogoleva, M.A.; Semenov, A.N.; Rodionov, S.A.; Novoselova, M.V.; Gayer, A.V.; Kovalev, A.V.; Bernakevich, A.I.; Fadeev, V.V.; Armaganov, A.G. Label-free characterization of white blood cells using fluorescence lifetime imaging and flow-cytometry: molecular heterogeneity and erythrophagocytosis. *Biomedical optics express* 2019, *10*, pp 4220-4236.
39. van der Meel, R.; Fens, M.H.; Vader, P.; Van Solinge, W.W.; Eniola-Adefeso, O.; Schiffelers, R.M. Extracellular vesicles as drug delivery systems: lessons from the liposome field. *Journal of controlled release* 2014, *195*, pp 72-85.
40. Guo, D.; Xu, S.; Huang, Y.; Jiang, H.; Yasen, W.; Wang, N.; Su, Y.; Qian, J.; Li, J.; Zhang, C. Platinum (IV) complex-based two-in-one polyprodrug for a combinatorial chemo-photodynamic therapy. *Biomaterials* 2018, *177*, pp 67-77.
41. Fernandez, A.; Le Bon, C.; Baumlin, N.; Giusti, F.; Crémel, G.; Popot, J.-L.; Bagnard, D. In Vivo Characterization of the Biodistribution Profile of Amphipol A8-35. *The Journal of membrane biology* 2014, *247*, pp 1043-1051.
42. González, M.I.; Martín-Duque, P.; Desco, M.; Salinas, B. Radioactive labeling of milk-derived exosomes with 99mTc and in vivo tracking by SPECT imaging. *Nanomaterials* 2020, *10*, p 1062.
43. Almeida, J.P.M.; Chen, A.L.; Foster, A.; Drezek, R. In vivo biodistribution of nanoparticles. *Nanomedicine* 2011, *6*, pp 815-835.

CHAPTER 6 . GOAT MILK EXOSOMES AS NATURAL NANOPARTICLES FOR DETECTING INFLAMMATORY PROCESSES BY OPTICAL IMAGING

The content of this chapter has been published as follows: González, M.I.*, Santos-Coquillat, A.*, Clemente-Moragón, A., González-Arjona, M., Albaladejo-García, V., Peinado, H., Muñoz, J., Ximénez-Embún, P., Ibañez, B., Oliver, E., Desco, M., Salinas, B. *Goat Milk Exosomes As Natural Nanoparticles for Detecting Inflammatory Processes By Optical Imaging* Small 2021, 2105421.

Authors signaled by an asterisk (*) have contributed equally to the research article.

In this chapter, only part of the published research article has been included.

6.1. Introduction

Extracellular vesicles (EVs) are signaling particles without replicative capacity, released by cells to the biological fluids with the aim of controlling intercellular communication [1,2]. Among these secreted particles, exosomes have been described as one of the smallest EVs (30–150 nm) and are of endosomal origin [3]. They carry and exchange proteins, lipids, miRNA, or DNA between diverse cell types [1,4]. These nanometric EVs have important roles in different biological processes, including tumor metastasis and tissue regeneration, and have been proposed as prognostic markers for different diseases [5].

In light of their transport function, exosomes are currently under consideration as novel agents for diagnosis and therapy, especially as drug delivery systems (DDS). Traditionally, this application has been covered by various synthetic nanoparticles, principally liposomes [6,7]. Current barriers to the clinical use of biofunctionalized nanoparticles include lack of batch to batch reproducibility and toxicity. Naturally derived nanoparticles such as exosomes are increasingly being proposed as an alternative to synthetic nanoparticles to overcome some of those limitations, thanks to their natural origin, (phospho)lipid bilayer structure, and nanometric size [8].

Among the possible sources, milk exosomes are notable for their easy production and high sample volumes in comparison with culture fluid or blood plasma. With this approximation, a high yield, harmless, and cost-effective production of non-tumor exosomes can be obtained for use as a scalable source [9]. In addition, the non-toxic and non-immunogenic behavior of milk exosomes in healthy models has been demonstrated [10,11], as has as their application as carriers for chemotherapeutic/ chemopreventive agents [12]. Although these characteristics have been evaluated in exosomes from different milk sources such as human, pig, rat, camel, and horse [8], to the authors' knowledge goat milk exosomes have not yet been investigated.

Aside from the great potential of EVs in cancer therapy [5,6], milk exosomes have been implicated in the regulation of inflammatory processes through miRNA tracking [13]. Moreover, milk exosomes are rapidly trapped by macrophages [14,15] as part of the

clearance activity that these cells, along with neutrophils, carry out when foreign agents are detected [16-18]. This natural targeting and their nanometric size support the use of milk exosomes in the diagnosis and therapy of inflammation underlying the pathogenesis of diseases such as atherosclerosis, chronic obstructive pulmonary disease, asthma, and cancer [19,20].

The main aim of this work was the evaluation of exosomes isolated from goat milk for use as natural nanoprobes in the detection of inflammatory processes. This evaluation was performed through their fluorescent labeling and further in vitro and in vivo assessment by means of optical imaging. The internalization of these fluorescent exosomes in inflammatory M0, M1, and M2 macrophages in vitro was evaluated by means of confocal imaging and flow cytometry. Once the capacity of macrophages to internalize the exosomes was demonstrated in vitro, it was evaluated in vivo in a mouse peritonitis model in comparison with healthy mice by assessing the biodistribution of the probe through optical imaging. Finally, exudates from the peritonitis model were analyzed using flow cytometry and confocal imaging to confirm the in vivo uptake of the nanoparticles by specific inflammatory cell populations (macrophages and neutrophils).

6.2. Materials and Methods

6.2.1. Isolation of Milk Exosomes

Exosomes were isolated by differential centrifugation and ultracentrifugation, complemented with size exclusion chromatography. All steps of the isolation protocol were carried out at 4 °C in an AVANTI J-30I centrifuge (Beckman Coulter Instruments, CA, USA), fitted out with a Ja 30,50 Ti fixed-angle rotor (k factor = 280) and 30-mL polycarbonate tubes, as already described in the literature [21,22]. Commercial pasteurized semi-skimmed goat's milk (El Cantero de Letur, Spain) was centrifuged at 5,000 x g for 10 min to remove fat globules (MFGs). Microbial rennet was then added to improve the precipitation of casein. Resultant milk whey was centrifuged at 5,000 and 13,000 x g for 10 and 35 min respectively, then 15 min at 35,000 x g and finally 70 min at 100,000 x g. This process enables the precipitating of exosomes excluding large extracellular vesicles and cell debris. The exosomal pellet was washed thrice with phosphate-buffered saline (1X PBS) and then purified with PD-10 columns (GE Healthcare Bio-Sciences AB, IL, USA). Exosomes were re-isolated at 100,000 x g for 90 min and the resultant pellet was dispersed in 100–200 µL of 1X PBS. Exosomes suspension was stored at −20 °C until used.

6.2.2. Fluorescence Labeling of Exosomes

Goat milk exosomes were labeled with BODIPY-FL NHS ester (BDP) or Sulfo-Cyanine 5 (SCy-5) (Lumiprobe, Germany), following previously described protocols [22]. Suspension of 100 µg of milk exosomes in 100 µL of 1X PBS was adjusted to pH 8.5 using a 0.1 M $NaHCO_3$ solution. Then, exosomes were mixed with 10 µL of BDP-FL (12.5 mM) or SCy-5 (17 mM) and vortex for 2 h at 4 °C. Free fluorophore residues were removed by purification with Exosome Spin Columns (Invitrogen, CA, USA).

6.2.3. Fluorescence Labeling Characterization

Flow cytometry: Flow cytometry analysis was performed using a Gallios ten color Flow Cytometer (Beckman Coulter Instruments, CA, USA). Exo-BDP suspensions were excited employing a blue light laser (Excitation: 488 nm; detection FL1 Emission: 525/20nm) and a red light laser (Excitation: 633 nm detection FL6 Emission: 660/20nm) was used for the excitation of Exo-SCy5 suspensions. Data were analyzed using FlowJo (Ashland, OR, USA) software.

Fluorescence emission assessment: The fluorescence spectra of Exo-BDP and Exo-SCy5 were recorded using a NanoDrop 3300 fluorospectrometer (Thermo Fisher Scientifc, CA, USA), measuring Exo-BDP with the Blue LED with λ excitation = 515 nm and Exo-SCy5 with the White LED with λ excitation = 665 nm.

6.2.4. Cell Culture

RAW 264.7 (ATCC TIB-71) murine cell line was used as a model of inflammatory response mediated by macrophages. For maintenance of the cell line the medium was changed every other day and cells were cultured in Dulbecco's MEM (D6429, Sigma Aldrich, MO, USA) with 10 % Fetal Bovine Serum (FBS, gibco, 10 270) and 1 % penicillin, streptomycin and amphotericin B (17-745H, Lonza, Switzerland) incubated at 37 °C with 5 % CO_2. Subculturing was performed with a cell scraper (3011, Corning Costar, NY, USA).

6.2.5. XTT Assay

Metabolic activity of macrophages was measured at 24 and 48 h using CyQUANT TM XTT assay (Invitrogen, Thermo Fisher Scientifc, CA, USA), a non-toxic technique that quantitatively measures the cellular redox potential, providing an estimation of viability. 1.5×10^4 cells were seeded on a 48-well plate (Corning Costar, NY, USA) and 5, 0.5, and 0.05 μg/mL dose of exosomes were added (Mi-Exo, Exo-BDP, Exo-SCy5). Each well received 140 μL of XTT dye, and the plates were incubated for 180 min at 37 °C. Absorbance of each well was measured using a plate-reader (680 XR, BIO-RAD Laboratories, CA, USA) at 450 nm. Each condition was analyzed in triplicate.

6.2.6. LDH Assay

LDH Cytotoxicity assay kit (Pierce, Thermo Fisher Scientifc, CA, USA) is a colorimetric method that quantifies cellular cytotoxicity based on the plasma membrane damage. RAW 264.7 were seeded on 96-well plates at a concentration of 1.5×10^4 cells and evaluated after 48 h of Mi-Exo, Exo-BDP or Exo-SCy5 incubation (5, 0.5, and 0.05 μg/mL). Briefly, 10 μL of sterile ultrapure water or lysis buffer were added to control conditions, corresponding to spontaneous release or maximum LDH release, and cultured for 45 min in an incubator at 37 °C with 5 % CO_2. After this time, 50 μL of each condition/sample medium was transferred to a 96-well plate and mixed with 50 μL of reaction Mixture. The new plate was incubated at RT for 30 min in darkness and finally, 50 μL of Stop Solution was added to each sample. Absorbance of each well was measured using a plate-reader (680 XR, BIO-RAD Laboratories, CA, USA) at 450/655 nm.

6.2.7. In Vitro Fluorescence Uptake

RAW 264.7 cells were plated on 24-well plates with glass coverslips at 1.5×10^4 cells per cm^2 in complete DMEM. 5, 0.5, and 0.05 μg/mL dose of Exo-BDP were added to evaluate the uptake level after 5 min, 1, 4, and 24 h. Cells growing on the glass coverslips were fixed with 3.7 % formaldehyde solution for 10 min after the exosomes uptake. After formaldehyde was removed, cells were washed three times with PBS and stained with Phalloidin-iFluor 555 Reagent (ab176756, Abcam, UK) for actin and DAPI staining (D9542, Sigma Aldrich, MO, USA) for nuclei during 20 min at RT (Room Temperature) and in darkness. Dako Fluorescence Mounting Medium (Agilent, CA, USA) was used to prepare the coverslips for microscopy and left to cure overnight. Cells were observed using a confocal microscope (Leica-SPE, Leica Microsystems, Germany) at 488 nm (Exo-BDP), 555 nm (Phalloidin) and 405 nm (DAPI). ROI (region of interest) of the fluorescent images was calculated using ImageJ software taking an average 50 cells per condition.

6.2.8. Macrophages Activation

Macrophages were activated with 30 ng/mL IL-4 (Peprotech, UK) for M(IL-4) and 20 ng/mL of IFN-γ (Peprotech, UK) and 100 ng/mL LPS (Sigma Aldrich, MO, USA) for M(IFN-γ+LPS). M(IL-4) population was identify as M2 and M(IFN-γ+LPS) as M1. RAW 264.7 cells were seeded on 24-well plates with glass coverslips or 12-well plates at 1.5×10^4 cells per cm^2 in complete DMEM for confocal microscopy or flow cytometry, respectively. After 24 h of stimuli, 0.5 μg/mL of Exo-BDP were added to be evaluated by confocal microscopy and flow cytometry.

6.2.9. In Vitro Flow Cytometry

For flow cytometry RAW 264.7 cells were seeded at a concentration of 2×10^6 cells per cm^2 in 12-well plates. Cells were detached with trypsin/EDTA (T3924, Sigma Aldrich, MO, USA) and washed twice with PBS after each centrifugation. Propidium iodide (P4864, Sigma Aldrich, MO, USA) was used in order to evaluate the cell viability after the stimuli and Exo-BDP uptake. A Gallios flow cytometer was used and analyzed with the Flowjo (Ashland, OR, USA) software.

6.2.10. In Vivo and Ex Vivo Fluorescence Imaging

All animal experiments were carried out in accordance with the EU Directive (2010/63EU) and Recommendation 2007/526/EC, enacted in Spanish law under Real Decreto 53/2013. Animal protocols were approved by the local ethics committees and the Animal Protection Area of the Comunidad Autónoma de Madrid.

In vivo assessment of the selectivity of the nanoparticle towards inflammatory processes was assessed using a well-established mouse model of thioglycolate-induced peritonitis [23,24]. Briefly, 8–13-week-old wild-type C57BL/6 mice (n = 6) were intraperitoneally injected with 1 mL of thioglycolate (BD211716). Three hours after the thioglycolate injection, the animals received an intravenous (i.v.) administration of Exo-SCy5 (100 μL in PBS, 20 μg) through the tail vein. As control group for the evaluation of the natural biodistribution of the nanoparticles, healthy animals (n = 6) were also injected

with the nanoparticles, employing same imaging protocol. In vivo fluorescence image acquisition was performed with an IVIS Spectrum 200 In vivo Imaging System (Perkin Elmer, MA, USA) 6 and 21 h after exosome injection, both in peritonitis and control mice, using a Cy5.5 filter, Em = Cy5.5, Ex = Cy5.5. During image acquisition mice were kept anesthetized with 2.5 % isofluorane in 100 % of O_2 via facemask. Analysis and quantification of the images was performed with Living Image 4.4 Software (Perkin Elmer).

After the last time point of the image acquisition (24 h post injection of thioglycolate and 21 h post Exo-SCy5 administration) animals were sacrificed, a peritoneal lavage was carried out and organs of interest (intestine, liver, spleen, heart, and lungs) were harvested to perform ex vivo assessment by fluorescence imaging. Fluorescence was quantified as average radiant efficiency, expressed as mean ± SD, in $(p/s/cm^2/sr)/(\mu W/cm^2)$.

6.2.11. Flow Cytometry of Exudates

Exosome uptake by myeloid cells (macrophages and neutrophils) was assessed by flow cytometry after in vivo imaging acquisition. Exudates were obtained from thioglycolate-induced peritonitis mice (n = 6), after the latest imaging time-point (21 h). For the evaluation of autofluorescence of inflammatory cells, we also included a control group with peritonitis but without nanoparticles administration (n = 6). For exudate collection, animals were sacrificed and peritoneal lavage performed with 2 mL of saline (NaCl, 0.9 %). Samples were gently centrifuged (200 g, 5 min) and washed with 1X PBS. Cells were then incubated for 30 min with a rat PE-conjugated anti-mouse Ly6G (Clone: 1A8, 551 461, BD Pharmingen, CA, USA) antibody or a rat PE-Cy7-conjugated anti-mouse F4/80 antigen pan-macrophage marker (Clone: BM8, 123 114, BioLegend, CA, USA) antibody. After the incubation, cell nuclei were stained with DAPI (D8417, Sigma Aldrich, MO, USA). All samples were filtered using 100 µm Cell Strainer (352 360, Falcon) before the analysis for exactly 60 s of constant medium flow in a FACS Canto-3L flow cytometer equipped with DIVA software (BD Biosciences, NJ, USA). All experiments were conducted at the CNIC-Cellomics Unit.

6.2.12. Exosome Uptake Analyses

Flow cytometry was used to evaluate the uptake of fluorescent exosomes into myeloid cells isolated from peritoneal exudates. The entire cell sample was labeled with DAPI and dead cells (positive labeling for DAPI) were excluded from the analysis. Within the live cell population, macrophage and neutrophil populations were selected using F4/80 and Ly6G markers, respectively. On the identified populations we measured the median fluorescence intensity (MFI) in the FL6 channel (APC), corresponding to Exo-SCy5. In addition, the percentage of the population positive for probe incorporation was determined in both cell lines. All results were analyzed using FlowJo software (Ashland, OR, USA).

6.2.13. Cell Sorting and Immunofluorescence

To confirm and visualize the internalization of the Exo-SCy5 probe by confocal microscopy, the cell populations present in the peritoneal exudates were isolated by sorting, at the wavelength of the probe (630 nm), using an Aria Cell Sorter at the CNIC-Cellomics Unit.

Once sorted, cells were gently centrifuged (200 G, 5 min) and fixed in 2 % paraformaldehyde. After fixation, cells were washed with 1X PBS and placed onto Superfrost Plus slides (Thermo Fisher Scientifc, CA, USA), until samples were dehydrated and cells stuck to the slide. Then, cells were blocked in 1X PBS and 3 % normal goat's serum, and then incubated overnight at 4 °C with a rat anti-mouse CD68 (Clone: FA-11, MCA1957, BIO-RAD Laboratories, CA, USA) antibody. After that, cells were incubated for 1 h with an anti-rat Alexa Fluor-488 conjugated-secondary antibody. After washing thrice with 1X PBS, they were incubated overnight at 4 °C with a rat PE-conjugated anti-mouse Ly6G antibody, counterstained with DAPI to visualize the nuclei and covered with Fluoroshield (F6182, Sigma Aldrich, MO, USA). Images were then acquired with a Leica SP8 Confocal Navigator Microscope available at CNIC's Microscopy Unit.

6.2.14. Statistics

All data are represented as mean ± standard deviation (SD). Comparisons between PBS group and Mi-Exo treated group were performed with Student's t tests. XTT statistical analysis was performed using two-way Analysis of Variance (ANOVA) and Tuckey's multiple comparison test. LDH statistical analysis was performed using one-way ANOVA and Tuckey's multiple comparison. Statistical analysis of macrophages uptake employing different concentrations and time points in confocal imaging was performed by two-way ANOVA and post-hoc Student-NewmanKeuls multiple comparisons test. Analysis of the fluorescence intensity of the macrophages populations was performed using two-way ANOVA and Tuckey's multiple comparison test. For in vivo and ex vivo peritonitis data a KS Normality test was used to determine if variables followed a normal distribution. Comparisons between control and Exo-SCy5 groups were performed by Student's t test. All data were analyzed using Prism software 8.4.3 (Graph pad, Inc.) except confocal macrophages uptake, performed with SPSS. Differences were considered statistically significant for p values below 0.05.

6.3. Results and Discussion

6.3.1. Fluorescence Labeling and Physicochemical Characterization of Exo-BDP and Exo-SCy5

In order to assess the behavior of goat milk exosomes in inflammatory processes, we used a chemical approach previously published by our group to fluorescently label the nanoparticles, creating two exosome-based optical probes [22]. The specific dyes employed in the labeling were selected based on the biological application: for in vitro assessment, the nanoparticles were labeled with the commercial fluorophore BODIPYFL (Exo-BDP) as in our previous studies [22], while for in vivo experiments,

Sulfo-Cyanine 5 (Exo-SCy5) was selected for its favorable emission in the far red spectrum. The labeling success was demonstrated by fluorescence emission measurements using a fluorospectrometer, which registered over 4000 relative fluorescent units in both cases. Additionally, the fluorescence of the resulting probes was evaluated by flow cytometry (Figure 6.1), showing an intense peak between 10^5 and 10^6 for both Exo-BDP and Exo-SCy5. The whole analyzed population could be considered 100 % positive for the labeling, as the control's autofluorescence of 10^1–10^3 relative fluorescent units did not overlap with that of the labeled exosomes in either wavelength.

The absence of morphological modifications after labeling was proven using TEM, showing that exosomes maintained their typical cup-shape appearance after the labeling reaction (Figure 6.1). Moreover, NTA eliminated the possibility of any significant alterations in the sizes of the exosomes, which measured 142.20 ± 2.80 nm (Exo-BDP) and 140.10 ± 3.80 nm (Exo-SCy5) (Figure 6.1). NTA also confirmed that the samples were highly enriched with exosomes after optical labeling and purification, showing values of $2.46 \cdot 10^{11} \pm 3.81 \cdot 10^9$ particles/mL for Exo-BDP and $2.72 \cdot 10^{11} \pm 4.00 \cdot 10^9$ particles/mL for Exo-SCy5. The slight reduction in the number of labeled particles compared with the control was acceptable, considering the loss of sample during purification.

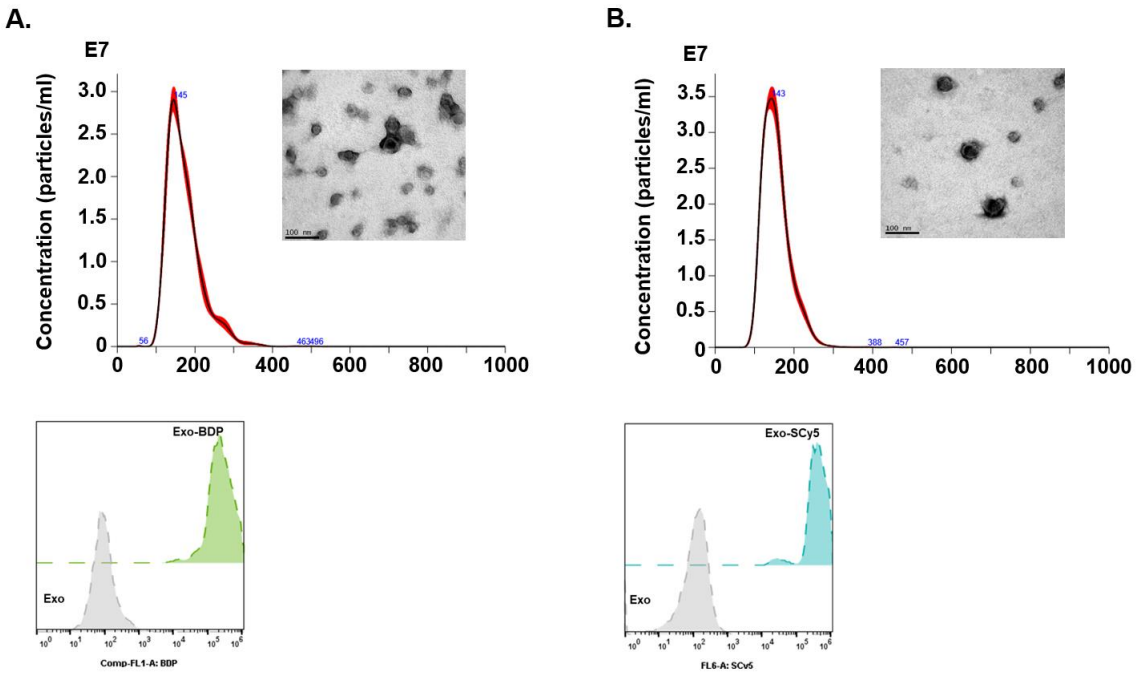

Figure 6.1 Physicochemical characterization of fluorescent milk exosomes.

The assessment includes NTA analysis, TEM images (100,000 X), and flow cytometry for (A) Exo-BDP and (B) Exo-SCy5.

6.3.2. Cytocompatibility Evaluation

XTT assay results (Figure 6.2) showed that cells maintained their viability in the presence of different doses of Mi-Exo, Exo-SCy5, and Exo-BDP at 24 h and 48, despite

the labeling of the nanoparticles. Nevertheless, at 24 h an increase in metabolic activity was found at the higher dose (5 µg/mL) of each nanoparticle type. This behavior has also been observed with other extracellular vesicles, for instance as a macrophage proliferation after 24 h and 48 of exposure [25]. A similar effect was previously found with other milk exosomes [26-28], with cell metabolic activity increasing after exposure to the nanoparticles at different time points. This effect could be related to the fact that the macrophages are phagocytosing at 24 h and therefore, the metabolic activity increases at 24 h and decreases at 48 h, as most of the exosomes have already been internalized. An LDH assay was also performed with our novel nanoparticles (data not shown) to evaluate their cytotoxicity, based on the release of lactate dehydrogenase due to potential damage to the plasma membrane. These studies showed no significant differences 48 h after the addition of exosomes at various concentrations (5, 0.5, and 0.05 µg/mL), in accord with the results obtained with XTT.

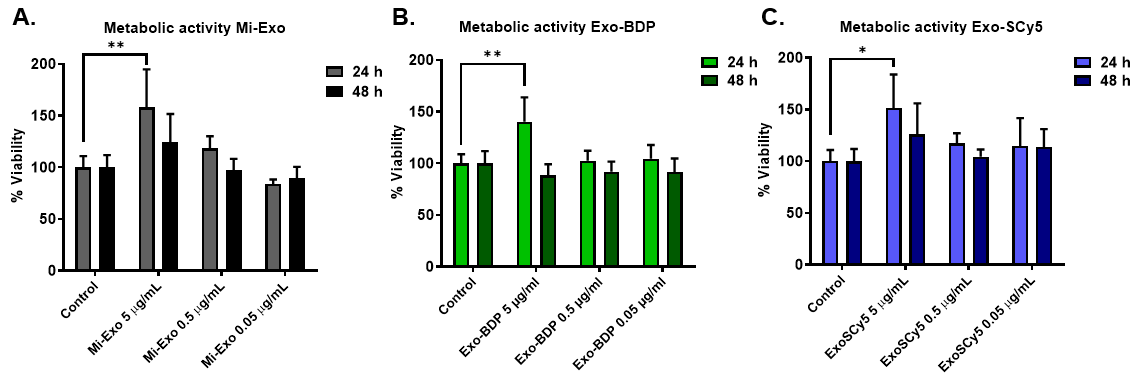

Figure 6.2 In vitro metabolic activity evaluation with RAW 264.7 cells.

Metabolic activity levels by XTT assay after 24 and 48 h of dose of (A) Mi-BDP, (B) Exo-BDP, and (C) Exo-SCy5 (5 µg/mL, 0.5 µg/mL, and 0.05 µg/mL). Statistical analysis by two-way ANOVA and Tukey's multiple comparisons test; P values below 0.05: * $p < 0.05$, ** $p < 0.01$.

6.3.3. In Vitro Uptake Studies Using Confocal Imaging of RAW 264.7 Cells

The evaluation of intracellular uptake of Exo-BDP at different concentrations (5, 0.5, and 0.05 µg/mL) by RAW 264.7 cells was assessed using confocal microscopy at 5 min, 1, 4, and 24 h (Figure 6.3). Figure 6.3A presents the confocal images 24 h after exosome addition at the three dosages. The 5 µg/mL dose induced the greatest incorporation of the exosomes into the cells, with almost all the cytoplasmic area positive for the Exo-BDP (green). This result can be correlated with the increase in metabolic activity observed at 24 h as measured with the XTT assay (Figure 6.2C). Figure 6.3B shows the uptake time course for the different concentrations of Exo-BDP (5, 0.5 and 0.05 µg/mL). All concentrations showed significant differences over time and between dosages ($p < 0.00001$ for both time and dosage).

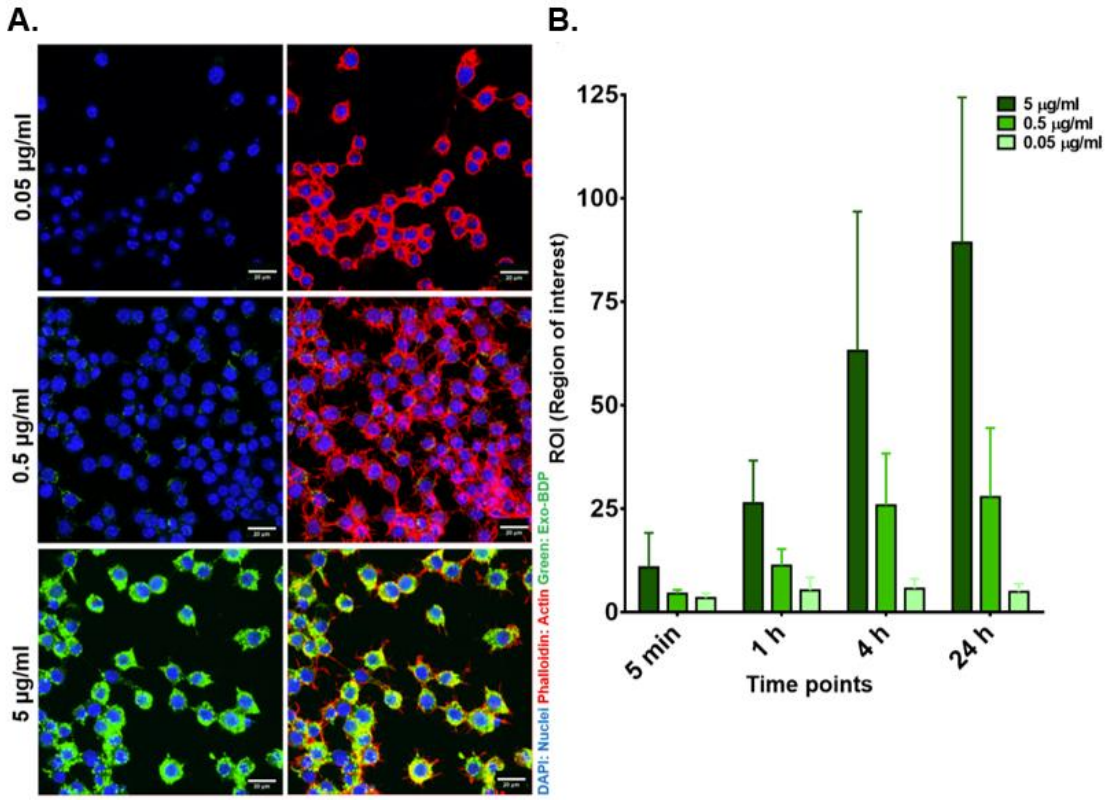

Figure 6.3 Assessment of exosome uptake by RAW 264.7 macrophages.

(A) Confocal images of macrophages after 24 h of exposure to different concentrations of exosomes. Blue (DAPI), red (phalloidin) and green (Exo-BDP). (B) Quantification of fluorescent exosome uptake by RAW 264.7 cells in confocal imaging. Statistical analysis by ANOVA and post-hoc Student-Newman-Keuls multiple comparisons test.

6.3.4. In Vitro Assessment of Selective Uptake of Exo-BDP by M1, M2, and M0 Macrophages

Once we confirmed the uptake of the probe in macrophages, we evaluated the selectivity of the nanoprobe toward specific macrophage populations. Macrophage phenotypes (non-activated or activated) depend on their function and localization. Macrophages with these different phenotypes may incorporate the nanoprobe differently, showing different in vivo uptake. Activated macrophages (Mϕ) are mainly classified as M1 (proinflammation) and M2 (anti-inflammation) macrophages [29,30]. M1 macrophages induce a type I immune response, killing microorganisms and tumor cells. M2 macrophages participate in a type II immune response by removing cellular debris residues and promoting angiogenesis [31].

Using flow cytometry, we quantified Exo-BDP uptake in the different macrophage populations. To this purpose, we selected the intermediate concentration (0.5 µg/mL) of exosomes to better mimic the in vivo scenario. M0, M1, and M2 populations were evaluated after 1, 4, and 24 h of exposure to the exosomes (Figure 6.4A). The activated population with the proinflammatory stimuli (M1) presented higher uptake than the untreated cells (M0) and M2 (two-way ANOVA, $p < 0.01$). These differences were

greater at 24 h, when the M1 population presented a fivefold increase in fluorescence compared with M0 and M2 (Figure 6.4B). This result was confirmed by confocal microscopy at the same time points (Figure 6.4C). At 1 h, Exo-BDP uptake did not differ among the macrophage populations, but from 4 h and up to 24 h there was a clear difference in the cytoplasmic disposition of the nanoparticles, with the proinflammatory phenotype M1 presenting tighter packing in contrast to a more diffuse distribution in the control M0 cells.

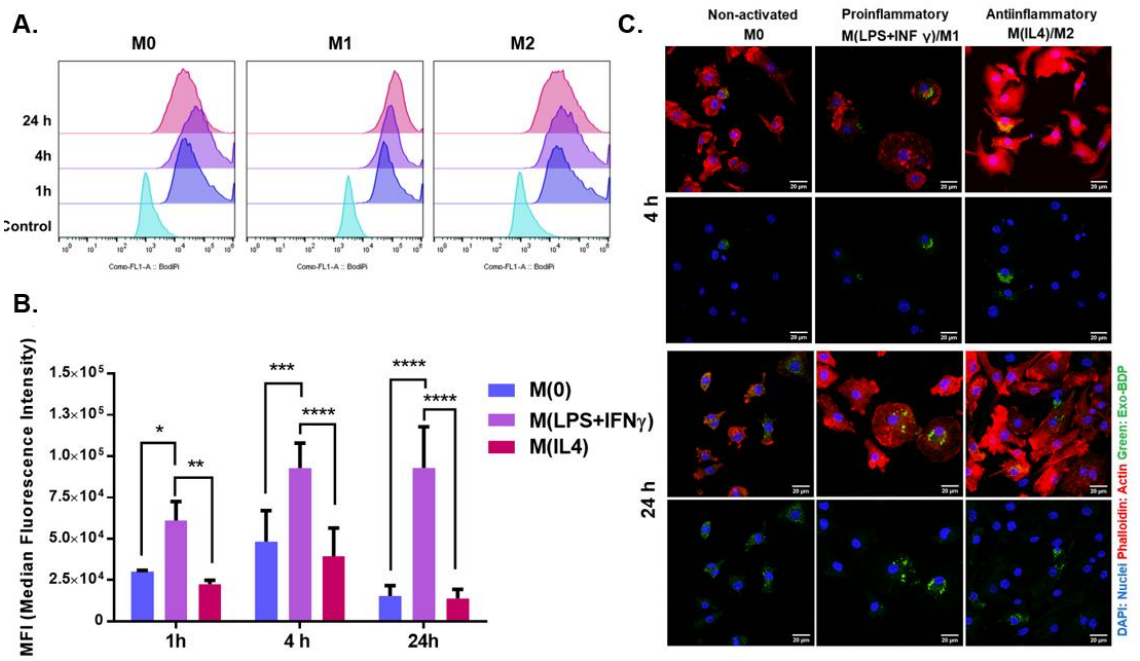

Figure 6.4 In vitro evaluation of Exo-BDP uptake in macrophage populations.

(A) Flow cytometry of M0, M1, and M2 populations after 1, 4, and 24 h of incubation with 0.5 µg/mL Exo-BDP. (B) Quantification of fluorescence intensity by flow cytometry. Statistical analysis by two-way ANOVA and Tukey's multiple comparisons test; p values below 0.05: * $p < 0.05$, ** $p < 0.01$, *** $p < 0.001$, **** $p < 0.0001$. (C) Confocal images of Exo-BDP uptake in M0, M(IFN-γ+LPS)/M1, and M(IL-4)/M2 populations. IFN-γ, interferon gamma; LPS, lipopolysaccharide; IL-4, interleukin-4.

6.3.5. In Vivo Optical Imaging

Once we confirmed the in vitro capacity of inflammatory cells to incorporate the labeled exosomes, we carried out an in vivo assessment of our milk exosome-based probe to verify its ability to detect inflammatory processes. To this end we used a thioglycolate-induced mouse peritonitis model and chose the far-red exosome-based probe Exo-SCy5 to minimize interference by tissue autofluorescence. Based on previous studies with this animal model [32-35], we selected 9 and 24 h time points (6 and 21 h after exosome administration) for image acquisition. In parallel, we carried out a similar imaging protocol employing healthy mice as a control group to evaluate the natural biodistribution of the probe.

In vivo optical imaging showed clear differences in the uptake of the nanoprobe between healthy mice and the thioglycolate-induced peritonitis model mice (Figure

6.5A). In the inflammation model, intense fluorescence was recorded 6 h post injection in the abdominal area, with progressive clearance up to 21 h after administration. This peritoneal accumulation associated with the inflammatory pathology was observed both in vivo and ex vivo. Control animals showed uptake of the nanoprobe mostly in the bladder and liver (Figure 6.5A, 5B) but not in the peritoneal area. The renal and hepatobiliary metabolism of the probe were observed in both the controls and the peritonitis model mice. Early uptake of intravenously injected exosomes in the liver has been reported and attributed to physiological phagocytosis of exosomes by macrophages [21,36]. In addition, an increase in the optical signal in the bladder due to the renal clearance of exosomes has also been described, with a progressive reduction of exosome accumulation in the liver as bladder activity increases [37,38].

After the last time point of in vivo imaging, the mice were sacrificed, the skin of the abdominal area was removed, and the mice were imaged again. Figure 6.5B shows a higher signal in the liver and intestine of the peritonitis mice compared with the healthy controls, which mainly accumulated Exo-SCy5 in the bladder. Next, excised organs were imaged ex vivo (data not shown) and the signal was quantified (Figure 6.5C). In the peritonitis model we observed higher exosome content in the kidneys and intestines and lower fluorescence in liver and spleen compared with the controls, but not reaching statistically significant differences (Student's t-test) (Figure 6.5C).

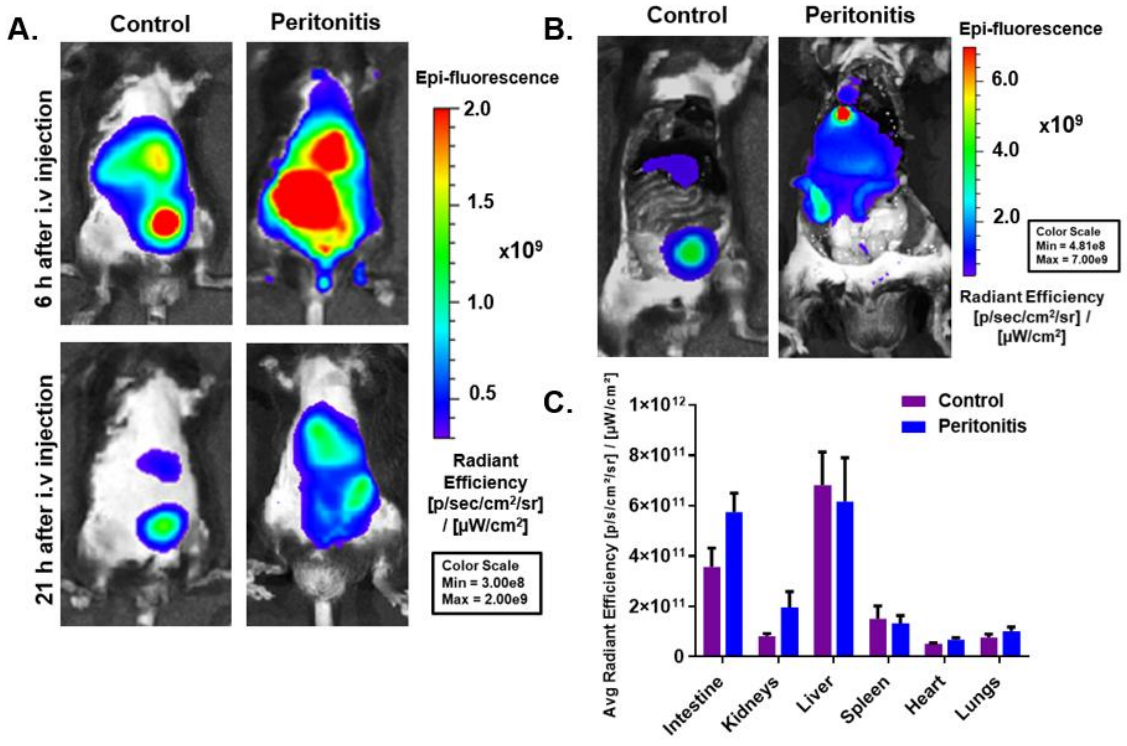

Figure 6.5 Abdominal in vivo uptake in a mouse peritonitis model.

(A) In vivo fluorescence imaging 6 and 21 h after Exo-SCy5 injection in a healthy mouse (control) and peritonitis model. (B) Ex vivo fluorescence imaging after sacrifice and skin removal. (C) Quantification of fluorescence signals of excised organs (intestine, kidneys, liver, spleen, heart, and lungs) from animals sacrificed 21 h after Exo-SCy5 injection.

6.3.6. Flow Cytometry of Peritonitis Exudates

To quantify the uptake of the Exo-SCy5 probe by the myeloid population (macrophages and neutrophils), we isolated peritoneal exudates from Exo-SCy5-treated and from untreated peritonitis model mice, which were used to assess cell autofluorescence. Figure 6.6A shows fluorescence intensity corresponding to exosomes (APC) for the neutrophil (Lys6G+) and macrophage (F4/80+) populations of the untreated control group (top) and the group treated with Exo-SCy5 (bottom). Probe intensity was quantified in terms of median fluorescence intensity (MFI) (Figure 6.6B). A statistically significant increase in MFI was observed in both cell populations with respect to the controls ($p = 0.0037$ and $p = 0.0006$ for macrophages and neutrophils, respectively). Exo-SCy5 was taken up by 27.8 ± 7.1 % of the total macrophage population (Figure 6.6C) based on the fluorescence signal versus 3.7 ± 2.7 % of the control due to their autofluorescence. In the case of neutrophils (Figure 6.6C) 18.4 ± 6.4 % of the total population took up the probe, versus 1.8 ± 1.2 % of the control population.

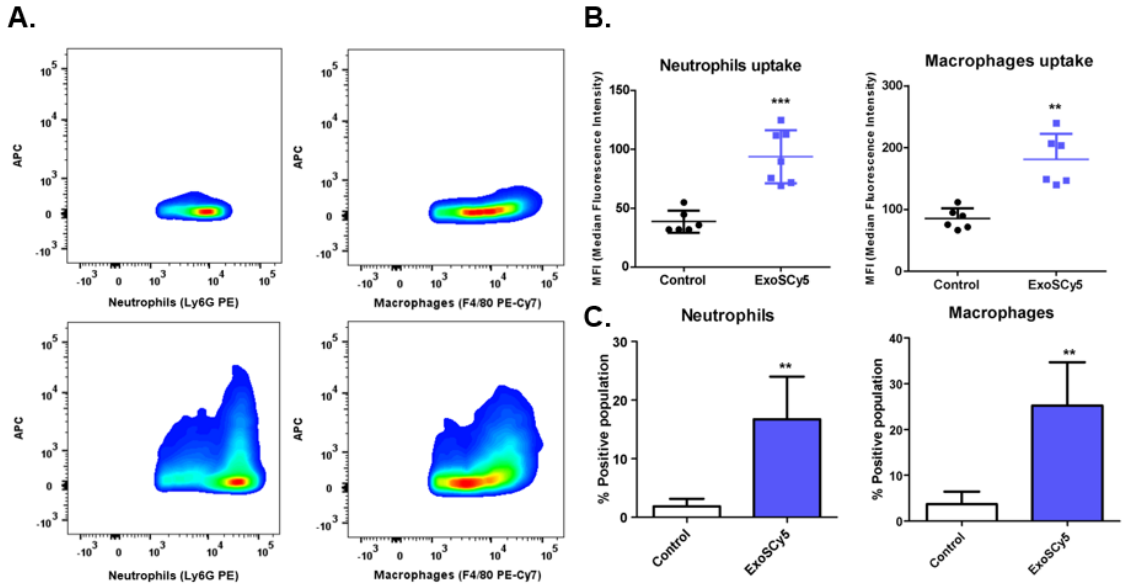

Figure 6.6 Flow cytometry of Exo-SCy5 in exudate neutrophils and macrophages.

(A) Representative dot plots of markers Ly6G in PE and F4/80 in PE-Cy7, respectively, versus exosome fluorescence (Cy5/APC). Untreated controls with peritonitis (upper) and treated with Exo-SCy5 (lower). (B) MFI values of Exo-SCy5 uptake by neutrophils (left) and by macrophages (right), represented by median values from mice with peritonitis without Exo-SCy5 and treated with Exo-SCy5. (C) Percentages of neutrophils and macrophages that have taken up fluorescent exosomes (Cy5/APC); control values stand for cell autofluorescence. p values below 0.05 indicate significant differences: * $p < 0.05$, ** $p < 0.01$, *** $p < 0.001$.

6.3.7. Confocal Imaging of Cells Sorted From Peritoneal Exudates

Finally, to visualize the uptake of our nanoprobe by the targeted cell population, we sorted positive SCy5 exudate samples. Figure 6.7 presents a representative image of the final sorted pool. The incorporation of our nanoparticles can be observed in a neutrophil (stained for Ly6G) at the top of the image and in macrophages (stained for CD68) at the

bottom of the figure. Similar to the in vitro results previously described (Figure 6.3), exosome fluorescence was observed in the perinuclear area, especially in neutrophils where the Exo-SCy5 seemed more localized in rounded packages.

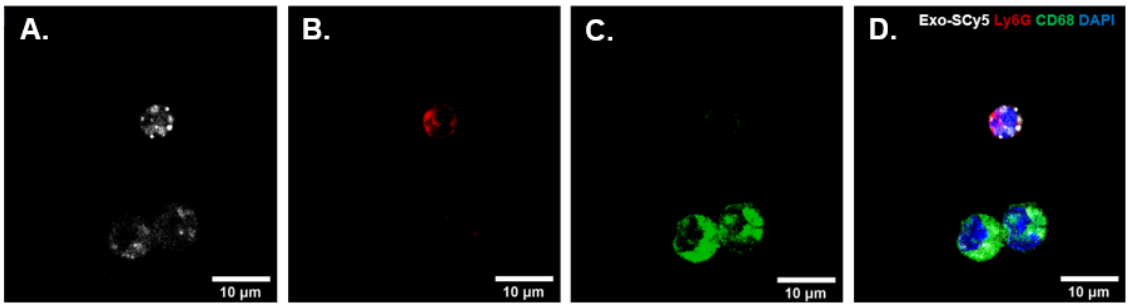

Figure 6.7 Confocal imaging of cells obtained from FACS and immunostained with specific antibodies.

(A) The Exo-SCy5 signal is white. (B) Neutrophils stained for Ly6G are red. (C) Macrophages stained for CD68 are green. (D) Four-channel merged image. Cellular nuclei were stained with DAPI (blue).

6.4. Conclusions

In this work we present for first time goat milk exosomes as natural liposome-like nanoparticles in the development of optical probes for the detection of inflammatory diseases. XTT and LDH assays confirmed the excellent cytocompatibility of the exosomes and in vitro studies in RAW 264.7 macrophages showed a time and dose dependent uptake, and a higher uptake of the M1 proinflammatory activated population compared to M(0) and M2. In addition, successful in vivo internalization of the fluorescent nanoparticles by macrophages and/or neutrophils was demonstrated in a peritonitis mouse model. All these findings suggest that goat milk exosomes are able to localize inflammatory processes and support its potential use as markers for the in vivo detection of inflammatory processes by optical imaging.

6.5. Bibliography

1. Mathivanan, S.; Ji, H.; Simpson, R.J. Exosomes: Extracellular organelles important in intercellular communication. *Journal of Proteomics* 2010, *73*, pp 1907-1920.
2. Thery, C.; Witwer, K.W.; Aikawa, E.; Alcaraz, M.J.; Anderson, J.D.; Andriantsitohaina, R.; Antoniou, A.; Arab, T.; Archer, F.; Atkin-Smith, G.K., et al. Minimal information for studies of extracellular vesicles 2018 (MISEV2018): a position statement of the International Society for Extracellular Vesicles and update of the MISEV2014 guidelines. *J Extracell Vesicles* 2018, *7*, p 1535750.
3. Abels, E.R.; Breakefield, X.O. Introduction to Extracellular Vesicles: Biogenesis, RNA Cargo Selection, Content, Release, and Uptake. *Cellular and Molecular Neurobiology* 2016, *36*, pp 301-312.
4. Armstrong, J.P.; Holme, M.N.; Stevens, M.M. Re-Engineering Extracellular Vesicles as Smart Nanoscale Therapeutics. *ACS Nano* 2017, *11*, pp 69-83.
5. Peinado, H.; Aleckovic, M.; Lavotshkin, S.; Matei, I.; Costa-Silva, B.; Moreno-Bueno, G.; Hergueta-Redondo, M.; Williams, C.; Garcia-Santos, G.; Ghajar, C.,

et al. Melanoma exosomes educate bone marrow progenitor cells toward a pro-metastatic phenotype through MET. *Nat Med* 2012, *18*, pp 883-891.
6. Li, X.; Corbett, A.L.; Taatizadeh, E.; Tasnim, N.; Little, J.P.; Garnis, C.; Daugaard, M.; Guns, E.; Hoorfar, M.; Li, I.T.S. Challenges and opportunities in exosome research-Perspectives from biology, engineering, and cancer therapy. *APL bioengineering* 2019, *3*, pp 011503-011503.
7. Man, F.; Gawne, P.J.; T.M. de Rosales, R. Nuclear imaging of liposomal drug delivery systems: A critical review of radiolabelling methods and applications in nanomedicine. *Advanced Drug Delivery Reviews* 2019, *143*, pp 134-160.
8. Sergey E. Sedykh, E.E.B., Lada V. Purvinsh, Daria A. Klemeshova, Elena I. Ryabchikova and Georgy A. Nevinsky. Milk Exosomes: Isolation, Biochemistry, Morphology, and Perspectives of Use. *IntechOpen, Ed.* 2019, 10.5772/intechopen.85416.
9. Sedykh, S.; Kuleshova, A.; Nevinsky, G. Milk Exosomes: Perspective Agents for Anticancer Drug Delivery. *Int J Mol Sci* 2020, *21*.
10. Wiklander, O.P.B.; Nordin, J.Z.; O'Loughlin, A.; Gustafsson, Y.; Corso, G.; Mäger, I.; Vader, P.; Lee, Y.; Sork, H.; Seow, Y., et al. Extracellular vesicle in vivo biodistribution is determined by cell source, route of administration and targeting. *Journal of Extracellular Vesicles* 2015, *4*, p 26316.
11. Zhu, X.; Badawi, M.; Pomeroy, S.; Sutaria, D.S.; Xie, Z.; Baek, A.; Jiang, J.; Elgamal, O.A.; Mo, X.; Perle, K., et al. Comprehensive toxicity and immunogenicity studies reveal minimal effects in mice following sustained dosing of extracellular vesicles derived from HEK293T cells. *J Extracell Vesicles* 2017, *6*, p 1324730.
12. Munagala, R.; Aqil, F.; Jeyabalan, J.; Gupta, R.C. Bovine milk-derived exosomes for drug delivery. *Cancer letters* 2016, *371*, pp 48-61.
13. Galley, J.D.; Besner, G.E. The Therapeutic Potential of Breast Milk-Derived Extracellular Vesicles. *Nutrients* 2020, *12*.
14. Izumi, H.; Tsuda, M.; Sato, Y.; Kosaka, N.; Ochiya, T.; Iwamoto, H.; Namba, K.; Takeda, Y. Bovine milk exosomes contain microRNA and mRNA and are taken up by human macrophages. *J Dairy Sci* 2015, *98*, pp 2920-2933.
15. Lässer, C.; Alikhani, V.S.; Ekström, K.; Eldh, M.; Paredes, P.T.; Bossios, A.; Sjöstrand, M.; Gabrielsson, S.; Lötvall, J.; Valadi, H. Human saliva, plasma and breast milk exosomes contain RNA: uptake by macrophages. *J Transl Med* 2011, *9*, p 9.
16. Gustafson, H.H.; Holt-Casper, D.; Grainger, D.W.; Ghandehari, H. Nanoparticle Uptake: The Phagocyte Problem. *Nano today* 2015, *10*, pp 487-510.
17. Lin, M.H.; Lin, C.F.; Yang, S.C.; Hung, C.F.; Fang, J.Y. The Interplay Between Nanoparticles and Neutrophils. *J Biomed Nanotechnol* 2018, *14*, pp 66-85.
18. Manca, S.; Upadhyaya, B.; Mutai, E.; Desaulniers, A.T.; Cederberg, R.A.; White, B.R.; Zempleni, J. Milk exosomes are bioavailable and distinct microRNA cargos have unique tissue distribution patterns. *Scientific Reports* 2018, *8*, p 11321.
19. Kim, Y.; Mok, H. Citraconylated exosomes for improved internalization into macrophages. *Applied Biological Chemistry* 2019, *62*, p 26.
20. Okin, D.; Medzhitov, R. Evolution of inflammatory diseases. *Current biology : CB* 2012, *22*, pp R733-R740.
21. Gonzalez, M.I.; Martin-Duque, P.; Desco, M.; Salinas, B. Radioactive Labeling of Milk-Derived Exosomes with (99m)Tc and In Vivo Tracking by SPECT Imaging. *Nanomaterials (Basel)* 2020, *10*.

22. González, M.I.; González-Arjona, M.; Santos-Coquillat, A.; Vaquero, J.; Vázquez-Ogando, E.; de Molina, A.; Peinado, H.; Desco, M.; Salinas, B. Covalently Labeled Fluorescent Exosomes for In Vitro and In Vivo Applications. *Biomedicines* 2021, *9*, p 81.
23. Clemente-Moragón, A.; Gómez, M.; Villena-Gutiérrez, R.; Lalama, D.V.; García-Prieto, J.; Martínez, F.; Sánchez-Cabo, F.; Fuster, V.; Oliver, E.; Ibáñez, B. Metoprolol exerts a non-class effect against ischaemia–reperfusion injury by abrogating exacerbated inflammation. *European heart journal* 2020, *41*, pp 4425-4440.
24. Garcia-Prieto, J.; Villena-Gutierrez, R.; Gomez, M.; Bernardo, E.; Pun-Garcia, A.; Garcia-Lunar, I.; Crainiciuc, G.; Fernandez-Jimenez, R.; Sreeramkumar, V.; Bourio-Martinez, R., et al. Neutrophil stunning by metoprolol reduces infarct size. *Nat Commun* 2017, *8*, p 14780.
25. Cao, L.; Xu, H.; Wang, G.; Liu, M.; Tian, D.; Yuan, Z. Extracellular vesicles derived from bone marrow mesenchymal stem cells attenuate dextran sodium sulfate-induced ulcerative colitis by promoting M2 macrophage polarization. *Int Immunopharmacol* 2019, *72*, pp 264-274.
26. Chen, T.; Xie, M.-Y.; Sun, J.-J.; Ye, R.-S.; Cheng, X.; Sun, R.-P.; Wei, L.-M.; Li, M.; Lin, D.-L.; Jiang, Q.-Y., et al. Porcine milk-derived exosomes promote proliferation of intestinal epithelial cells. *Scientific Reports* 2016, *6*, p 33862.
27. Hock, A.; Miyake, H.; Li, B.; Lee, C.; Ermini, L.; Koike, Y.; Chen, Y.; Määttänen, P.; Zani, A.; Pierro, A. Breast milk-derived exosomes promote intestinal epithelial cell growth. *Journal of Pediatric Surgery* 2017, *52*, pp 755-759.
28. Wang, L.; Shi, Z.; Wang, X.; Mu, S.; Xu, X.; Shen, L.; Li, P. Protective effects of bovine milk exosomes against oxidative stress in IEC-6 cells. *European Journal of Nutrition* 2020, 10.1007/s00394-020-02242-z.
29. Genin, M.; Clement, F.; Fattaccioli, A.; Raes, M.; Michiels, C. M1 and M2 macrophages derived from THP-1 cells differentially modulate the response of cancer cells to etoposide. *BMC Cancer* 2015, *15*, p 577.
30. Park, S.-J.; Kim, B.; Choi, S.; Balasubramaniam, S.; Lee, S.-C.; Lee, J.Y.; Kim, H.S.; Kim, J.-Y.; Kim, J.-J.; Lee, Y.-A., et al. Imaging inflammation using an activated macrophage probe with Slc18b1 as the activation-selective gating target. *Nature Communications* 2019, *10*, p 1111.
31. Shapouri-Moghaddam, A.; Mohammadian, S.; Vazini, H.; Taghadosi, M.; Esmaeili, S.-A.; Mardani, F.; Seifi, B.; Mohammadi, A.; Afshari, J.T.; Sahebkar, A. Macrophage plasticity, polarization, and function in health and disease. *Journal of Cellular Physiology* 2018, *233*, pp 6425-6440.
32. Chan, J.; Leenen, P.J.; Bertoncello, I.; Nishikawa, S.I.; Hamilton, J.A. Macrophage lineage cells in inflammation: characterization by colony-stimulating factor-1 (CSF-1) receptor (c-Fms), ER-MP58, and ER-MP20 (Ly-6C) expression. *Blood* 1998, *92*, pp 1423-1431.
33. Cook, A.D.; Braine, E.L.; Hamilton, J.A. The Phenotype of Inflammatory Macrophages Is Stimulus Dependent: Implications for the Nature of the Inflammatory Response. *The Journal of Immunology* 2003, *171*, pp 4816-4823.
34. Fiedler, U.; Reiss, Y.; Scharpfenecker, M.; Grunow, V.; Koidl, S.; Thurston, G.; Gale, N.W.; Witzenrath, M.; Rosseau, S.; Suttorp, N., et al. Angiopoietin-2 sensitizes endothelial cells to TNF-α and has a crucial role in the induction of inflammation. *Nature Medicine* 2006, *12*, pp 235-239.

35. Leijh, P.C.; van Zwet, T.L.; ter Kuile, M.N.; van Furth, R. Effect of thioglycolate on phagocytic and microbicidal activities of peritoneal macrophages. *Infection and Immunity* 1984, *46*, pp 448-452.
36. Kim, D.H.; Kothandan, V.K.; Kim, H.W.; Kim, K.S.; Kim, J.Y.; Cho, H.J.; Lee, Y.K.; Lee, D.E.; Hwang, S.R. Noninvasive Assessment of Exosome Pharmacokinetics In Vivo: A Review. *Pharmaceutics* 2019, *11*.
37. Royo, F.; Cossío, U.; Ruiz de Angulo, A.; Llop, J.; Falcon-Perez, J.M. Modification of the glycosylation of extracellular vesicles alters their biodistribution in mice. *Nanoscale* 2019, *11*, pp 1531-1537.
38. Banerjee, A.; Alves, V.; Rondão, T.; Sereno, J.; Neves, Â.; Lino, M.; Ribeiro, A.; Abrunhosa, A.J.; Ferreira, L.S. A positron-emission tomography (PET)/magnetic resonance imaging (MRI) platform to track in vivo small extracellular vesicles. *Nanoscale* 2019, *11*, pp 13243-13248.

CHAPTER 7 . GENERAL DISCUSSION AND CONCLUSIONS

The main goal of this thesis is the development of novel imaging nanoprobes based on natural milk exosomes and their further in vivo evaluation as imaging agents in animal models.

To reach this objective, the thesis assesses the physicochemical properties of goat milk exosomes, isolated by an innovative biophysical protocol, and proposes labeling strategies based either on the passive incorporation of the isotope Technetium-99 into the exosome structure or the covalent binding of commercial fluorophores on the nanovesicle surface . Pharmacokinetics and biodistribution of the resultant nanoprobes were evaluated by nuclear and optical imaging techniques in healthy mice and the diagnostic capability of fluorescently labeled goat milk exosomes was assessed on an inflammatory mouse model, due to the proven involvement of these nanovesicles in inflammatory response pathways.

More in detail, the first part of this thesis project describes a novel biophysical approach for the isolation of a pure and homogeneous sample of exosomes from commercial goat milk and the presentation of this goat milk exosomes as natural nanoparticles. This source of exosomes was chosen because exosomes contained in goat milk are still quite unexplored in comparison to human breast or bovine milk, although their protective and immunomodulatory effects have already been demonstrated [1]. Several methodologies for the purification of milk exosomes have been published [2,3], but the nature and composition of the raw material have a considerable influence on the yield and quality of the isolation. In the case of goat milk, its composition includes high fat and casein content, which may limit the effectiveness of the isolation protocols currently reported. Thus, the first part of this thesis optimized an innovative methodology that, for the first time, combined usual physical techniques for exosome isolation with a biological approach employing microbial rennet, to successfully remove residual milk components that could contaminate the exosome sample. This methodology enables the isolation of a large number of vesicles with characteristics traditionally associated with exosomes, such as nanometric size and cup-shape morphology, and with a homogeneous and stable population distribution, confirmed by different physicochemical techniques as Transmission Electron Microscopy (TEM), Dynamic Light Scattering (DLS) and Nanoparticle Tracking Analysis (NTA). The confirmation of the exosomal nature of these nanovesicles was carried out by Western Blot and proteomic analysis, demonstrating the presence of exosomal biomarkers in their composition. The latter assay also linked the isolated exosomes to the activity of the immune system. Finally, a biochemical analysis, performed as proof of concept in healthy mice, determined that the administration of goat milk exosomes in these animals showed no signs of toxicity at the basic biochemical, hepatic or inflammatory levels.

Once isolated, goat milk exosomes were fully characterized, and different labeling strategies were explored to develop exosome-based nanoprobes. The objective of this stage involved not only the labeling of the exosomes, but also the development of new

chemical methodologies to overcome the limitations of current techniques developed for the same purpose. These include the lack of the probe stability or the sensitive chemical processes to which these natural nanoparticles are subjected [4-6].

In the case of the Technetium-99 radiolabeling of exosomes, the proposed methodology was based on the straightforward incorporation and internal chelation of the radiometal with the phospholipids present in the external exosome membrane. Optimized labeling conditions involved physiological pH and temperature, without the need for chelators or exosomal surface modifications. This strategy, in comparison with those described in previous protocols, led to decreasing the reaction time and the presence of chemical reagents needed for the radiolabeling, reaching an appropriate labeling yield and high purity, and maintaining the isotope "trapped" in the exosomal structure over time. The harmlessness of the reaction conditions is proven by physicochemical characterization, which confirmed that the original properties of the exosomes are not modified.

For the exosome-based optical probes, the fluorescent labeling methodology evaluated in the thesis resulted in the development of a highly stable nanoprobe due to the strong covalent binding stablished between the functional chemical groups available in the exosome surface and commercial fluorophores. This strategy is the usual one for connecting N-HydroxySuccinimide (NHS) fluorescent labels with amino biomolecules and had been previously suggested for the labeling of extracellular vesicles [4]. Nevertheless, to the author knowledge, this is the first time that these specific labeling conditions are described and the results of the physicochemical characterization of the probes, as well as their purity and stability, are presented. The major improvement offered by this procedure is the stability of the fluorescent probe obtained, as opposed to the limitations of unspecificity and instability presented by previously developed labeling methodologies [4].

The novel radioactive and optical milk exosome-based probes were assessed both in vitro and in vivo. Nuclear imaging, supported by the ex vivo assays, revealed that the route of administration of the exosomes significantly influenced their pharmacokinetics and biodistribution. The impact of this finding directly affects the use of exosomes in diagnostics or therapy, especially in hepatic or neurological applications, since the bioavailability of these vesicles is increased in the liver when injected intravenously or in the brain if administered via intranasal instillation. In this sense, the significant and rapid uptake of both radioactive and fluorescent probes in the liver of healthy mice after being administered via intravenous injection, supported by in vitro uptake assays in hepatocytes, opens the door to evaluate the potential use of goat milk exosomes in hepatic disorders, for example in targeted drug delivery.

Finally, this thesis not only provides imaging tools to further the study of cell internalization, pharmacokinetics and natural in vivo behavior of exosomes but also evaluates the potential use of these nanovesicles as probes for diagnosis. The ability of fluorescently labeled goat milk exosomes to detect inflammation foci has been studied in the last part of in this thesis, based on the literature supporting its natural role in the immune system activity and inflammatory processes [1,7]. As expected, cellular uptake

assays performed using fluorescently labeled exosomes revealed internalization of these nanovesicles by macrophages, one of the main cell populations involved in the immune response. Among the different macrophage phenotypes, exosome uptake was more significant in the activated M1 proinflammatory population, highlighting them as targets of these nanovesicles. The in vivo analysis of the intravenously injected nanoprobe in a peritonitis mouse model as well as the ex vivo evaluation of the uptake in inflammation-associated cells confirmed the capacity of fluorescent exosomes to signal the inflammatory process, internalizing in vivo in both neutrophils and, again, macrophages.

7.1 Conclusions

I.- An innovative isolation protocol has been proposed for the purification of exosomes from commercial goat milk, based on the combination of physical and biological approaches. This reproducible method guarantees the purity and homogeneity of the nanovesicles and maintains their expected physicochemical properties as well as their non-toxicity.

II.- Novel chemical strategies for the radioactive and fluorescent labeling of goat milk exosomes have been developed and optimized, improving the limitations of current methodologies. Technetium-99 radiolabeling enabled the straightforward incorporation of the radioisotope in the exosomal structure under physiological conditions, without using chelators. In the case of the fluorescent labeling, the proposed methodology resulted in a highly stable nanoprobe by the covalent binding between the fluorophore and the exosome surface, avoiding false positives in optical imaging assays. Both radioactive and fluorescent exosome-based probes maintained the original physicochemical properties of the nanovesicles. [^{99m}Tc]-exosome tracer was validated by SPECT imaging, gamma-counter biodistribution and autoradiography. Applicability of fluorescent exosomes was assessed by in vivo optical imaging and confocal microscopy.

III.- The evaluation of the pharmacokinetic profile of the developed nanoprobes in healthy mice revealed significant differences in pharmacokinetics and biodistribution of exosomes depending on the route of administration.

IV.- The in vivo assessment of the fluorescent nanoprobe in a peritonitis mouse model have demonstrated the ability of goat milk exosomes to target inflammatory processes underlying pathologies by specific interactions with inflammatory cell populations. The exosome-based nanoprobes were in vivo taken up by neutrophils and macrophages, confirmed by flow cytometry assay, and the in vitro evaluation carried out using non-activated and activated macrophages revealed significant accumulation of the exosomes in the proinflammatory phenotype.

7.2 Future research lines derived from this thesis project

Different lines of research could be further developed from the results achieved in this thesis:

- Due to the novelty of the combined physical/biological isolation protocol proposed of this thesis, it would be interesting to evaluate whether this technique can improve the isolation of exosomes from other milk sources, reducing the presence of contaminating milk components that are normally co-isolated.
- As the radioactive labeling conditions reported are intended to be "exosome friendly", their applicability to other types of extracellular vesicles less resistant than milk exosomes, such as those derived from cell cultures or clinical samples, could be evaluated, as was evaluated in the case of the fluorescent labeling.
- This thesis presents in vitro studies and one in vivo proof of concept related to the evaluation of the possible toxic effects of goat milk exosomes, carried out in different cell lines and healthy mice. However, considering their potential translation to the clinic, it is crucial to further evaluate the immunogenicity, immunoreactivity and possible adverse effects of these nanovesicles, also ruling out its participation in the development of certain pathologies.
- The results achieved in this thesis confirm the promising application of goat milk exosomes for the development of novel imaging agents, especially for detecting pathologies with associated inflammatory response. However, one of the objectives of future research lines should be to reduce the accumulation of these nanovesicles in secondary organs not related to the specific biological target. To this aim, the developed exosome-based platforms can be optimized by bioengineering through the enrichment of the exosomal surface with specific target-relevant vectors, such as proteins or antibodies, enhancing their bioaccumulation in the target area.
- The physicochemical properties of these nanovesicles not only support their use in diagnostic imaging but also point to their promising application as drug delivery systems. The structural characteristics of the exosomes enable them to incorporate hydrophobic molecules inside, improving their bioavailability and being able to transport them as "Trojan horses" to a specific biological target. In different assays of this thesis, goat exosomes have exhibited significant liver targeting in addition to their selectivity for inflammatory processes, highlighting the importance of developing drug encapsulation strategies to explore their potential use as drug transporters for hepatic disorders or inflammatory-related diseases.

7.3 Bibliography

1. Mecocci, S.; Gevi, F.; Pietrucci, D.; Cavinato, L.; Luly, F.R.; Pascucci, L.; Petrini, S.; Ascenzioni, F.; Zolla, L.; Chillemi, G. Anti-Inflammatory Potential of Cow, Donkey and Goat Milk Extracellular Vesicles as Revealed by Metabolomic Profile. *Nutrients* 2020, *12*, p 2908.
2. Vaswani, K.; Koh, Y.Q.; Almughlliq, F.B.; Peiris, H.N.; Mitchell, M.D. A method for the isolation and enrichment of purified bovine milk exosomes. *Reproductive biology* 2017, *17*, pp 341-348.
3. Munagala, R.; Aqil, F.; Jeyabalan, J.; Gupta, R.C. Bovine milk-derived exosomes for drug delivery. *Cancer letters* 2016, *371*, pp 48-61.

4. Yi, Y.W.; Lee, J.H.; Kim, S.-Y.; Pack, C.-G.; Ha, D.H.; Park, S.R.; Youn, J.; Cho, B.S. Advances in analysis of biodistribution of exosomes by molecular imaging. *International journal of molecular sciences* 2020, *21*, p 665.
5. Varga, Z.; Gyurkó, I.; Pálóczi, K.; Buzás, E.I.; Horváth, I.; Hegedűs, N.; Máthé, D.; Szigeti, K. Radiolabeling of extracellular vesicles with 99mTc for quantitative in vivo imaging studies. *Cancer Biotherapy and Radiopharmaceuticals* 2016, *31*, pp 168-173.
6. Hwang, D.W.; Choi, H.; Jang, S.C.; Yoo, M.Y.; Park, J.Y.; Choi, N.E.; Oh, H.J.; Ha, S.; Lee, Y.-S.; Jeong, J.M. Noninvasive imaging of radiolabeled exosome-mimetic nanovesicle using 99mTc-HMPAO. *Scientific reports* 2015, *5*, pp 1-10.
7. Ahmed, F.; Tamma, M.; Pathigadapa, U.; Reddanna, P.; Yenuganti, V.R. Drug Loading and Functional Efficacy of Cow, Buffalo, and Goat Milk-Derived Exosomes: A Comparative Study. *Molecular Pharmaceutics* 2022, *19*, pp 763-774.

SCIENTIFIC OUTPUT DERIVED FROM THE THESIS: PUBLISHED AND SUBMITTED CONTENT

Papers Published in Scientific Journals

- González, M.I., Martín-Duque, P., Desco, M., Salinas, B. *Radioactive Labeling of Milk-Derived Exosomes with ^{99m}Tc and In Vivo Tracking by SPECT Imaging*. Nanomaterials 2020, 10, 1062. Impact Factor: 4.324 (Q2 Nanoscience and Nanotechnology). DOI: 10.3390/nano10061062. This item has been wholly included in this thesis (Chapter 4). Whenever material from this source is included in this thesis, it is singled out with typographic means and an explicit reference.
- González, M.I., González-Arjona, M., Santos-Coquillat, A., Vaquero, J., Vázquez-Ogando, E., de Molina, A., Peinado, H., Desco, M., Salinas, B. *Covalently Labeled Fluorescent Exosomes for In Vitro and In Vivo Applications*. Biomedicines 2021, 9, 81. Impact Factor: 4.757 (Q2 Biochemistry and Molecular Biology). DOI: 10.3390/biomedicines9010081. This item has been wholly included in this thesis (Chapter 5). Whenever material from this source is included in this thesis, it is singled out with typographic means and an explicit reference.
- González, M.I.*, Santos-Coquillat, A.*, Clemente-Moragón, A., González-Arjona, M., Albaladejo-García, V., Peinado, H., Muñoz, J., Ximénez-Embún, P., Ibáñez, B., Oliver, E., Desco, M., Salinas, B. *Goat Milk Exosomes As Natural Nanoparticles for Detecting Inflammatory Processes By Optical Imaging*. Small 2021, 18 (6), 2105421. Impact Factor: 15.153 (Q1 Nanoscience and Nanotechnology). DOI: 10.1002/smll.202105421. González, M.I. and Santos-Coquillat, A. contributed equally to this project. This item has been wholly included in this thesis (Chapter 3 and Chapter 6). Whenever material from this source is included in this thesis, it is singled out with typographic means and an explicit reference.

Papers Submitted in Scientific Journals / Under Preparation

- González, M.I.*, Gallardo, B.*, Cerón, C., Aguilera-Jiménez, E., Cortés-Canteli, M., Peinado, H., Desco, M., Salinas, B. *Isolation of Goat Milk Small Extracellular Vesicles by Novel Combined Biophysical Methodology*. Under preparation to be submitted to Molecular Nutrition and Food Research (Impact Factor 2021: 6.575, Q1 Food science & technology). González, M.I. and Gallardo, B. contributed equally to this project. This item has been partially included in this thesis (Chapter 3). Whenever material from this source is included in this thesis, it is singled out with typographic means and an explicit reference.
- González, M.I., Santos-Coquillat, A., Sánchez-Redondo, S., Hergueta-Redondo, M., Peinado, H., Desco, M., Salinas, B. *Fluorescent Goat Milk Small Extracellular Vesicles for In Vivo Detection of Melanoma by Optical Imaging.* Under preparation to be submitted to Cancers (Impact Factor 2021: 6.575, Q1 Oncology).

Contributions to Conferences

Presenter of the communication has been singled out with an asterisk (*)

- González, M.I.*, Santos-Coquillat, A., Sánchez-Redondo, S., Herreros-Pérez, D., Hergueta-Redondo, M., Peinado, H., Desco, M., Salinas, B. *Milk small extracellular vesicles as natural nanoprobes for tumor detection by optical imaging*. The World Molecular Imaging Congress (WMIC) 2022. Miami, USA. Poster presentation.
- González, M.I.*, Santos-Coquillat, A., Clemente-Moragón, A., González-Arjona, M., Sobrino, G., Albaladejo-García, V., Peinado, H., Muñoz, J., Ximénez-Embún, P., Ibañez, B., Oliver, E., Desco, M., Salinas, B. *Nano-sondas fluorescentes basadas en vesículas extracelulares de leche de cabra para la detección in vivo de procesos inflamatorios*. IX Jornadas de Investigación e Innovación del Instituto de Investigación Sanitaria Gregorio Marañón (IiSGM) 2022. Madrid, Spain. Poster presentation.
- González, M.I.*, González-Arjona, M., Santos-Coquillat, A., Sobrino, G., Vaquero, J., Vázquez-Ogando, E., de Molina, A., Peinado, H., Desco, M., Salinas, B. *Novel strategies for the fluorescent labeling of extracellular vesicles for in vitro and in vivo imaging*. International Society of Extracellular Vesicles (ISEV) anual meeting 2022. Lyon, France. Oral presentation.
- González, M.I.*, Santos-Coquillat, A., Clemente-Moragón, A., González-Arjona, M., Sobrino, G., Albaladejo-García, V., Peinado, H., Muñoz, J., Ximénez-Embún, P., Ibáñez, B., Oliver, E., Desco, M., Salinas, B. *Fluorescent nanoprobes based on goat milk small extracellular vesicles for in vivo detection of inflammation processes*. International Society of Extracellular Vesicles (ISEV) anual meeting 2022. Lyon, France. Poster presentation.
- Santos-Coquillat, A.*, González, M.I., Clemente-Moragón, A., González-Arjona, M., Albaladejo-García, V., Ibáñez, B., Oliver, E., Desco, M., Salinas, B. *Goat's milk exosomes as natural nanoparticles in detection of inflammatory processes by optical imaging.* 16th European Molecular Imaging Meeting (EMIM) 2021. Göttingen, Germany. Poster presentation.
- González, M.I.*, Santos-Coquillat, A., Sánchez-Redondo, S., Hergueta-Redondo, M., Peinado, H., Desco, M., Salinas, B. *Natural exosome-based nanoprobes for melanoma detection by optical imaging*. 16th European Molecular Imaging Meeting (EMIM) 2021. Göttingen, Germany. Poster presentation.
- González, M.I.*, Martín-Duque, P., Desco, M., Salinas, B. *Radioactive labeling and in vivo tracking of milk exosomes by SPECT/CT imaging.* Student Network on Extracellular Vesicles (SNEV) 2021 Virtual Conference. Virtual online. Oral presentation, awarded for the 'Best Oral Communication'.
- González, M. I.*, Salinas, B.*, Desco, M. *Exosomas de leche y teragnóstico*. 1er Simposio Vesículas Extracelulares en Hepatología. Madrid, Spain. Oral presentation

- Santos-Coquillat, A.*, González, M.I., Clemente-Moragón, A., González-Arjona, M., Albaladejo-García, V., Ibáñez, B., Oliver, E., Desco, M., Salinas, B. *In vitro and in vivo fluorescent detection of inflammatory processes using milk exosomes*. The World Molecular Imaging Congress (WMIC) 2020. Virtual online. Oral presentation.
- González, M.I.*, Sobrino, G., Hergueta-Redondo, M., Sánchez-Redondo, S., Peinado, H., Desco, M., Salinas, B. *Goat milk exosomes: natural nanoplatforms in tumor detection by molecular imaging*. 5th International GEIVEX 2019 Symposium. Granada, Spain. Oral presentation.
- Santos-Coquillat, A.*, González, M.I., Albaladejo-García, V., Desco, M., Salinas, B. *Non-invasive detection of inflammation processes using fluorescent milk exosomes*. 5th International GEIVEX 2019 Symposium. Granada, Spain. Oral presentation.
- González, M.I.*, Sobrino, G., Desco, M., Salinas, B. *In vivo tracking of exosomes by nuclear imaging*. 5th International GEIVEX 2019 Symposium. Granada, Spain. Poster presentation, awarded for the 'Best Poster Communication'.
- González, M.I.*, Sobrino, G., Santos-Coquillat, A., Martín-Duque, P., Desco, M., Salinas, B. *Evaluation of milk-derivate exosomes as natural nanoplatforms in oncology*. 2nd Spanish Conference on Biomedical Applications of Nanomaterials (SBAN) 2019. Madrid, Spain. Oral presentation.
- González, M.I., Sobrino, G., Desco, M., Salinas, B*. *Evaluación de exosomas de leche como liposomas naturales en teragnóstico*. XXXVII Reunión bienal de la Real Sociedad Española de Química 2019. Madrid, Spain. Oral presentation.
- González, M.I.*, Sobrino, G., Desco, M., Salinas, B. *In vivo exosomal tracking by SPECT imaging*. VII Jornadas de Investigación e Innovación del Instituto de Investigación Sanitaria Gregorio Marañón (IiSGM) 2019. Madrid, Spain. Oral presentation, awarded for the 'Best Oral Communication'.
- González, M.I.*, Sobrino, G., Desco, M., Salinas, B. *In vivo exosomal tracking by SPECT imaging*. 14th European Molecular Imaging Meeting (EMIM) 2019. Glasgow, UK. Oral presentation.

Participation in Research Projects

This thesis has been developed as part of several research projects:

- Project name: PT20/00044, "Modelos animales e imagen biomédica". PI: Manuel Desco Menéndez. ISCIII, Ministerio de Ciencia e Innovación. 2021 – 2023. 72.600 €. Status: member.
- Project name: PI20/01632, "Monitorización de tratamiento y respuesta a infecciones estafilocócicas mediante imagen inmunoPET empleando trazadores específicos". PI: Beatriz Salinas Rodríguez. ISCIII, Ministerio de Ciencia e Innovación. 2021 – 2023. 68.970 €. Status: member.

- Project name: “Development of new approaches of molecular imaging for diagnosis and treatment of tumors and infectious diseases”. PI: Beatriz Salinas Rodríguez and Susanne Kossatz. Bavarian Funding Programme for the Initiation of International Projects. 2020 – 2021. 3.282 €. Status: member.
- Project name: Y2018/NMT-4949, “Nuevas aplicaciones de la nanotecnología en la enfermedad hepática crónica (NanoLiver-CM)”. PI: Manuel Desco Menéndez. Comunidad de Madrid. 2018 – 2022. 771.100 €. Status: member.
- Project name: S2017/BMD-3867, “Red Madrileña de Nanomedicina en Imagen Molecular (RENIM-CM)”. PI: Manuel Desco Menéndez. Comunidad de Madrid. 2018 – 2022. 1.020.100,65 €. Status: member.

Stays in National or International Research Centers

- Research Center: Technische Universität München (TUM, München, Germany). 07/03/2022 - 16/04/2022. Supervisor: Prof. Dr. Susanne Kossatz. Purpose: pre-doctoral stay.
- Research Center: Technische Universität München (TUM, München, Germany). 17/11/2021 - 12/12/2021. Supervisor: Prof. Dr. Susanne Kossatz. Purpose: pre-doctoral stay.
- Research Center: Centro Nacional de Investigaciones Oncológicas (CNIO) Carlos III (Madrid, Spain). 01/03/2019 – 01/03/2020. Supervisor: Dr. Héctor Peinado. Purpose: research collaboration.
- Research Center: Centro Nacional de Investigaciones Cardiovasculares (CNIC) Carlos III (Madrid, Spain). 01/07/2018 – currently. Supervisor: Prof. Dr. Manuel Desco. Purpose: associated researcher.

OTHER RESEARCH MERITS

Papers Published in Scientific Journals (not related to the thesis project)

- Gómez-Cid, L., López-Donaire, M. L., Velasco, D., Marín, V., González, M. I., Salinas, B., Cussó, L., García, Á., Bravo, S. B., Fernández-Santos, M. E., Elvira, C., Sierra, J., Arroba, E., Bañares, R., Grigorian-Shamagian, L., Fernández-Avilés, F. *Cardiac Extracellular Matrix Hydrogel Enriched with Polyethylene Glycol Presents Improved Gelation Time and Increased On-Target Site Retention of Extracellular Vesicles*. International Journal of Molecular Sciences 2021, 22(17), 9226. Impact Factor: 6.208 (Q1 Biochemistry and Molecular Biology). DOI: 10.3390/ijms22179226.

Papers Submitted in Scientific Journals / Under Preparation (not related to the thesis project)

- González, M.I.*, González-Arjona, M.*, Cussó, L., Morcillo, M.A., Kestler, M., Calle, D., Cerón, C., Cortés-Canteli, M., Muñoz, P., Bouza, E., Desco, M., Salinas, B. *Radiolabeled anti-alpha toxin antibodies for the in vivo detection of staphylococcal infection by PET imaging*. Submitted to Applied Microbiology and Biotechnology (Impact Factor 2021: 5.560, Q1 Biotechnology and Applied Microbiology). González, M.I. and González-Arjona, M. contributed equally to this project.
- González-Arjona, M.*, González, M.I.*, Burillo, A., Vázquez, S.N, Cussó, L., Rodríguez, B., Muñoz, P., Desco, M., Salinas, B. *Radiolabeled anti-IgM antibody for the in vivo detection of infectious diseases by immunoPET*. Under preparation to be submitted to ACS Infectious Diseases (Impact Factor 2021: 5.578, Q1 Chemistry, Medical). González-Arjona, M. and González, M.I. contributed equally to this project.
- Santos-Coquillat, A.*, Herreros-Pérez, D.*, Samaniego, R., González, M.I., Cussó, L., Desco, M., Salinas, B. *Dual-labeled nanoparticles based on small extracellular vesicles for tumor detection*. Biology Direct, in press (Impact Factor 2021: 7.173, Q1 Biology). Santos-Coquillat, A. and Herreros-Pérez, D. contributed equally to this project.
- Albaladejo-García, V.*, Morán, L.*, Santos-Coquillat, A., González, M.I., Gallardo-Alguacil, B., Ye, H., Vaquero, J., Vázquez-Ogando, E., Cubero, J., Desco, M., Salinas. B. *ExoCur as nanotherapeutic platform in liver acute diseases*. Under preparation to be submitted to Frontiers in Gastroenterology (Impact Factor not registered). Albaladejo-García, V. and Morán, L. contributed equally to this project.

Contributions to Conferences (not related to the thesis project)

Presenter of the communication has been singled out with an asterisk (*)

- González, M.I.*, Sobrino, G., Clemente-Moragón, A., González-Arjona, M., Gómez-Parriza, M., Ibáñez, B., Desco, M., Oliver, E., Salinas, B. *In vivo evaluation of neutrophils infiltration in acute lung injury by immunePET imaging*. The World Molecular Imaging Congress (WMIC) 2022. Miami, USA. Poster presentation.
- González-Arjona, M.*, Cussó, L., Aguilera-Correa, J.J., González, M.I., Burillo, A., N. Vázquez, S., Muñoz, P., Romero, E., Morcillo, M.A., Esteban, J., Desco, M., Salinas, B. *Detección in vivo de la infección por Staphylococcus aureus en un modelo de osteoartritis mediante inmunoPET*. IX Jornadas de Investigación e Innovación del Instituto de Investigación Sanitaria Gregorio Marañón (IiSGM) 2022. Madrid, Spain. Oral presentation, awarded for the 'Best Communication with Innovative Component'.
- Herreros-Pérez, D.*, Santos-Coquillat, A., Samaniego, R., González, M.I., González-Arjona, M., Aguilera-Jiménez, E., Cussó, L., Desco, M., Salinas, B. *Dual nanoparticles based on milk exosomes in glioblastoma detection*. 17th European Molecular Imaging Meeting (EMIM) 2022. Thessaloniki, Greece. Oral presentation.
- González-Arjona, M.*, Cussó, L., Aguilera-Correa, J.J., González, M.I., Burillo, A., N. Vázquez, S., Muñoz, P., Romero, E., Morcillo, M.A., Esteban, J., Desco, M., Salinas, B. *In vivo detection of Staphylococcus aureus infection in osteoarthritis model by immunoPET employing radiolabed Anti-alfa toxin antibody*. 17th European Molecular Imaging Meeting (EMIM) 2022. Thessaloniki, Greece. Oral presentation.
- González-Arjona, M.*, González, M.I., Burillo, A., N. Vázquez, S., Fernández, M. J., Muñoz, P., Desco, M., Salinas, B. *^{89}Zr-AntIgM radiotracer for the early detection of infectious processes by immunoPET imaging*. The World Molecular Imaging Congress (WMIC) 2021. Virtual online. Oral presentation.
- González-Arjona, M.*, Aguilera-Correa, J.J., González, M.I., Cussó, L., Burillo, A., N. Vázquez, S., Muñoz, P., Esteban, J., Desco, M., Salinas, B. *^{89}Zr-αTox immunotracer for the in vivo detection of S. aureus infection in osteoarthritis model*. The World Molecular Imaging Congress (WMIC) 2021. Virtual online. Oral presentation.
- González-Arjona, M.*, González, M.I., Burillo, A., N. Vázquez, S., Muñoz, P., Desco, M., Salinas, B. *IgM specific radiotracer for the in vivo detection of infectious diseases by immunoPET.* 16th European Molecular Imaging Meeting (EMIM) 2021. Göttingen, Germany. Oral presentation.
- González-Arjona, M.*, González, M.I., Burillo, A., N. Vázquez, S., Fernández, M. J., Muñoz, P., Desco, M., Salinas, B. *Detection of infectious diseases by non-invasive nuclear imaging*. Immuno-Imaging and Molecular Therapy Workshop 2021. Virtual online. Oral presentation.
- González, M.I.*, González-Arjona, M., Cussó, L., Kestler, M., Calle, D., Muñoz, P., Bouza, E., Desco, M., Salinas, B. *Detection of Sthaphylococcus aureus infections by*

specific alpha-toxin immunepet tracer. Immuno-Imaging and Molecular Therapy Workshop 2021. Virtual online. Oral presentation.

- González, M.I.*, González-Arjona, M., Cussó, L., Kestler, M., Calle, D., Muñoz, P., Bouza, E., Desco, M., Salinas, B. *Specific α-toxin radiotracer for the detection of S. aureus infections by immunoPET imaging*. The World Molecular Imaging Congress (WMIC) 2020. Virtual online. Oral presentation.
- González, M.I.*, González-Arjona, M., Kestler, M., Cussó, L., Calle, D., Muñoz, P., Bouza, E., Desco, M., Salinas, B. *Radiolabelled Anti-Staphylococcal antibodies for diagnosis of bacterial infection by immunoPET*. : 15th European Molecular Imaging Meeting (EMIM) 2020. Virtual online. Oral presentation.
- González, M.I.*, González-Arjona, M., Kestler, M., Cussó, L., Calle, D., Muñoz, P., Bouza, E., Desco, M., Salinas, B. *Diseño de radiotrazadores inmuno-PET para la detección de procesos infecciosos asociados a S. aureus*. Ciclo de Seminarios de Investigación "Alberto Tejedor" del Instituto de Investigación Sanitaria Gregorio Marañón (IiSGM). Madrid, Spain. Oral presentation.
- González, M.I.*, Calle, D., Cussó, L., Kestler, M., Muñoz, P., Bouza, E., Desco, M., Salinas, B. *^{89}Zr-αToxAb; a novel approach in the specific detection of S. aureus infection by immunoPET*. 3rd Young Spanish Molecular Imaging Network (ySMIN) 2019. Barcelona, Spain. Oral presentation.
- González, M.I., Kestler, M., Muñoz, P., Bouza, E., Desco, M., Salinas, B*. *^{89}Zr-alfaToxAb as novel immunoPET radiotracer for the detection of S. aureus in bacteremia model.* 14th European Molecular Imaging Meeting (EMIM) 2019. Glasgow, UK. Oral presentation.

Direction of Bachelor/Master Thesis

During her thesis period, the doctoral candidate has collaborated in the direction of the following bachelor or thesis:

- Corral-Bellón, M. *Title under consideration*. Bachelor thesis (Biomedical Engineering, Universidad Carlos III, currently in progress).
- Jiménez-Aguilera, A. *Synthesis of nanosystems based on silver sulphide nanoparticles encapsulated in exosomes for their use as probes in optical imaging*. Bachelor thesis (Biomedical Engineering, Universidad Carlos III, 25/03/2022) with grade: 10.
- Fernández-Montero, A. L. *Interacción de campos magnéticos con nanopartículas magnéticas alojadas en células sanguíneas*. Master thesis (Medical Physics, Universidad Nacional de Eduación a Distancia, 13/10/2020) with grade: 10.